SANDIA REPORT

SAND97-0844 • UC-902
Unlimited Release
Printed April 1997

Development of a Subsurface Gas Flow Probe

Robert P. Cutler, Sanford Ballard, Glenn T. Barker, Russell G. Keefe, Michael P. Chavez, Harlan W. Stockman, Louis Romero

Prepared by
Sandia National Laboratories
Albuquerque, New Mexico 87185 and Livermore, California 94550

Sandia is a multiprogram laboratory operated by Sandia Corporation, a Lockheed Martin Company, for the United States Department of Energy under Contract DE-AC04-94AL85000.

Approved for public release; distribution is unlimited.

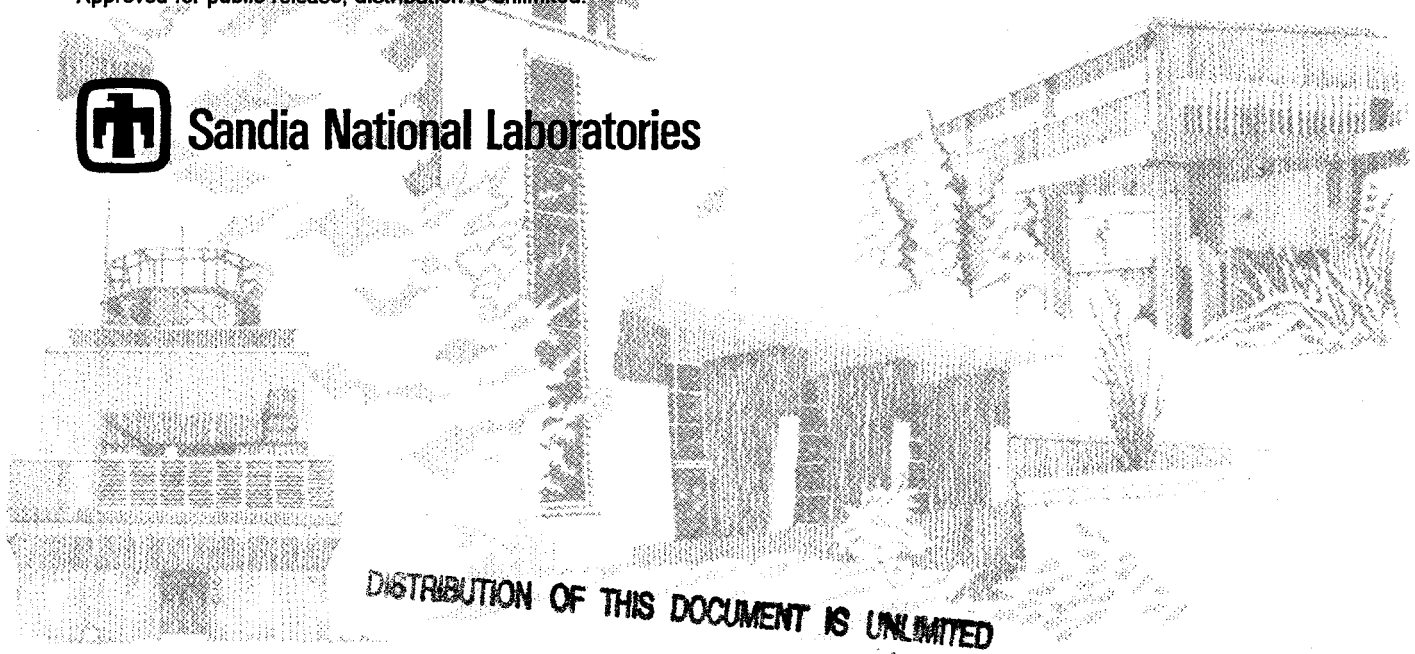

Sandia National Laboratories

Issued by Sandia National Laboratories, operated for the United States Department of Energy by Sandia Corporation.

Available to DOE and DOE contractors from
Office of Scientific and Technical Information
P.O. Box 62
Oak Ridge, TN 37831

Prices available from (615) 576-8401, FTS 626-8401

Available to the public from
National Technical Information Service
U.S. Department of Commerce
5285 Port Royal Rd
Springfield, VA 22161

NTIS price codes
Printed copy: A06
Microfiche copy: A01

SAND 97-0844
Unlimited Release
Printed April 1997

Distribution
Category UC902

Development of a Subsurface Gas Flow Probe

Robert P. Cutler, Sanford Ballard, Glenn T. Barker, Russell G. Keefe, Michael P. Chavez
Geophysical Technology Department

Harlan W. Stockman
Geochemistry Department

Louis Romero
Applied and Numerical Mathematics Department

Sandia National Laboratories
P.O. Box 5800
Albuquerque, NM 87185-0705

Abstract

This report describes a project to develop a flow probe to monitor gas movement in the vadose zone due to passive venting or active remediation efforts such as soil vapor extraction. 3-D and 1-D probes were designed, fabricated, tested in known flow fields under laboratory conditions, and field tested. The 3-D probes were based on technology developed for ground water flow monitoring. The probes gave excellent agreement with measured air velocities in the laboratory tests. Data processing software developed for ground water flow probes was modified for use with air flow, and to accommodate various probe designs. Modifications were made to decrease the cost of the probes, including developing a downhole multiplexer. Modeling indicated problems with flow channeling due to the mode of deployment. Additional testing was conducted and modifications were made to the probe and to the deployment methods. The probes were deployed at three test sites: a large outdoor test tank, a brief vapor extraction test at the Chemical Waste landfill, and at an active remediation site at a local gas station. The data from the field tests varied markedly from the laboratory test data. All of the major events such as vapor extraction system turn on and turn off, as well as changes in the flow rate, could be seen in the data. However, there were long term trends in the data which were much larger than the velocity signals, which made it difficult to determine accurate air velocities. These long term trends may be due to changes in soil moisture content and seasonal ground temperature variations.

Acknowledgments

This work was funded by the Strategic Environmental Research and Development Program and by the Office of Technology Development. We wish to thank James E. Studer and Souren Ala of Intera for their help with the remediation site field test. We also acknowledge the helpful comments of Marianne C. Walck and Ray E. Finley who reviewed this report. This work was supported by the United States Department of Energy under Contract DE-AC04-94AL85000. Sandia is a multiprogram laboratory operated by Sandia Corporation, a Lockheed Martin Company, for the United States Department of Energy.

Contents

List of Figures

List of Figures
(continued)

This Page Intentionally Left Blank

Introduction

Many techniques for remediating contaminated, unsaturated sediments involve inducing or controlling the flow of air through the sediments. Examples include in situ air stripping, air injection to enhance biodegradation of contaminants, and enhancing the naturally-occurring flow of air into and out of the subsurface due to changes in atmospheric pressure. In assessing the effectiveness, efficiency and zone of influence of these processes it is critical to understand the dynamics of the gas flow in the subsurface. Given the pronounced inhomogeneity of the pneumatic properties of natural sediments, air will travel along preferred, high permeability pathways. To effectively monitor the remediation process, it is necessary to accurately delineate these pathways and determine the degree to which the air flow is narrow and constricted or broad and diffuse.

The overall goal of this project was to develop an inexpensive, easily deployable probe to monitor subsurface gas flow velocity for air sparging and vapor extraction experiments and operations. If achievable, such a probe would find application in characterizing the gas flow fields in the vicinity of active and passive soil vapor extraction systems. It would have the potential to dramatically improve understanding of the dynamics of a wide range of environmental remediation technologies which involve air movements through unsaturated sediments. The availability of the gas flow probe technology would improve the cost effectiveness of these remediation techniques by providing information about the zone of influence of the process at a given site, thereby alleviating the necessity of conducting overly conservative cleanup sweeps.

The gas flow probe is an extension of a technology called the In Situ Permeable Flow Sensor which measures the full 3D groundwater flow velocity vector in saturated, permeable sediments, and was previously developed by Sandia [1,2,3]. Both technologies are based on the principle that the temperature distribution on the surface of a finite length, heated cylinder buried in a permeable flow field is related to the flow velocity of fluid past the cylinder. In essence, relatively cool temperatures are observed on the upstream side of the probe and relatively warm temperatures on the downstream side as heat emanating from the cylinder is advected around the probe by the moving fluid.

To accurately measure the fluid velocity, the cylinder must be directly buried in the sediment, in intimate contact with the formation, rather than being deployed inside a borehole. Boreholes, along with the casings, screens and gravel packs which surround them, alter the flow in and around the borehole in ways which are generally difficult to take into account. It was envisioned that in addition to versions of the gas flowmeter intended for direct burial in the ground, other versions would be tested that could be driven in place by a hammer, cone penetrometer, or other device without having to auger a hole in the ground. During the course of the investigation it became apparent that these versions were not practical.

The probes were tested in the laboratory, at demonstration field sites, and in an active remediation project. The work described in this document was conducted from February, 1995 through October, 1996, and was funded by SERDP and by the DOE Office of Technology Development, EM50.

The goals of this project were to:

1. Determine the feasibility of an in-situ air flow probe.
2. Develop a probe sensitive enough to monitor atmospheric pressure effects.
3. Develop fabrication and calibration procedures for the probes.
4. Determine the sensitivity and accuracy of the probes using known flow rates in controlled laboratory tests.
5. Modify existing data analysis software as needed for use with air flow probes.
6. Demonstrate the instruments at an active vapor extraction remediation site.
7. Make the probe more mechanically robust.
8. Reduce the cost of the probe compared to the 3D water flow probe.
9. Develop methods to deploy the probes at field sites without adversely affecting the flow field.

Tasks in this project included the design and fabrication of instruments, characterizing the accuracy, precision, resolution and response time of the technology, developing deployment methods, and dealing with the many variables that affect the temperature distribution in these shallow applications. Two versions of the hardware were envisioned. One of these, a 3D probe, would measure the magnitude and direction of the full three dimensional gas flow velocity. The second, a 1D probe, which it was hoped would be less expensive and easier to install, would measure only the magnitude and direction of the vertical component of the gas flow velocity. These probes and deployment schemes were analyzed using mathematical modeling, numerical simulations, laboratory testing, and field demonstrations. A controlled test facility was fabricated in which flow sensors could be exposed to known constant or oscillating air flow rates in homogenous media. Tests were conducted to determine the accuracy and sensitivity of the probes. The results were used in numerical simulations to guide probe modifications, in order to optimize the probe design for different velocity ranges, quicker response time, and easier deployment.

Background

Probe Description and Principle of Operation

Figure 1 shows a photograph of the 1D and 3D probes developed and tested for this project. Both probes operate on the same principle, but the 1D probe only measures the vertical velocity component, while the 3D probe measures the full 3D velocity vector.

The 3D probe is approximately 2" in diameter by 30" long. It contains a cylindrical flexible circuit heater element and an array of 30 temperature sensing thermistors on its surface. The probe is deployed in an augered hole in the ground, which is then backfilled. The heater element is turned on at a low power level (typically 15-20 watts), which heats the nearby soil. The thermistors on the flexible circuit monitor the soil temperature surrounding the probe.

In the absence of any fluid flow past the probe, the temperature distribution around the probe will be independent of azimuth and symmetric about the vertical midpoint of the probe. Any significant fluid flow past the probe will perturb the temperature distribution on the surface of the probe as some of the heat emanating from the heater is advected around the probe by the moving fluid. Relatively cool temperatures will be observed on the upstream side of the probe and relatively warm temperatures on the downstream side. The resulting temperature distribution data is used to compute the magnitude and direction of the air flow. The technique can be used to determine the full 3-dimensional fluid flow velocity vector in permeable media.

The 1-D probe operates in the same manner as the 3D probe, but only monitors the component of the flow along the long axis of the probe. It was felt that this probe could be much smaller, less expensive, and more robust than the 3D probe. It was also hoped that the 1-D probe could be emplaced by driving it into the ground without augering a hole, which would significantly reduce perturbations to the formation and gas flow field. However, it became apparent during the project that neither of the probes could be emplaced without augering holes, so a more robust probe was not needed. In addition, a number of changes were made to the 3D probe which reduced its cost to the point that the probe cost was a fairly small portion of the overall test costs. And the 3D probes provided better data since they had so many redundant channels that if a few channels gave bad data, they could be discarded and the velocities still calculated. Therefore, although the 1D probe was developed and tested, it is not a viable alternative to the 3D probe.

We built several different 1-D probe prototypes. The first one consisted of a metal tube with a nickel-chromium heater wire and a linear thermistor array, both potted inside the tube. This created a very rugged probe, but because there was little control of the relative radial position of the thermistors and the heater wire within the tube, and because there were variable lengths of potted material between a given thermistor and the heater wire and between the thermistor and the probe wall, this design did not produce satisfactory results. We investigated various highly conductive potting compounds including metal filled resins, to decrease this radial thermal

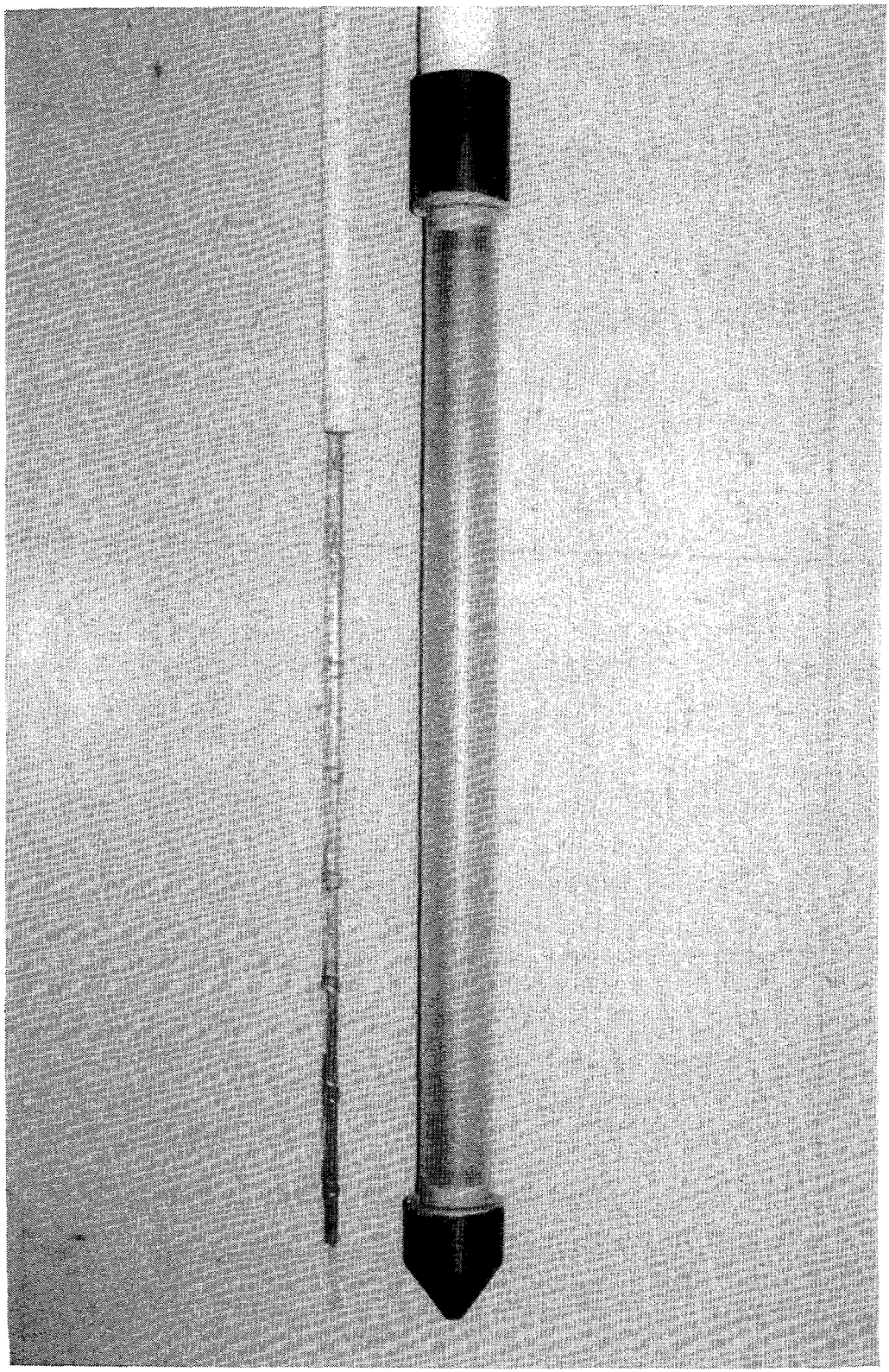

Figure 1: 1-D (left) and 3-D (right) Probes

gradient, and also different probe aspect ratios and construction methods to try to minimize axial heat transfer along the probe, but it was impractical to build a probe with a small enough diameter, long enough length, high radial heat transfer characteristics and low enough axial heat transfer characteristics, and at the same time to keep it rugged enough to be driven into the ground.

The 1D probe which we ended up using consists of a cartridge heater with a linear array of 8 to 11 thermistors attached to the outside of the heater and held in place by heat shrink tubing. This allowed the thermistors to be in close contact with the formation and eliminated the radial temperature gradient problems of the earlier design, but it also made the probe fragile enough that it could not be driven into the ground without first augering a hole.

Probe and Software Modifications

Drawings of the 1-D and 3-D Probes are shown in figures 2 through 6. The 3D gas flow probes were fabricated in a manner similar to the 3D water flow probes. Some modifications were made, which included the following:

Thermistor Spacing:
The original 3D probes used 3" vertical spacing between the rows of thermistors. This kept all of the thermistors well within the heated section of the probe. It was thought that by going to 4" spacing there would be a larger temperature range for the thermistors and hence a larger signal for a given flow. All of the 3D probes used in this test were built with flex circuits using 4" thermistor spacing. We later found that the top and bottom rings of thermistors were so close to the edge of the heater that they did not follow the other thermistors well, and did not match the mathematical model used to analyze the data, so the data from the upper and lower ring of thermistors were routinely discarded before doing data processing. In the future, it would be much better to go back to a closer vertical spacing.

Flush Design:
In the water flow probe [1,2], large machined end-caps were placed on the top and the bottom of the probe, which were considerably larger than the diameter of the heater portion of the probe. These were used to protect the flex circuit from abrasion during installation in the borehole, to help hold the probe in place while the hole was being backfilled, and to ensure a water tight seal at elevated pressures in deep boreholes. These large end-caps were not a problem in installations below the water table, because the saturated formation collapsed fairly uniformly around the probes over a matter of a few hours, sealing the probe in the emplacement hole. However, with dry soil in the vadose zone, the probe emplacement holes do not collapse, and have to be backfilled from the surface. Therefore, it was very important to eliminate these larger diameter pieces so that sand used in backfilling could flow down around the probe. In addition, modeling showed that a large diameter emplacement hole, even though backfilled with sand, presented a highly permeable conduit to vertical flow, and the vertical velocity near the probe was much

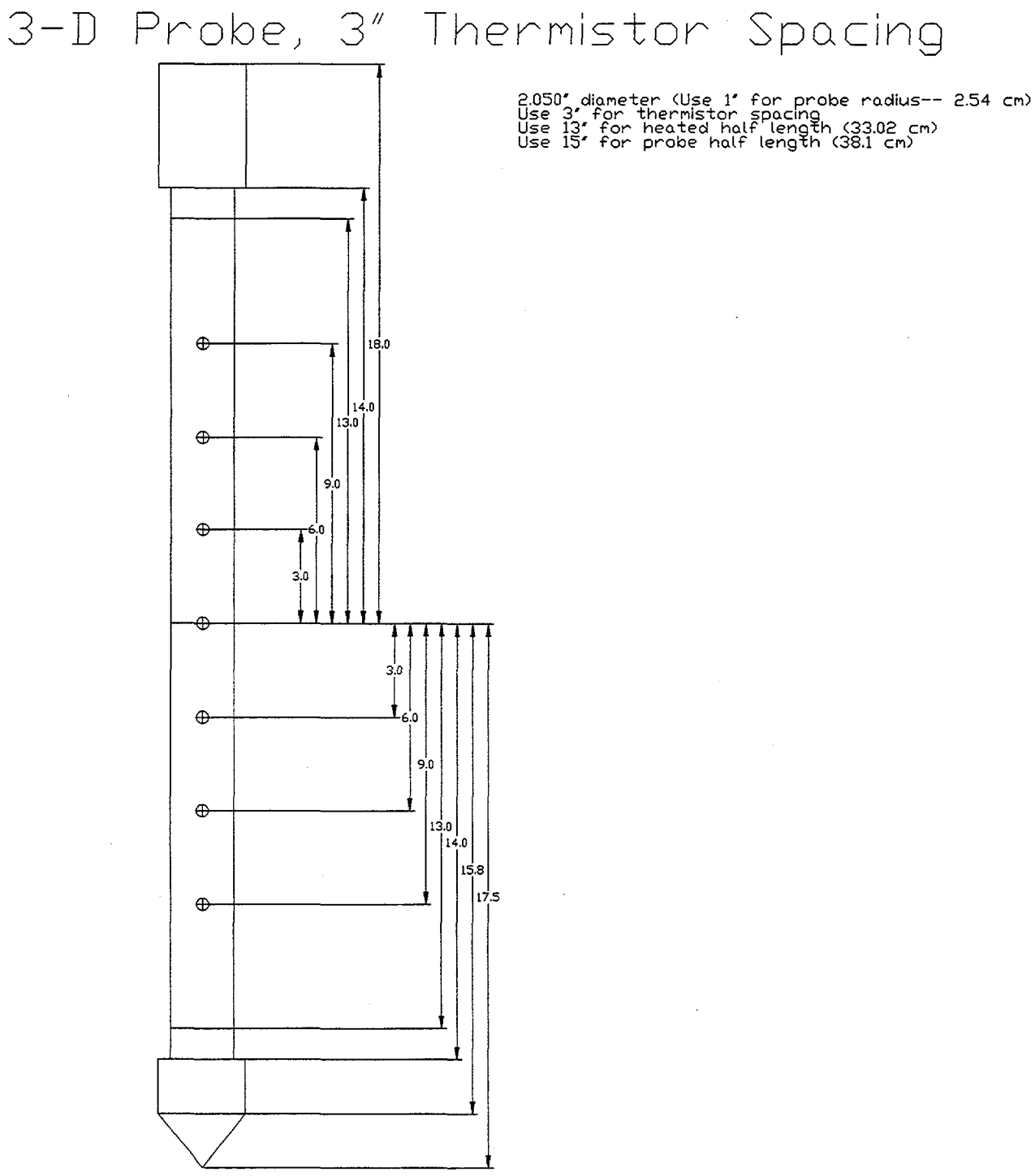

Figure 2: Probe Details—3-D Probe with 3" Thermistor Spacing

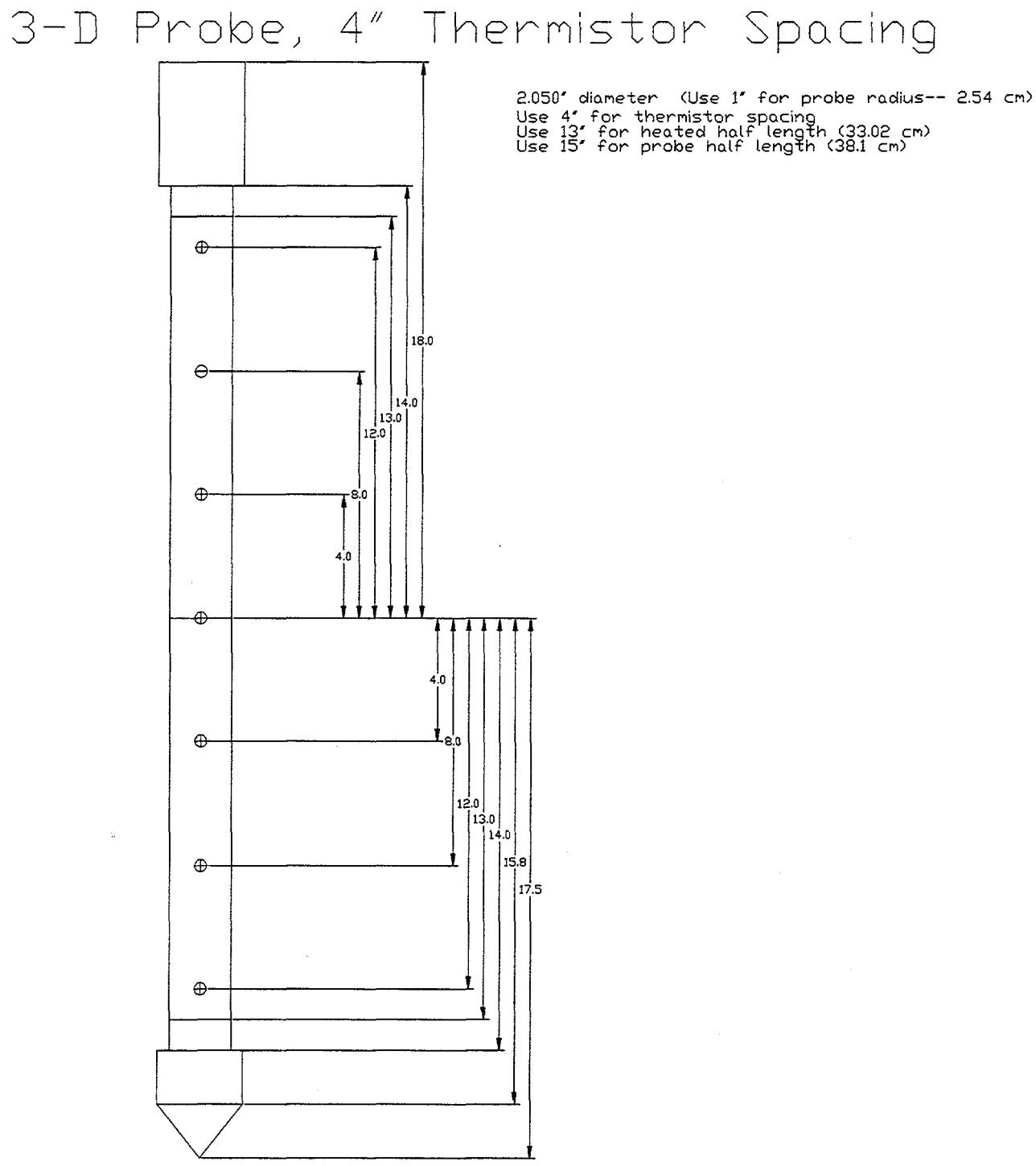

Figure 3: Probe Details—3-D Probe with 4" Thermistor Spacing

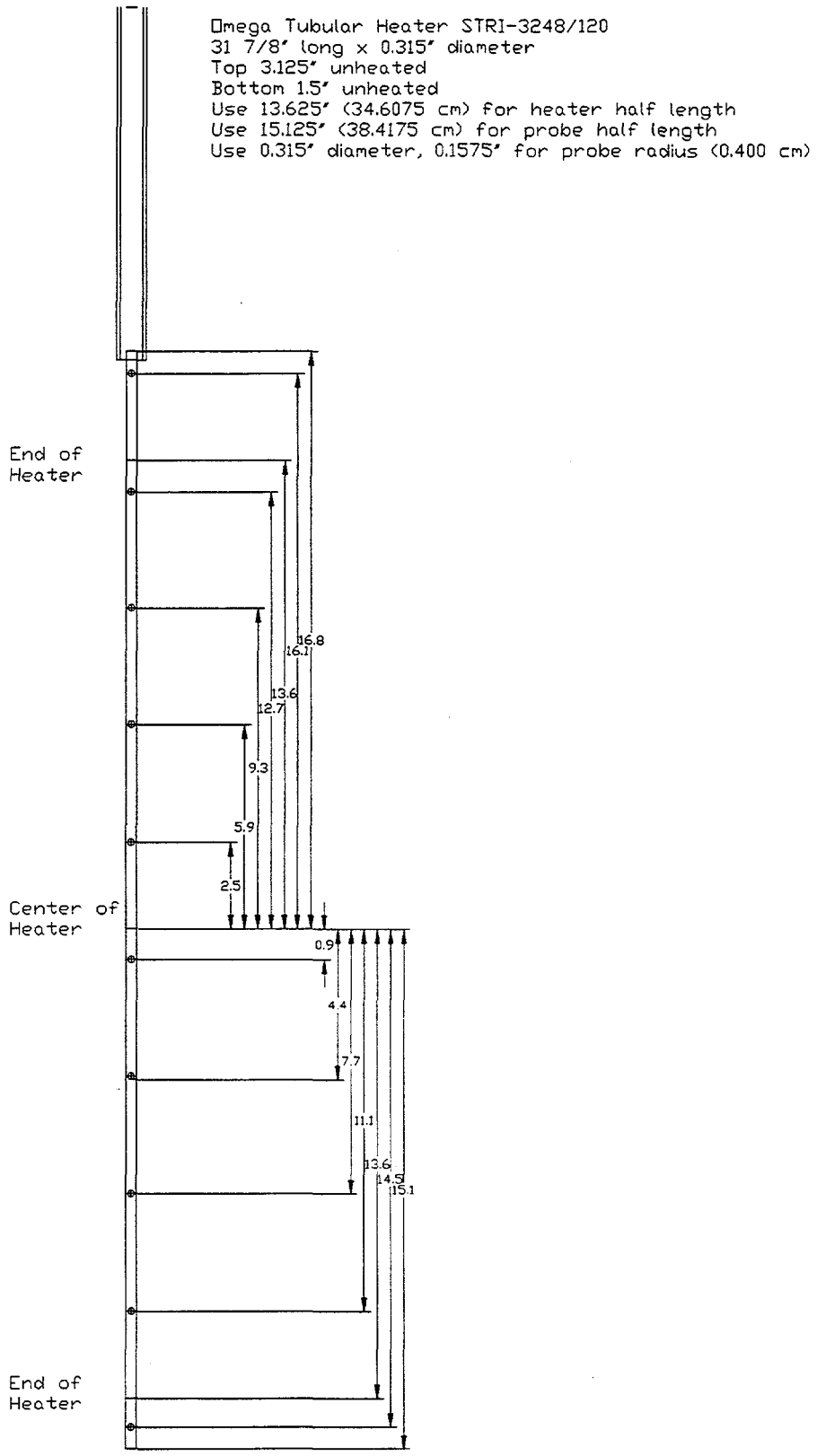

Figure 4: Probe Details—1-D Probe for Barrel Tests

1-D Probe, 4.5" spacing for Tank Tests

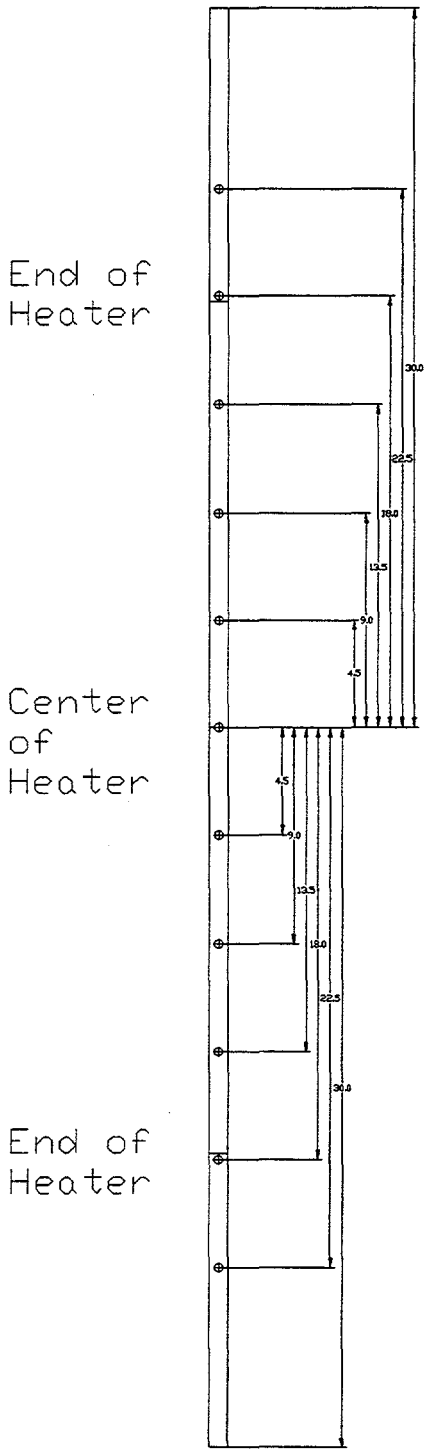

Figure 5: Probe Details—1-D Probe for Tank Tests

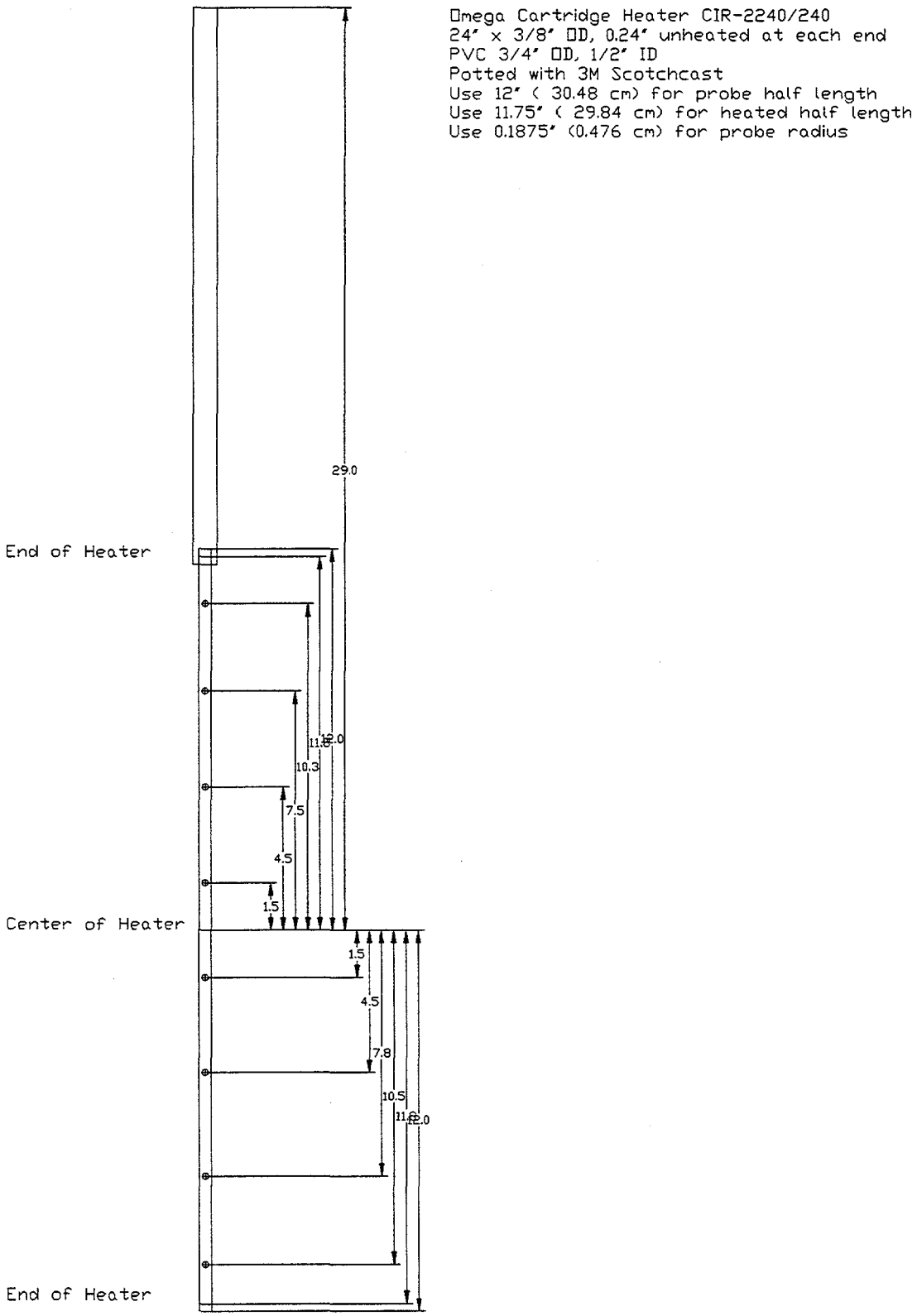

Figure 6: Probe Details—1-D Probe for Chemical Waste Land Fill (CWLF) Tests

different than without a hole present. Therefore, we redesigned the probe to make it flush along its entire length so that an emplacement hole could be drilled which was very close to the diameter of the probe. The machined end caps were replaced with flush potted ends. Oversized couplings and joints on the PVC pipe leading to the surface were also eliminated to keep the entire probe length close to the diameter of the probe body. In practice it proved not to be practical or desirable to try to drill a hole very close to the probe diameter due to the difficulty in back filling around the probe, so we ended up using larger diameter holes anyway.

Multiplexer:

One of the goals of the project was to reduce the cost of the probe compared to the water flow probe. One of the high cost items was long lengths of multi-conductor cables for the thermistors. To eliminate this, a downhole multiplexer was designed and fabricated and potted in place in a short length of PVC pipe a few inches above the top of the probe.

The 3-D flow probe contains 30 thermistors arranged in 6 columns, alternating between columns of seven thermistors and columns of three thermistors. Resistance values for these thermistors are calculated from voltage measurements made across each thermistor. The calculation is based on the voltage divider principle provided the excitation voltage and reference resistor values are known.

The down hole multiplexer was incorporated into the design of the flow probe for two primary reasons: (1) to simplify the installation process when the tool is deployed and (2) reduce the number of conductors required to span the distance between the deployed depth and surface data collection equipment. The second reason is mainly a cost savings, but only at relatively deep depths (> 100'). Physically, the multiplexer consists of two circuit boards ~1"x5" secured with a 1/4" stand-off at each corner using 4-40 hardware. After calibration, the assembly is potted into a 1-1/4" diameter section of PVC attached to the upper portion of the flow probe.

The multiplexer is connected with the surface data acquisition system by 7 conductors: +12V, 12V return, + analog signal, analog ground, clock, reset, and shield. At the input of the multiplexer, the 12V input is filtered and regulated down to 5V which is used by all of the CMOS devices. Current draw on the 12 VDC supply is approximately 6 mA. The heart of the down-hole multiplexer is a 1 x 16 analog multiplexer integrated circuit. This device connects 16 separate analog signals to a single common output channel. By stepping through a clock sequence each channel can be selected and measured. Since the flow probe contains thirty thermistors two of these integrated circuits are needed. The channels are selected using two control lines from the surface data acquisition system - (1) 5V clock line, (2) 5V reset. Initially, the reset line is held high (5V) and a single clock pulse is sent to start the sequence. This action causes the first multiplexer chip (input channels 1-16) to be active. Next, a series of 16 clock pulses are sent with a voltage measurement made on the common output channel between each clock pulse. The seventeenth clock pulse disables the first multiplexer chip and enables the second chip (channels 17-32) at channel 17. A voltage measurement is made on the common output channel and 15 more clock pulses/measurements complete a cycle. Multiplexer chip enabling and channel selection is accomplished by a combination of a 5 stage binary counter and a single "D" type flip-flop. A schematic of the multiplexer is shown in figure 7.

Flow Sensor Multiplexer Schematic

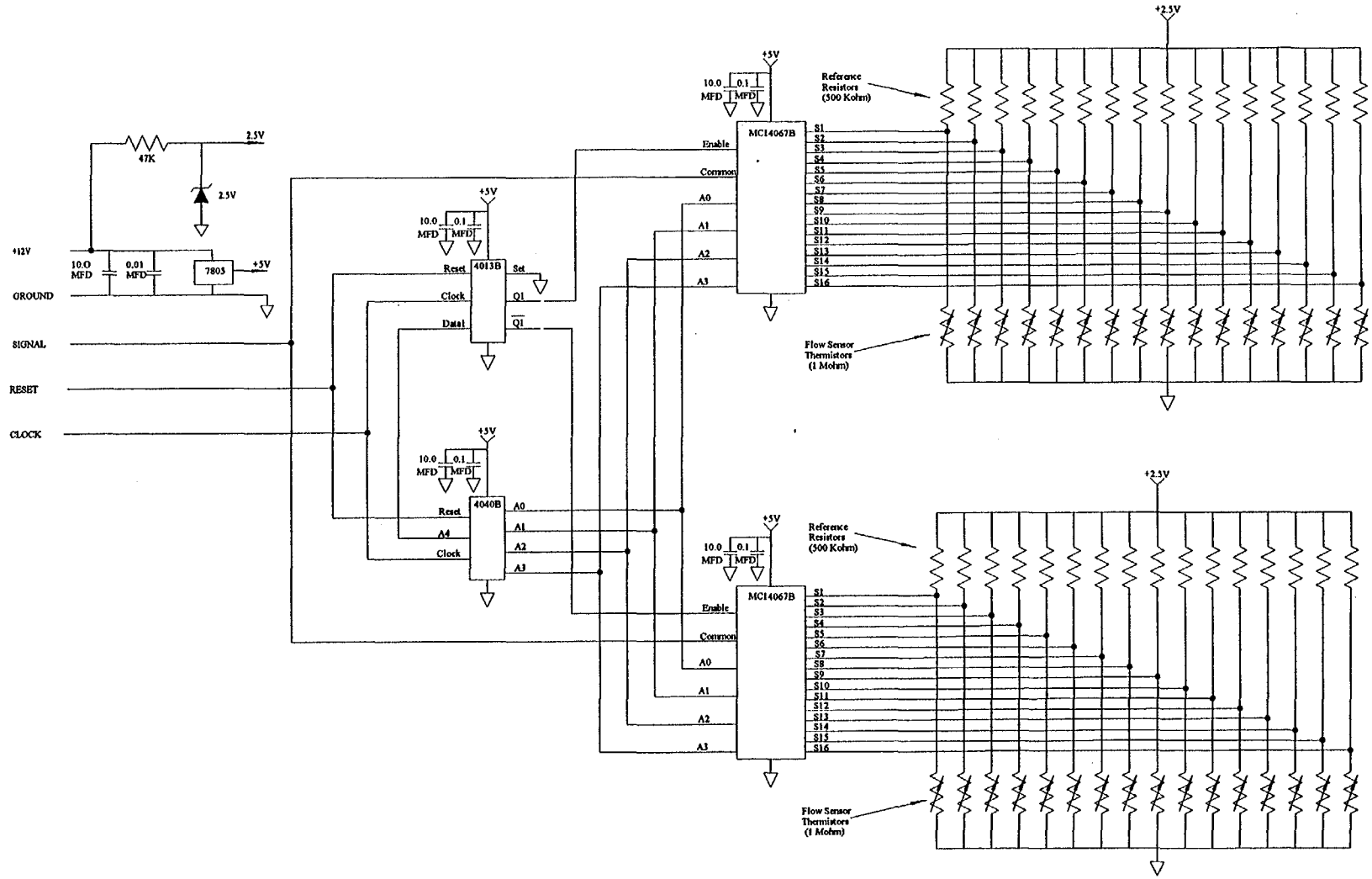

Figure 7: Probe Details—Multiplexer Schematic

Due to the desired accuracy of the voltage measurement, a separate reference resistor was used for each thermistor channel. This eliminates the need to sink the excitation current through the multiplexer itself, which is desirable due to the significant series resistance of the multiplexer and the temperature dependence of this resistance. A cable bundle of 32 conductors connects the thirty thermistors and two thermistor returns (one redundancy) between the solder tabs on the thermistor/heater flex circuit and one end of the appropriate reference resistor on the multiplexer boards. The other end of each reference resistor is connected to a common 2.5 volt precision reference standard mounted on one of the multiplexer boards. The two thermistor returns are connected to the analog multiplexer ground.

Since the multiplexer chips are 16 channels each, and there are only 30 thermistors, there are two available uncommitted data channels. For data integrity purposes, two fixed resistors were connected to these open channels, one fixed resistor was assigned to each multiplexer chip. By knowing the value of each fixed resistor (and their values sufficiently different from one another) two deductions can be made. The first one is confirmation that all 32 channels are getting address - not just the same 16 addressed twice. The second one is that a linear correction can be made to the data based on the measured values for those channels and their known values. This becomes important as the length of down-hole cable gets longer. The longer the cable, the larger the ground potential difference between the surface data acquisition system ground and the down-hole multiplexer ground. The two point linear correction process strips off this effect leaving only the true value obtained from the voltage divider. This ground potential difficulty can be circumvented entirely by making full differential measurements, however this would cause the complexity of the multiplexer to approximately double.

A single supply, unity gain operational amplifier is used to drive the analog signal line to the surface data acquisition system. The use of the buffer amp reduces the loading effect of the datalogger on the signal line and it also reduces the output impedance of the multiplexer making the long length of down-hole cable less susceptible to electrical noise from the underground environment.

Data analysis program:

The data from the laboratory and field tests was analyzed using FLOW, a modified version of the copyrighted Pascal program used to analyze data from the 3-D in-situ water flow probe. The basis for this program is described in references 2 and 3. This software had been written specifically for the 3-D water flow probe with 3" thermistor spacing. For our applications it was modified to use the thermal properties of air rather than water (ρc, which is the density times the specific heat, for water is 1, ρc for air is 3.096×10^{-4} cal/cm^3/°C) , to provide for variable 3-D probe thermistor spacing from 3" to 4", to provide for variable probe geometry (different lengths and diameters for 1-D probes), to calculate velocities for 1-D as well as 3-D probes, and to accommodate the use of fixed resistors on the multiplexer. In addition, for water flow probes, we typically determine and apply correction factors to accommodate erratic behavior during the first few minutes to hours of probe heater turn on. However, the data from the field tests was unusual, in that the erratic behavior continued for nearly two days. We performed a number of tests to determine the effects

of various correction factors. It turned out that the data were much more consistent if no correction factors were used.

Instrument Deployment

The mathematics used to calculate flow velocity from the surface temperature distribution on the probe assumes that the probe is deployed in a medium which is both thermally and hydrologically homogeneous and isotropic. Since these assumptions are grossly violated in a borehole environment, the probes must be buried directly in the soil, in intimate contact with the formation. This is accomplished by drilling a 3" diameter hole in the soil to the desired depth and placing the probe in the hole. The annulus between the probe and the formation is backfilled with material approximating the permeability of the formation, using either the material removed from the hole or sieved sand. However, since this material is un-compacted, it is always more permeable than the formation. Short cement plugs are poured above and below the probe to prevent vertical air flow along the augered hole. The hole is then backfilled to the surface. While this deployment strategy means that the probes cannot be recovered once installed, they can be monitored for extended periods (months to years). Wires from the probe are connected to a data logger on the surface by a multistrand cable inside a 1" PVC pipe. The data acquisition system can be monitored remotely via telephone/modem.

Proof of Concept Test at Hanford, WA:

A preliminary, proof-of-concept test of the gas flow probe idea was conducted at the Hanford Site, WA in 1994 using a water flow probe in the vadose zone. Three boreholes were augered in line with each other to a depth of 5 meters. A water flowmeter was buried 5 meters deep in the center hole. The other two holes had stainless steel casings, with 1 meter screened intervals at a depth of 5 meters. The probe was located 3 meters from one of the wells and 10 meters from the other well. Figure 8 shows a cross-section view of the test set up and details of the vapor extraction well and the probe.

The heater on the flowmeter was activated and the probes were allowed to approach thermal equilibrium for about 20 hours. The heater on the probe, which was operating with a total power output of 20 watts, warmed the soil and air around it by about 30°C (Figure 9). Due to time constraints during this brief proof of concept test, it was not possible to allow the probes to achieve complete temperature equilibrium.

Air was first extracted from the well that was 3 meters from the probe, at a rate 15 liters/sec. This extraction rate was maintained for approximately 22 hours. When the vapor extraction system was activated, the temperature distribution on the surface of the probe changed dramatically, with the difference in temperature between the upstream side and the downstream side of the probe increasing substantially. This change in the temperature distribution reflected a change in the air flow past the probe. The magnitude of the horizontal component increased to about 0.09 cm/s, directed roughly towards the extraction well. The direction of the horizontal component of the

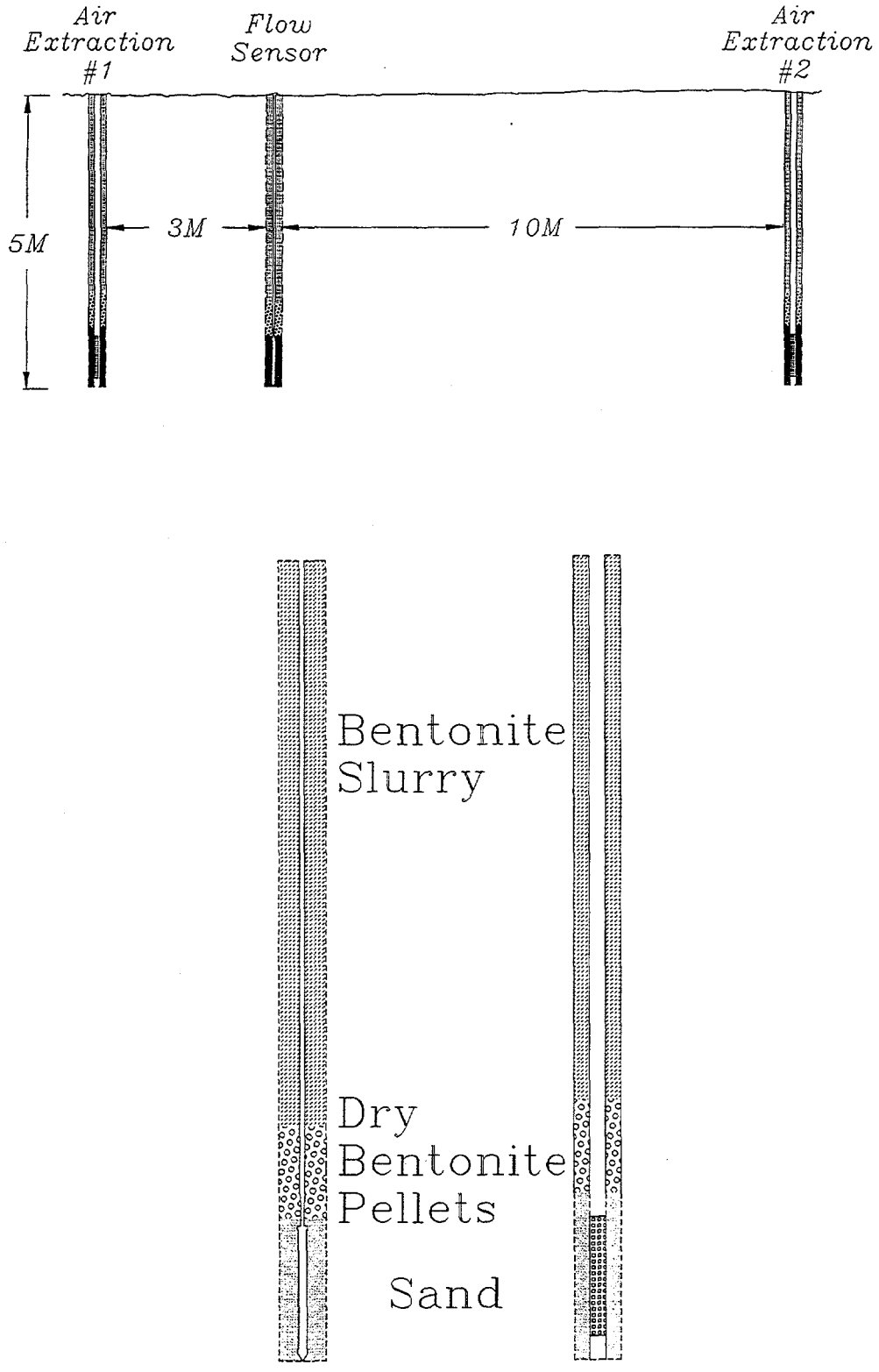

Figure 8: Hanford Test—Cross Section View and Well and Probe Details

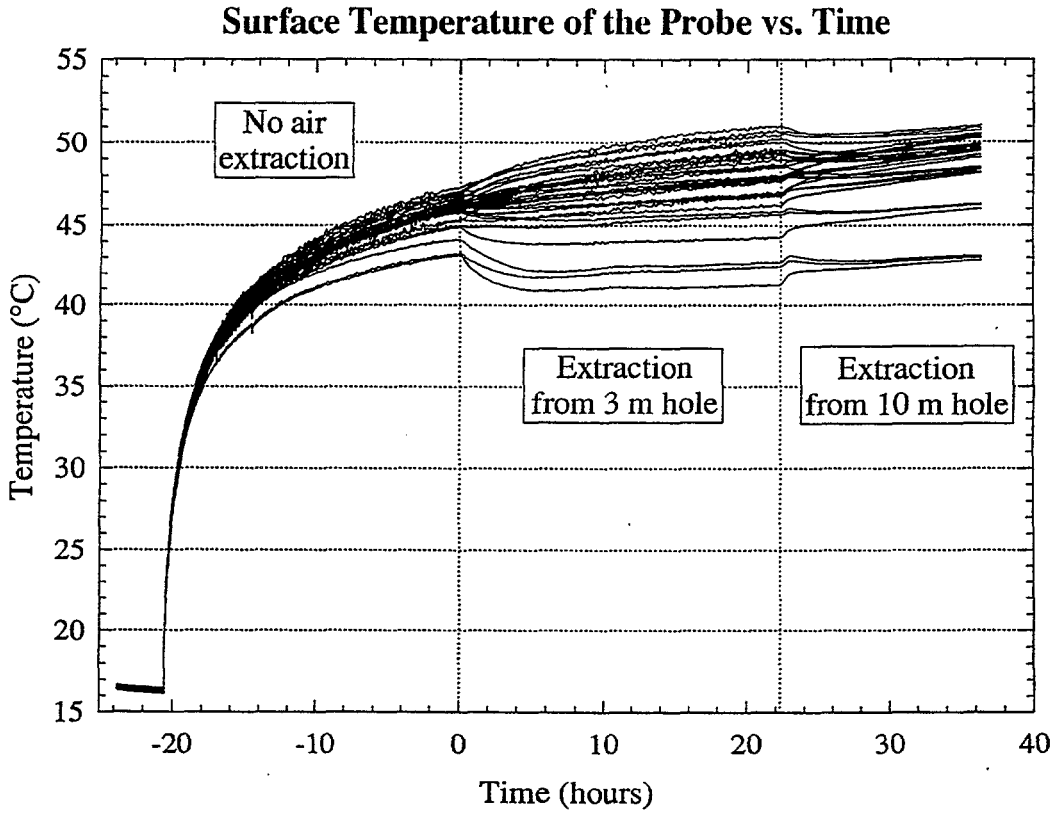

Figure 9: Hanford Test—Surface Temperature of the Probe vs. Time

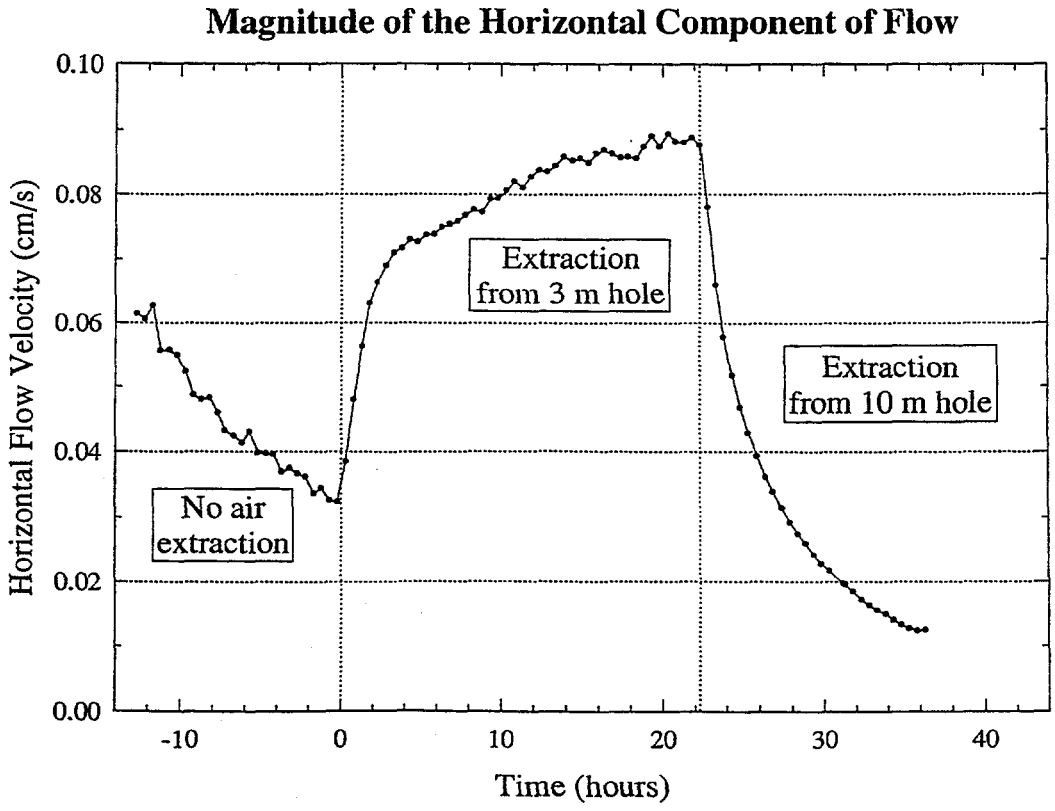

Figure 10: Hanford Test—Magnitude of the Horizontal Component of Flow

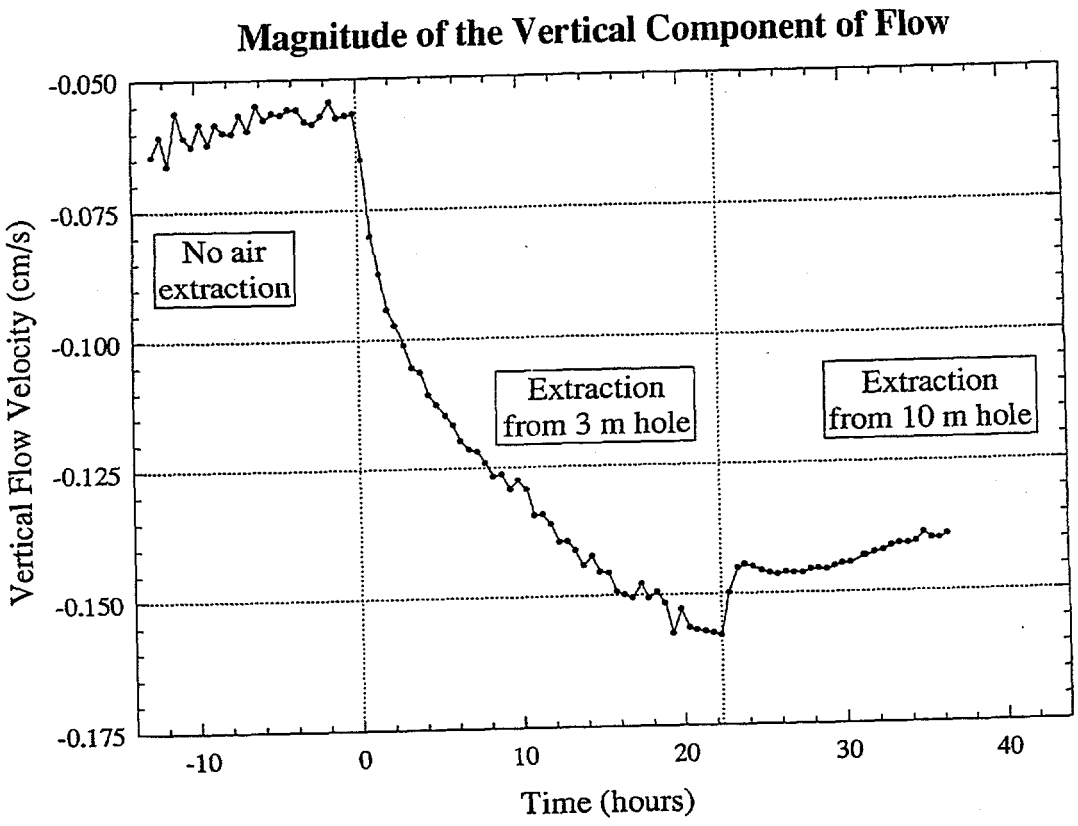

Figure 11: Hanford Test—Magnitude of the Vertical Component of Flow

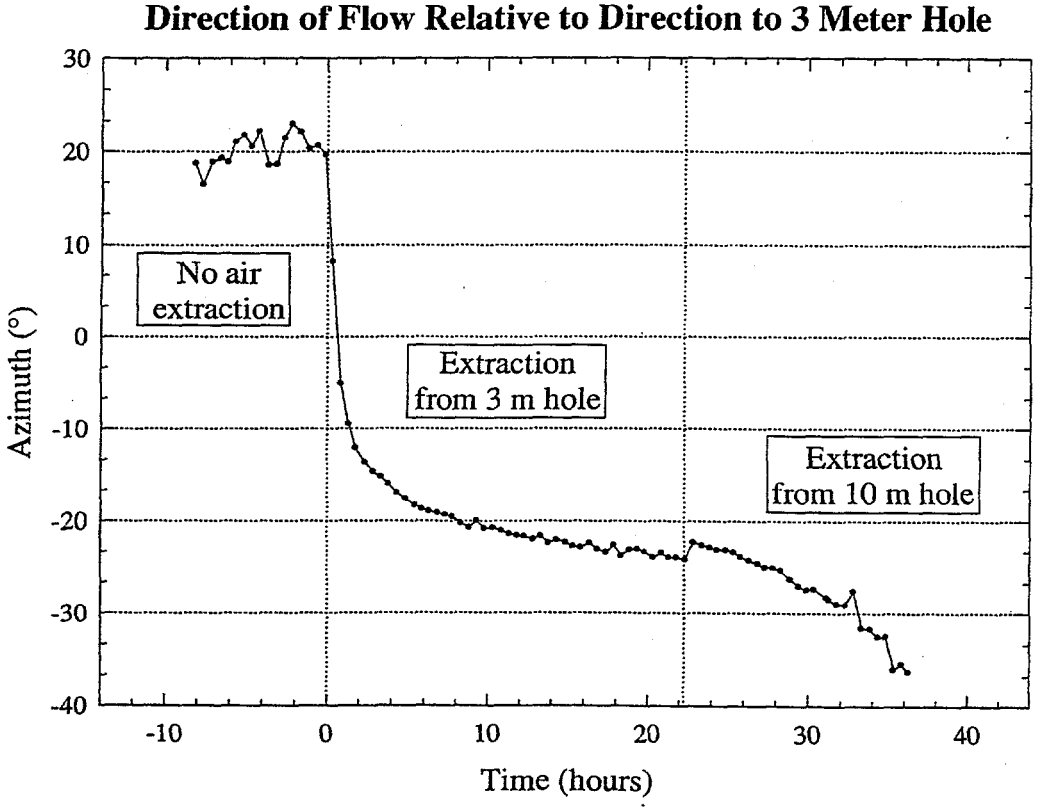

Figure 12: Hanford Test—Direction of Flow Relative to Direction of 3 meter hole

flow velocity was directed within 20° of the direction to the air extraction well. The flow velocity had a vertical component of -0.15 cm/s (negative magnitude indicated downward flow).

The measured flow had not reached equilibrium when the extraction system was moved to the other borehole, which was 10 meters away from the flow sensor and in the opposite direction. The direction of the flow velocity observed by the flow sensor began to change toward that well. The magnitude of the horizontal component decreased abruptly and approached zero. The direction of the horizontal component started to shift toward the 10 meter hole. After the vapor extraction system had operated on the 10 meter hole for about 14 hours, but before the observed flow velocity could equilibrate at the new orientation, the experiment unintentionally ended prematurely due to generator failure.

Figure 9 shows the surface temperature of the probe vs. time. Changes in the temperature distribution around the probe are clearly evident in the raw data at the start of each of the vapor extraction phases. Figure 10 shows the magnitude of the horizontal component of flow, and figure 11 shows the magnitude of the vertical component of flow. There is a large change in the indicated background or no-flow velocity at the time that the vapor extraction system is turned ON. Notice that the velocity had not stabilized before the extraction equipment was moved to the second well. Figure 12 shows the direction of the flow relative to the direction of the 3 meter hole.

This experiment demonstrated that the technology is clearly sensitive to the flow of air through unsaturated porous media.

Challenges

1. The In Situ Permeable Flow Sensor which had been developed for monitoring groundwater flow is sensitive to flow velocities in the range of 1×10^{-5} to 1×10^{-3} cm/s. However, a given volume of air can transport only about 0.001 times as much heat as can the same volume of water, so for a given flow rate the signals the gas flow probe needs to detect will be a thousand times smaller than for the same flow rate in water. This means that the background signals become much more of a problem.
2. There are problems in deploying the probe and insuring it is in intimate contact with the formation.
3. Many of the applications in the vadose zone are very shallow and are affected by daily and seasonal temperature, pressure, and moisture variations and long term trends. This can be corrected for by placement of monitoring instruments at the surface.
4. Another challenge is the relatively long response time of the instrument. During the tests, the actual air flow velocity past the instrument probably achieves equilibrium within a few minutes after activation of the air extraction system. The flow sensors however measure the temperature distribution, which is affected by a large volume of the formation surrounding the probe. Since the air transports so little heat, it can take a number of days for the temperature distribution to reach equilibrium. This indicates that if the flow sensors are exposed to velocity fields which oscillate with a period of a few days or less, such as daily atmospheric pressure oscillations, the measurements will be damped relative to the actual flow.

Modeling

A number of different probe configurations and deployment schemes were numerically modeled to gain insight into how to optimize the probe. These various modeling experiments included the following, which are discussed in more detail in this section:

1. Effects of the presence of an emplacement borehole, size of probe/borehole annulus, and length of borehole between solid plugs, on flow velocity
2. Effect of permeability contrast between backfill material and formation on flow velocity
3. Temperature distribution around probe for various flow velocities
4. Modeling of various probe designs

Channeling, Borehole Annulus, and Backfilling

During initial field tests the probes were placed in an emplacement borehole and the annulus between the probe and the borehole was backfilled with the same coarse 4-9 mesh sand (sand grain sizes between 0.079" and 0.19") that had been used in the laboratory experiments (see Laboratory Testing and Field Tests sections later in this report). It was found that almost all of the flow signal from the probes was vertical, although we had expected predominantly horizontal flow based on the test geometry. We conducted numerical modeling with the integrated finite difference code TOUGH2 [4] to determine the effects of the augered hole used for emplacing the probe on the overall flow field. The model used a cylindrically symmetric variable density mesh that could be adjusted to be fine near the probe and coarser further away. A generic model was constructed which assumed air flow at an angle of 45° relative to the probe axis. The bulk flow velocity could be varied, and the resulting horizontal and vertical velocity of the air flow in each cell of the model could be calculated and displayed.

When it became apparent from the borehole annulus modeling that the presence of the borehole annulus and the permeability of the backfill had a major effect on the flow field, we decided to model various configurations that might minimize this problem in actual deployments. The initial model was modified to allow different permeability contrasts between the formation and the backfill and to change the diameter and effective height of the augered hole. We modeled variations of the annulus between the probe and the formation from 0.05" to 6" to see if minimizing the annulus would minimize the disturbance in the flow field. We modeled an overall backfill height between the cement plugs (which are placed above and below the probe) of 1 meter and 5 meters. And we modeled the effect of replacing the 4-9 mesh sand used for backfilling with very fine sand that came closer to matching the permeability of the model "formation". We applied the results of these simulations to further tests in the lab and in our field deployments.

Figure 13 shows the model results for:

a) The condition where there is no borehole. While there are more arrows in the center where the grid is finest, there is no net change in the flow vectors at the location of the probe.
b) The condition of a 15 cm diameter by 1 meter high column of coarse sand placed around the probe, representing a typical 6" diameter augered hole for emplacing the probe, with as short a sand column between plugs as practical. As can be seen by comparing to the previous figure, there is a distortion of the flow field right at the probe due to the presence of the sand column, which increases the vertical flow. In figures 13 b,c, and d there is a permeability contrast ratio between the "formation" and the sand column of 100:1.
c) A close-up of the area immediately surrounding the probe. It is apparent from this figure that the probe will read an incorrect velocity due to the emplacement method.
d) The condition of a 15 cm diameter by 5 meter sand column placed around the probe. As can be seen, with this wider spacing between cement plugs, the distortion in the vertical flow is greatly increased.

Figure 14 compares the effect of no sand column, a short 1 meter sand column, and a long 5 meter sand column on the horizontal and vertical components of the flow. As can be seen, the horizontal component changes by a factor of 2 to 3 times due to the presence of the borehole, while the vertical component changes by a factor of 25 to 100 times, compared to the undisturbed flow with no borehole present.

Since the modeling showed that a probe emplacement hole distorts the flow field near the probe, we conducted further modeling to determine whether minimizing the annulus between the probe and the borehole would help to reduce this distortion, and also whether backfilling the hole with a material approaching the permeability of the undisturbed soil would minimize this distortion. Figure 15 shows the effect of varying the borehole/probe annulus and of varying the permeability ratios between the backfill material and the undisturbed formation on the flow velocity in terms of the horizontal and vertical components. As can be seen, there is a very steep gradient for any annulus less than 10-20 mm. Beyond that, the gradient is fairly flat. This means that rather than trying to drill a hole exactly the diameter of the probe, that we should drill one at least 20-40 mm oversize on the diameter. In other words, since it is impractical to auger a hole exactly the same size as the probe, it is better to use a larger hole (which allows backfilling uniformly with a fine material), since the affect of a larger annulus on the measured flow is more predictable than that of a smaller annulus.

Another thing that these plots show is that for permeability ratios where the backfill material is less permeable than the formation, there is little distortion of the flow field. And for permeability ratios where the backfill material is more permeable than the formation, as long as that ratio is less than 10, the change in the magnitude of the calculated velocity is less than a factor of 2-3. Therefore, we decided to measure the grain size of the material removed from the emplacement hole and use that to try to select a backfill material which would come as close as possible to matching the permeability of the undisturbed formation. One should be conservative in estimating the backfill permeability. It is better to err on the side of making the backfill less permeable, rather than more permeable than the surrounding formation.

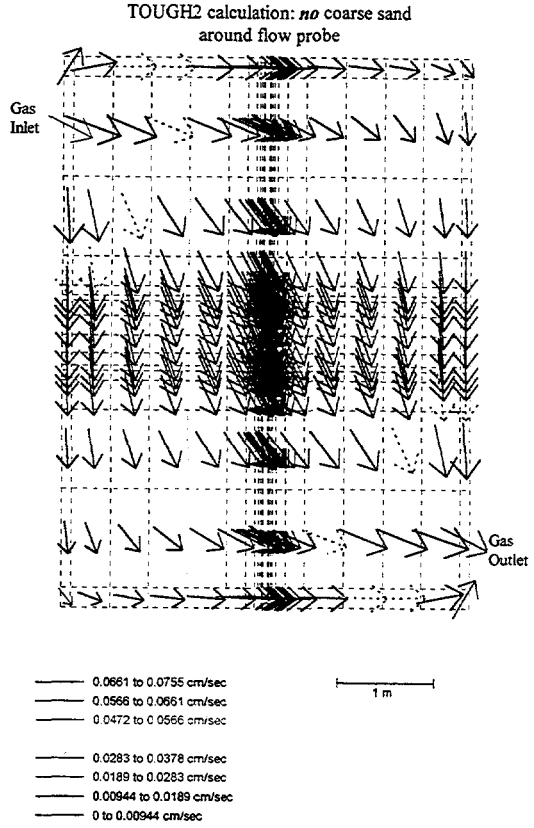

a) no borehole

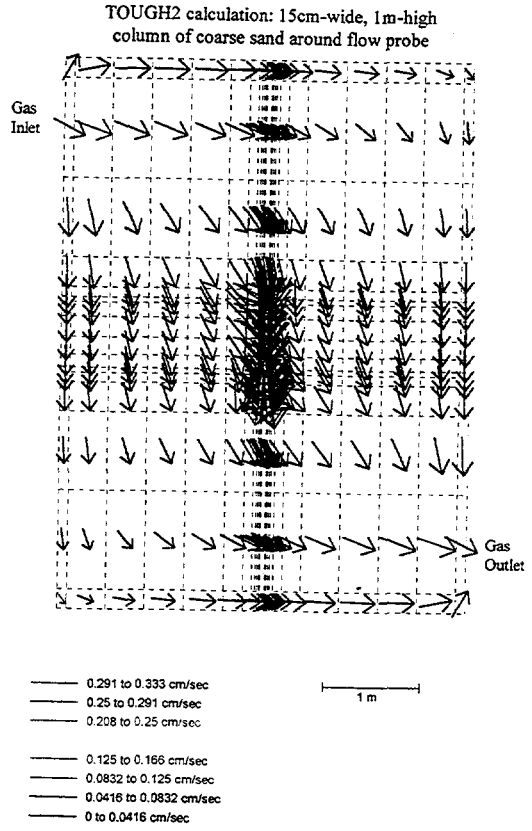

b) 15 cm x 1 m sand backfill

c) 15 cm x 1 m sand backfill (close-up)

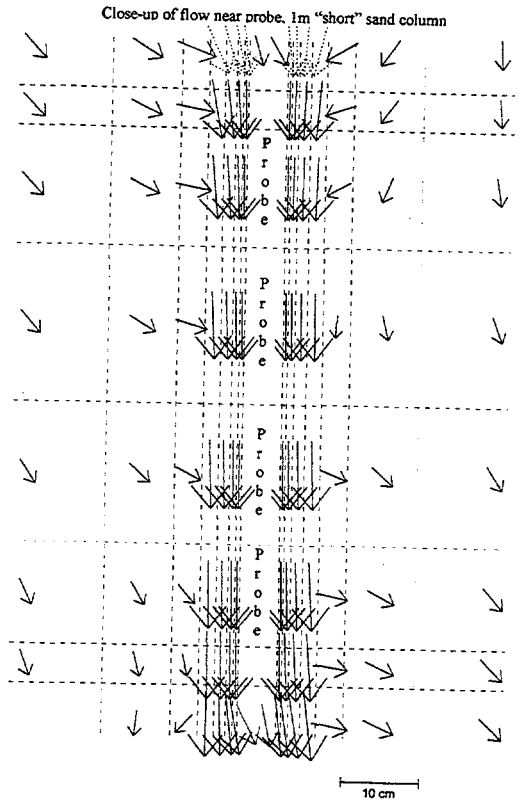

d) 15 cm x 5 m sand backfill

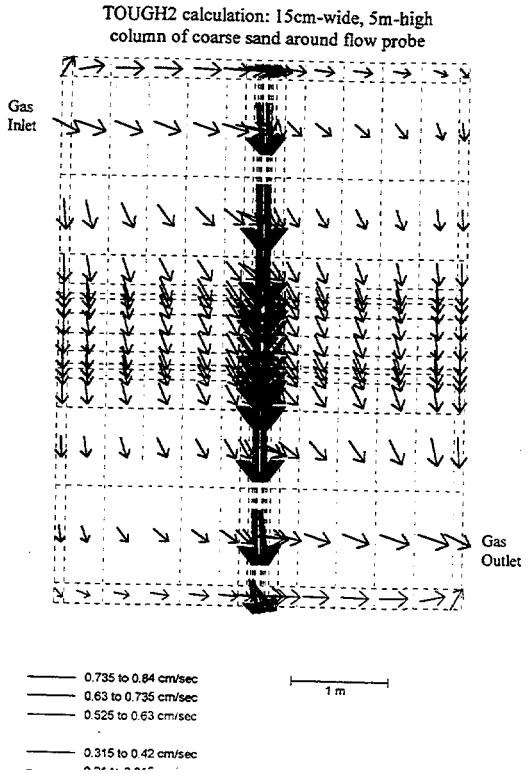

Figure 13: Model Results for Probe with a) no borehole b) 15 cm x 1 m sand backfill c) 15 cm x 1 m sand backfill (close-up) d) 15 cm x 5 m sand backfill (Note—The original plots were color coded and the legend shown corresponds to the flow velocity indicated by each arrow. However, the trends in the flow can be seen in these black and white copies)

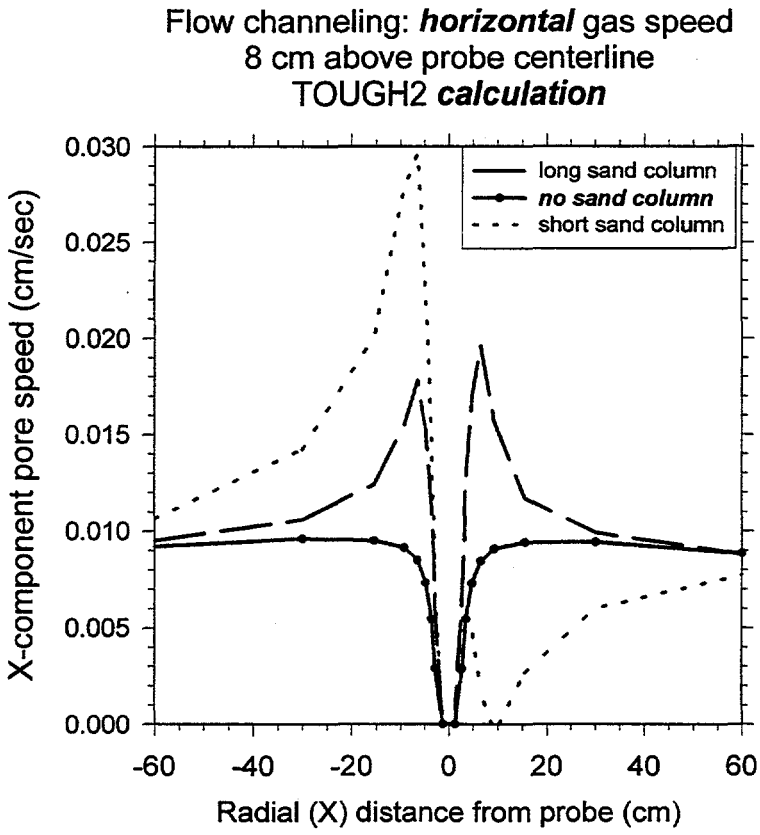

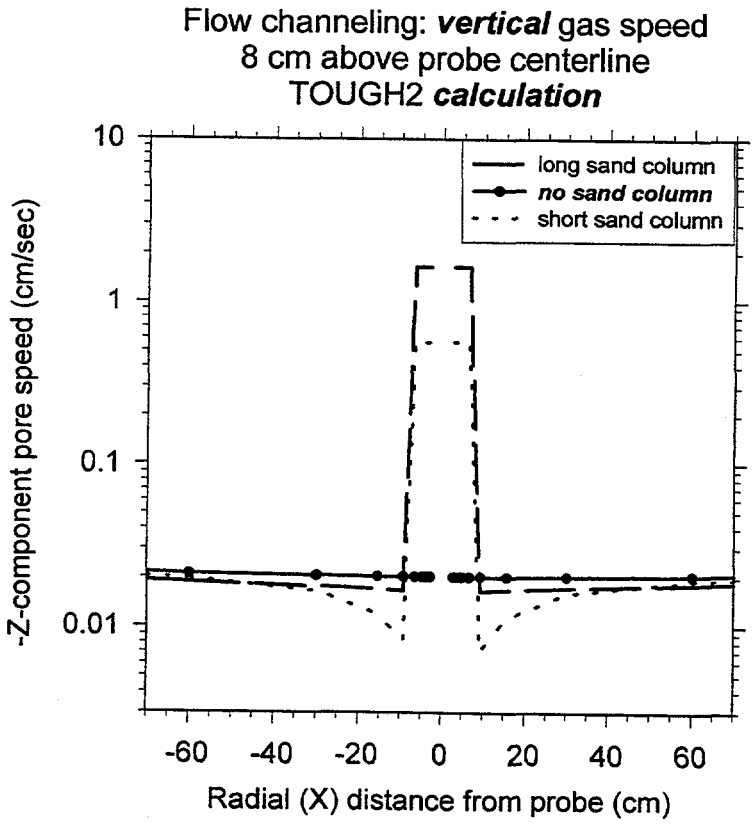

Figure 14: Model Results—Effect of Flow Channeling on a) Horizontal Gas Speed, b) Vertical Gas Speed

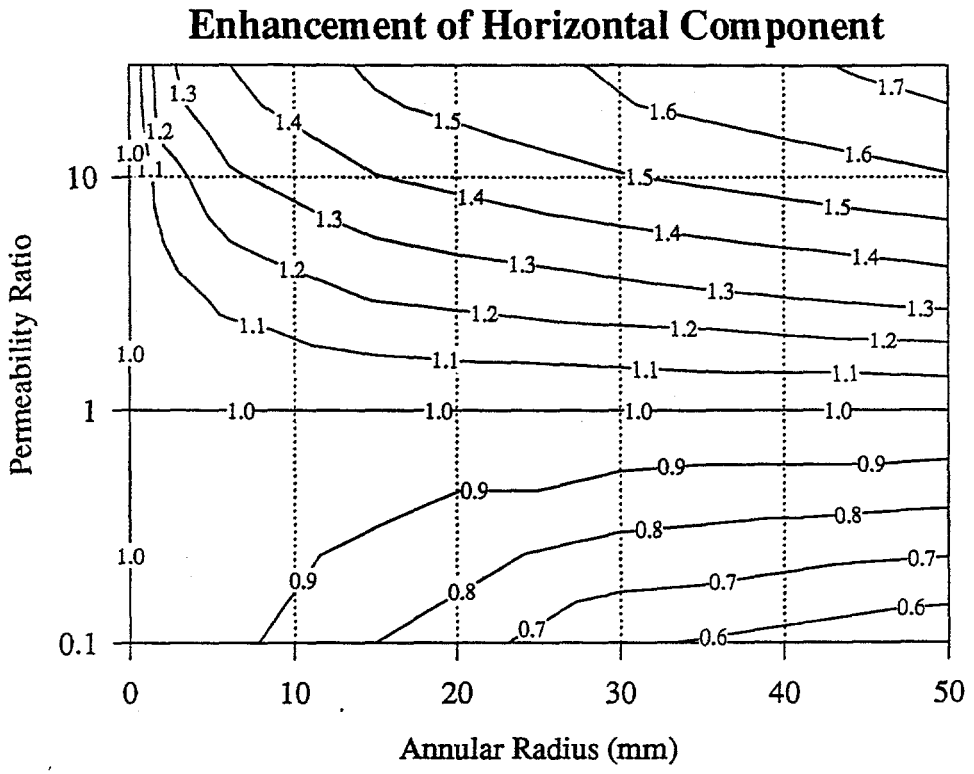

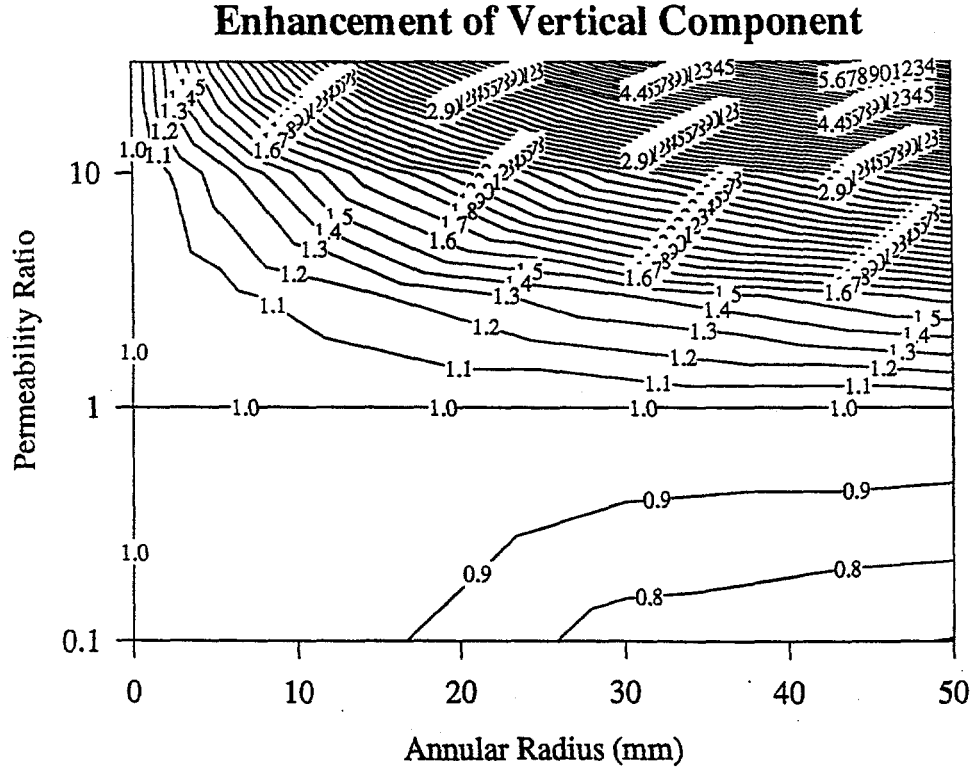

Figure 15: Model Results--Enhancement of a) Horizontal Component of Flow, b) Vertical Component of Flow

Temperature Distribution

The analysis software that is used to process temperature data from the flow probes is based on an analytical mathematical model which relates the temperature distribution on the surface of a finite length heated cylinder to the thermal properties of the porous medium surrounding the cylinder and the fluid flow velocity past the cylinder [3]. As a check that the data processing software and the mathematical model upon which it is based yield results consistent with the numerical model, the computed temperature distribution from a numerical simulation was input into the data processing software and the velocity and medium thermal properties calculated and compared to the thermal properties and velocities used in the numerical simulations. The two compared very favorably. The thermal properties agreed to within 15% and the velocities within 30%. The results for one set of operating conditions are shown in figure 16.

Additional Modeling Needed

Following the field tests which we conducted, and seeing the discrepancies between the laboratory data we obtained and the field test data, we feel that a major factor that was not modeled but which should be in the future was the effect of varying water content of the formation and of the air near the probe, due to rainfall, heating and drying of the soil by the probe, water used while emplacing the probe, etc.

Modeling of Various Probe Designs

The 3D probe relies on all of the heat being generated at the surface of the probe, with no appreciable heat transfer through the interior of the probe. This is accomplished by making the outer skin of the probe a thin flex circuit heater, and the interior of the probe a low thermal conductivity closed cell foam. This gives the probe excellent thermal properties, but makes the probe fairly fragile. One of the goals of the project was to make the probe much more robust, to the point that it could be driven into the ground with a hammer or cone penetrometer, rather than having to auger holes. This required a metal outer sheath for the probe, putting the heater and the thermistors together inside the metal sheath (i.e. not in direct contact with the formation), and eliminating the foam. This led to temperature gradients within the probe and between the thermistors and the formation, and also appreciable heat flow along the length of the probe. Modeling was conducted to determine if the wall could be made thin enough, the internal probe potting thermally conductive enough, and the thermistor locations within the probe accurate enough to overcome these problems. We considered filling the probe with powdered metal or metal filled pastes, making the probe wall extremely thin to minimize axial heat flow, etc. As it turned out, none of these concepts proved practical.

While reviewing the mathematical modeling of the flow probe, it was proposed that an instrument could be fabricated which used fundamentally different mathematics to determine the flow velocity and to also determine various formation thermal properties. The present probe relies on a uniform, steady state heat flux from a finite length cylinder, with the temperature sensing being

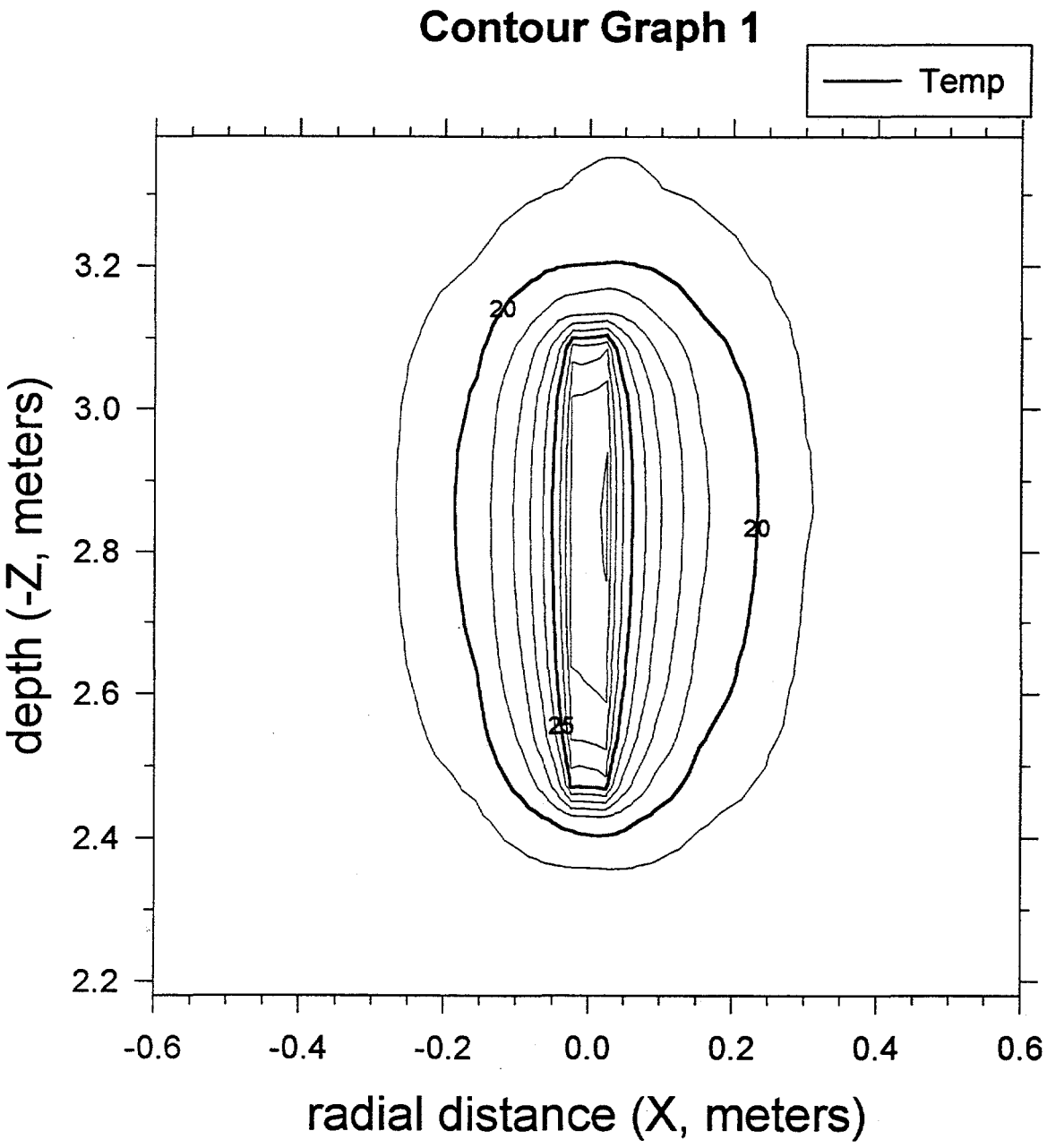

Figure 16: Model Results—Temperature Contour vs. Distance from Probe

done within the heated length of the cylinder. The new proposal was to fabricate a point source heater, to oscillate the heat output from the heater in a sinusoidal manner, and to monitor the temperature at various distances outside of the heater area. The temperature distribution on the upstream side of the heater and on the downstream side of the heater would match different mathematical curves. In addition, by observing the phase shift of the fluctuating temperature as a function of distance from the heater, one could determine formation thermal properties. A brief write-up of the modeling for these two ideas is included in Appendix A: "The Temperature Distribution Outside the Heated Section" and in Appendix B: "An Analysis of a Groundwater Probe with a Core of Highly Conducting Material". Some preliminary laboratory test data was collected using this concept and is included in Appendix C.

Laboratory Testing

A number of laboratory tests were conducted using the 1-D and 3-D probes under controlled, uniform flow conditions in homogenous media in order to determine the sensitivity and accuracy of the probes. We compared velocities calculated by the analysis software using the probe data to the known flow rates

Two similar test stands were constructed, one slightly larger than the other and with a different air flow capacity. Figure 17 shows the two test barrels, the inlet air manifold, and the coarse sand used in the test. Each test fixture consists of a large barrel (one 36" diameter by 7' tall, the other 22" diameter by 6' tall). The bottom of the barrel is closed, and the top is open to the room air. The bottom, sides and top of the barrel are insulated with approximately 3" of fiberglass insulation.

An air distribution manifold was fabricated of PVC pipe with numerous holes for air flow. The manifold was placed in the bottom of the barrel, and was connected to a building compressed air supply. A mass flow controller in the air supply line was used to set the desired volumetric flow rate. We had mass flow controllers that covered the range from 0.01 liter/minute to 200 liters per minute. For the smaller barrel geometry, 1 standard liter per minute (SLM) equals 0.0069 cm/sec air velocity past the probe. For the larger barrel, 1 SLM equals 0.00257 cm/sec air velocity past the probe.

The barrel was then filled with clean dry sieved 4-9 mesh sand. The coarse, uniform dry sand and the large manifold nearly covering the bottom of the barrel were used to produce a uniform vertical air flow field. A flow probe was buried in the sand either vertically (for axial flow experiments) or at a known angle (for cross flow experiments). The thermal conductivity of the sand in the barrel was measured using a thermal conductivity probe, and was found to be 0.00069 cal/sec °C cm.

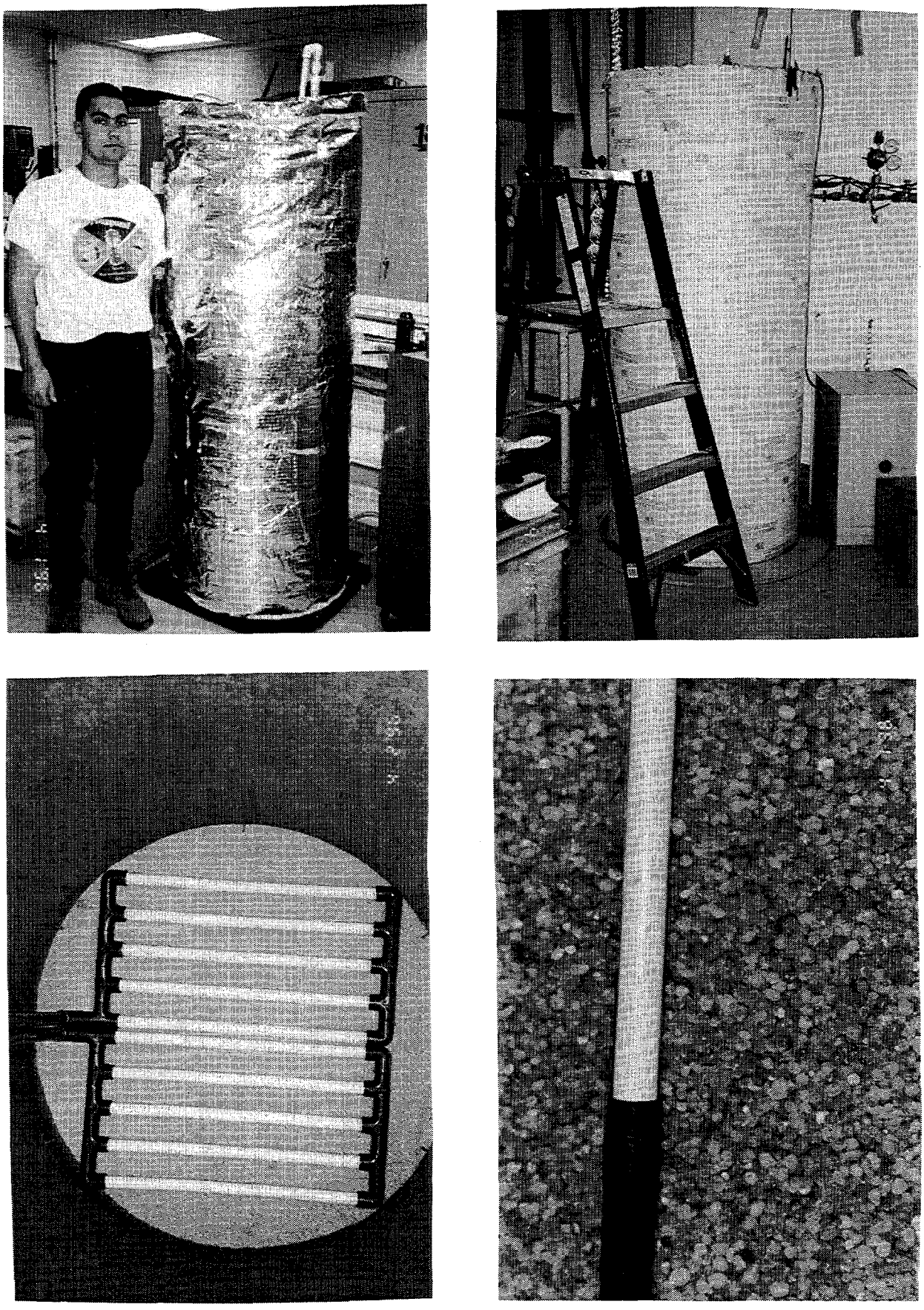

Figure 17: Laboratory test set-up a) Small test barrel b) Large test barrel c) Inlet air manifold d) Coarse 4-9 mesh sand in barrel
(Note: Object in photo d is a ball point pen for size comparison)

The heater circuit in the probe was attached to a regulated DC power supply. The thermistors in the probe were attached to a data logger, which in turn was connected to a PC to continuously record the temperature of the 10 to 30 thermistors on the probe. The thermistors on the probe can resolve temperature differences of approximately 0.01 °C, and are accurate to ~0.1 °C. The data logger also recorded the volumetric air flow through the mass flow controller, and additional thermistors on the wall of the test barrel.

The barrel, sand, and probe were allowed to reach thermal equilibrium with the room air. The heater on the probe was then turned on to an appropriate power level (typically 10-15 watts) by means of a controlled power supply. After the probe had heated to a steady state temperature (typically 3-5 days), the air flow was turned on at a fixed level through the mass flow controller. The probe thermistor readings were continuously recorded, and when they reached a steady state value the flow rate was set to a different level.

A number of tests were conducted on the 1-D and 3-D probes at various flow rates using this set-up. We conducted tests with the probes oriented parallel to the air flow. We conducted a test with the 3-D probe oriented at 30° to the air flow. We also filled an annulus around a 3D probe with a finer sand than the coarse sand in the barrel to investigate the effects of a permeability contrast between the backfill material and the formation on the probe response. Each of these tests are discussed below.

Test #1: 1D Probe in vertical flow field

The 1D probe was fabricated using a commercial cartridge heater, 31 7/8" long by 0.315" diameter, with thermistors arranged along the length of it and held in place with a layer of heat shrink tubing. Since the 1D probe can only sense vertical flow, not horizontal or azimuth, all of the tests of the 1D probe were done with the probe oriented vertically in the test fixture and with the flow directed vertically upwards from the bottom of the barrel.

Sequence of Events:

Julian Day	Date	Time	Event
64	3/4/96	10:30 a.m.	Heater ON at 10 watts
73	3/13/96		Flow set to 10 Standard Liters per Minute (SLM)
81	3/21/96		Flow set to 5 SLM
85	3/25/96		Flow set to 1 SLM
128	5/7/96		Flow set to 50 SLM
138	5/17/96		Flow set to 20 SLM
145	5/23/96		Flow set to 0.5 SLM
152	5/31/96	4:20 p.m.	Flow set to 0.25 SLM
158	6/6/96	4:30 p.m.	Turned heater off

Figure 18a shows sample raw data from the 1D probe for a period of 35 days. Figure 18b shows the same data but with the initial reading of all thermistors before flow turn on forced to zero, and

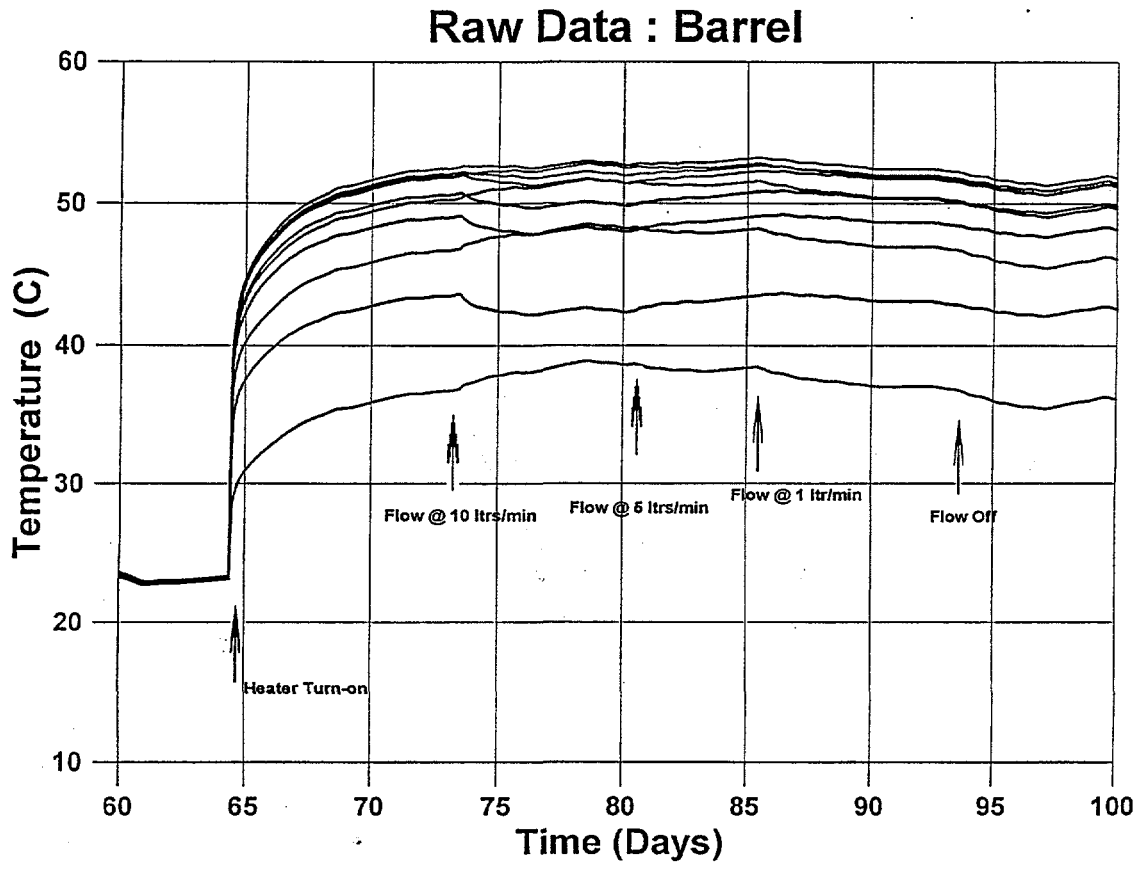

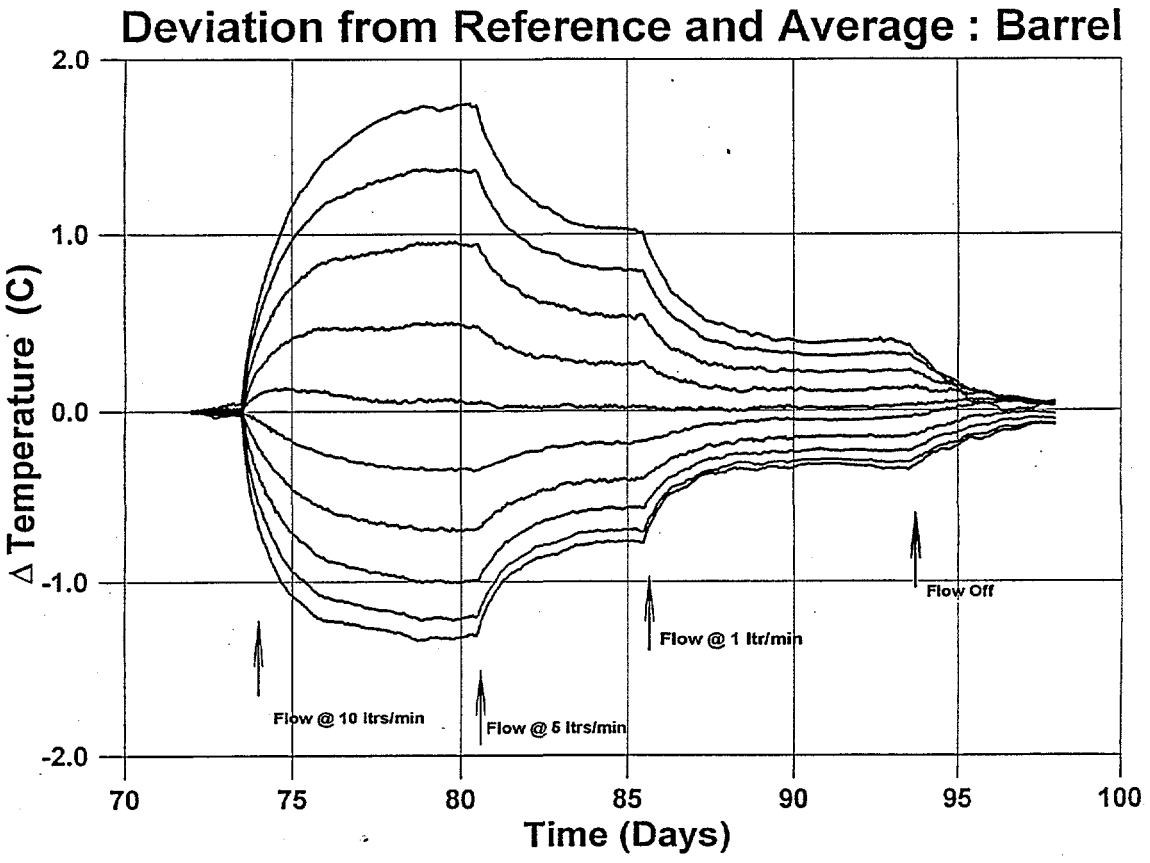

Figure 18: **Laboratory test of 1-D Probe a) Raw Data, b) Deviation from Reference and Average**

then looking at the deviation from this reference value and from the trace by trace average. This helps one to visualize the events in the data, but is not used by the data processing program to calculate velocities. The various flow rate steps can clearly be seen in this figure. The top thermistor is relatively warm and the bottom thermistor is relatively cool as the heat emanating from the tool is advected upward by the upwardly flowing air.

Figure 19 shows the corresponding calculated velocity for these various flow rates, and also shows the known air flow velocity as determined from the mass flow controller. As can be seen, there is excellent agreement between the velocities measured by the flow probe in the barrel and the known flow rates from the mass flow controller. It can also be seen that there is a 5-7 day settling time required before the probe reaches a steady state reading. A wide range of flow rates were tested. Figure 19 shows approximately 3 months worth of calculated and measured velocity data for the 1D probe. Figure 20a shows a plot of the air velocity measured by the probe vs. the known velocity, as measured by the mass flow controller. Figure 20b shows the probe temperature profile as it changed for 5 different flow rates.

Test #2: 3D Probe oriented 30 degrees off vertical in vertical flow field

In this test series the 3D probe was placed in the large test barrel at an angle of 30 degrees from vertical, in a vertical flow field. The purpose of this test was to determine how well the probe could resolve the flow direction. Figure 21 shows the orientation of the probe in the test barrel.

We also monitored the differential pressure between the bottom and top of the barrel of sand for various flow rates. We used the pressure differential and the flow rate to determine the permeability of the sand in the laboratory test barrel for modeling purposes.

Flow (SLM)	Differential Pressure (psi)
25	.0086
50	.0288
60	.048
70	.0736
80	.0832
90	.096
100	.1152

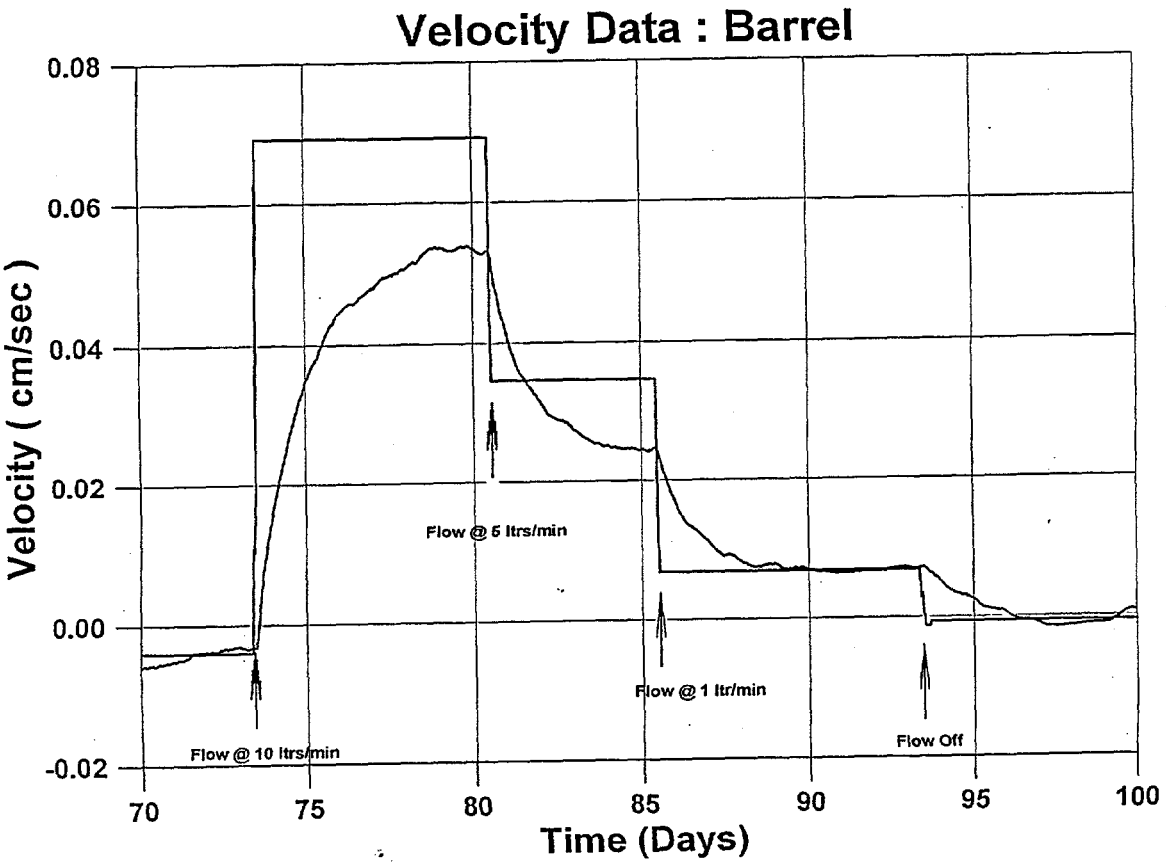

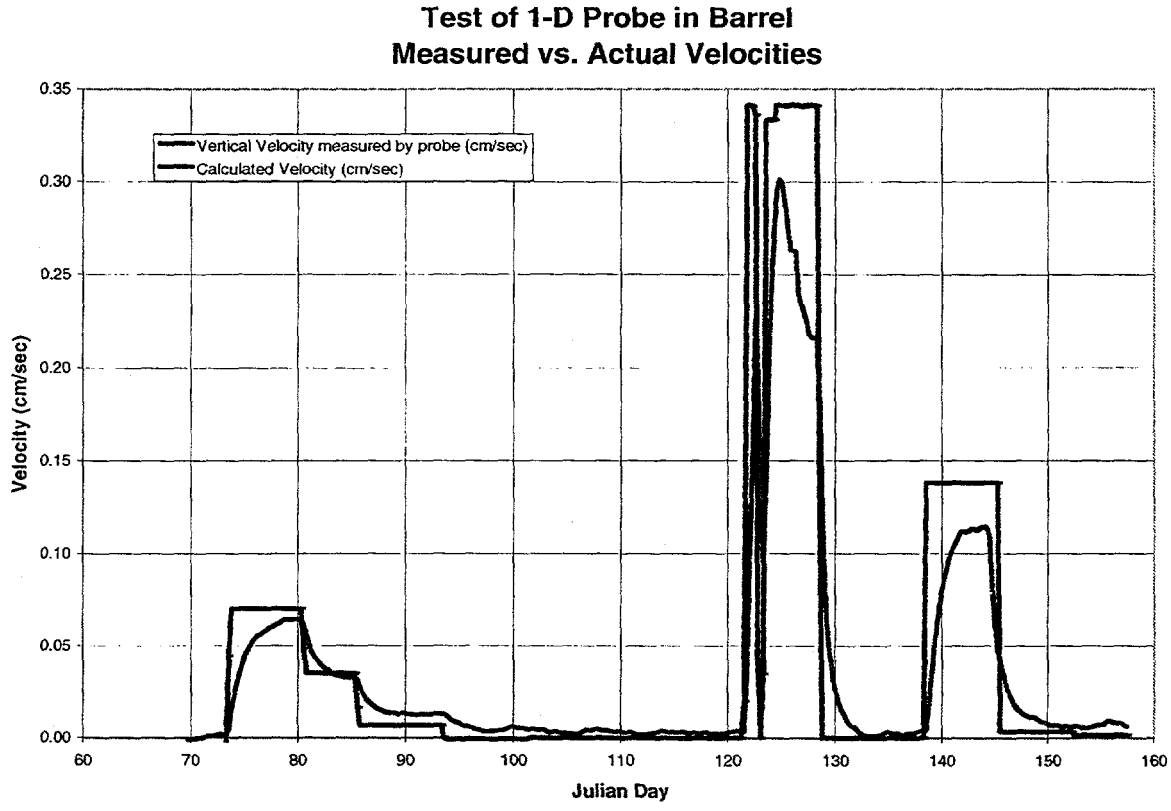

Figure 19: **Laboratory test of 1-D Probe a) Measured vs. Actual Velocity b) Additional Measured vs. Actual Velocity Data**

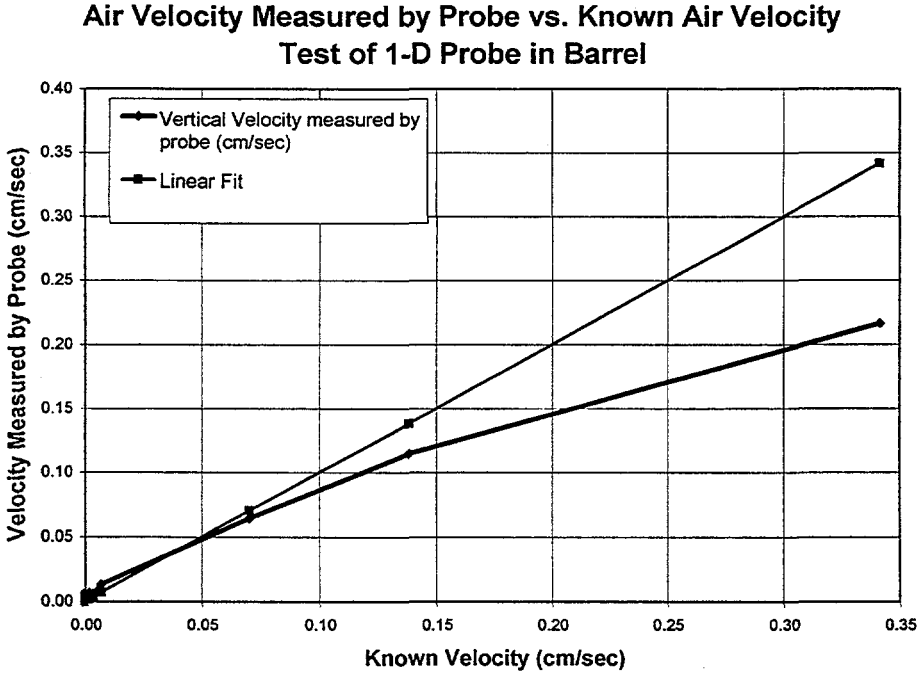

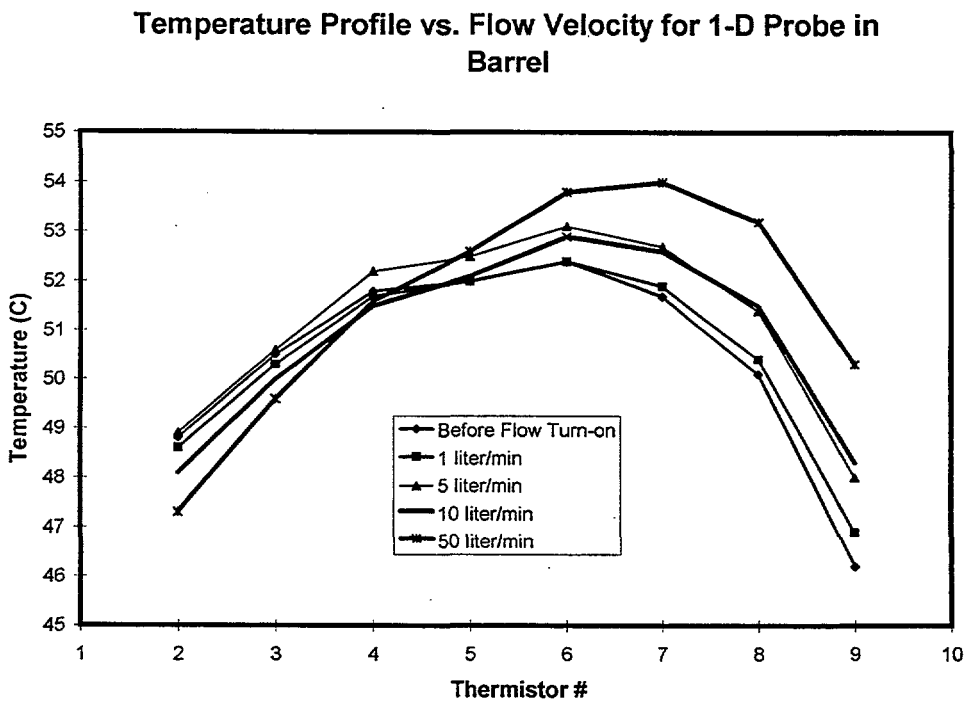

Figure 20: Laboratory test of 1-D Probe a) Air Velocity Measured by Probe vs. Known Air Velocity, b) Probe Temperature Profile vs. Air Flow Rate

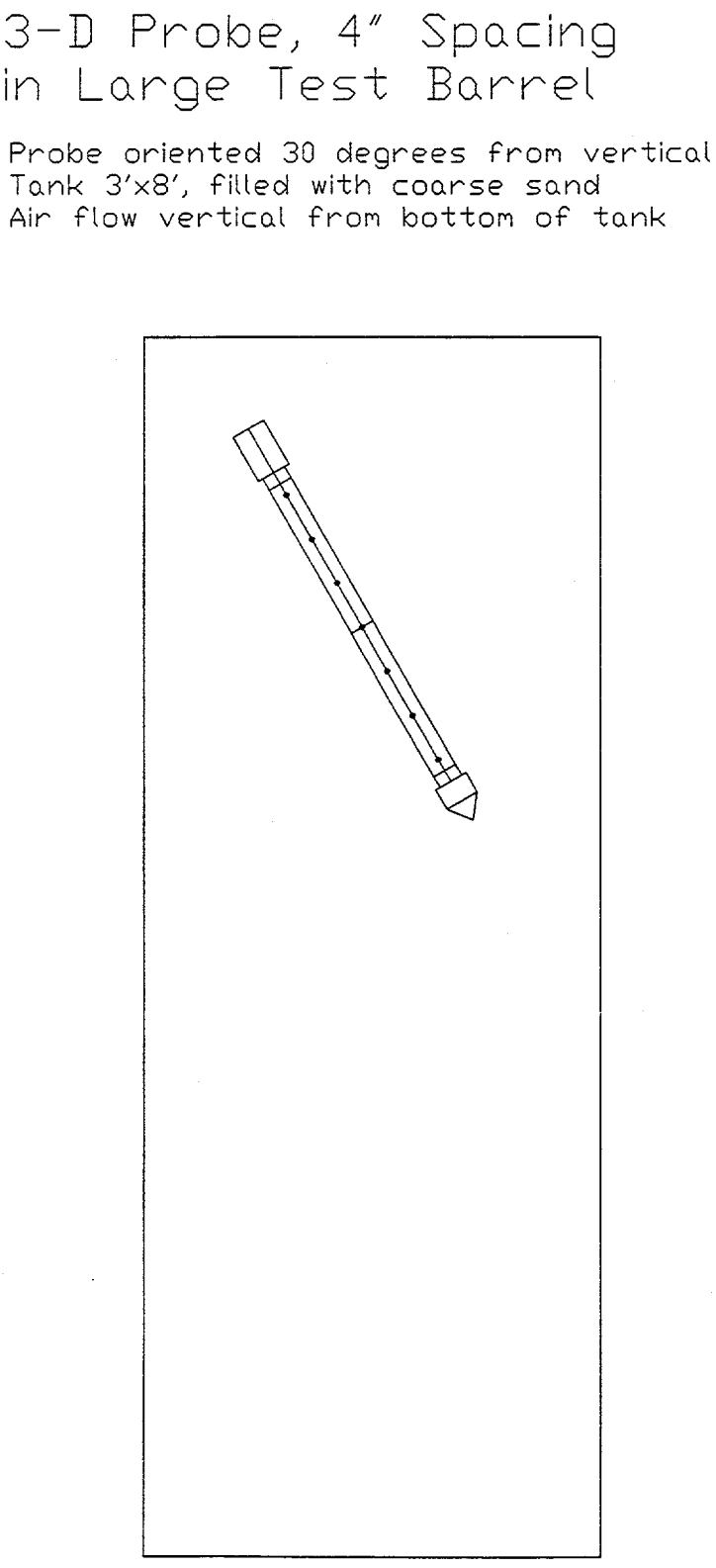

Figure 21: Laboratory test of 3-D Probe at 30°—Orientation of Probe in Barrel

Sequence of Events:

Julian Day	Date	Time	Event
114	4/23/96		3D probe installed
116	4/25/96	2:30 p.m.	Heater turned on to 20 watts
120	4/29/96	9:00 a.m.	Heater reduced to 12 watts
122	5/1/96	4:19 p.m.	Flow set at 10 SLM
128	5/7/96	12:35 p.m.	Flow OFF
129	5/8/96	3:22 p.m.	Flow set to 5 SLM
138	5/17/96	2:37 p.m.	Flow set at 30 SLM
144	5/23/96	3:45 p.m.	Flow set at 2 SLM
159	6/7/96	4:14 p.m.	Flow OFF
159	6/7/96	4:50 p.m.	Flow set to 0.5 SLM
166	6/14/96	2:30 p.m.	Flow set to 0.25 SLM
180	6/28/96	3:48 p.m.	Flow OFF, probe removed

Figure 22a shows the raw data from this test, with the known flow velocity in cm/sec indicated. Figure 22b shows the deviation from reference and average temperature. In this plot, all of the changes in flow rate are clearly visible, as is the required settling time of the probe. Figure 23a shows the magnitude of the velocity as determined by the probe, compared to the known velocity. As can be seen, the flow events above about 0.002 cm/sec are clearly visible in the data. However, the magnitude is only about half of the known velocity. Figure 23b shows the deviation from horizontal during these tests. During the 0.025 and 0.075 cm/sec flow rates, the angle is close to 60 degrees, which it should have been. At 0.012 cm/sec there is an error of about 20 degrees. At flow rates lower than this the angle measurement does not correspond at all with the known direction of flow.

Test #3: 3D Probe oriented Vertically, with Permeability contrast

The modeling that was conducted earlier showed a large difference in the vertical velocity component near the probe when the probe was backfilled with a material coarser (more permeable) than the formation. We needed to be able to backfill the thin annulus around the probe with something that would approximate the permeability of the formation. We could not use any liquids, since that would dramatically change the thermal conductivity near the probe. The back-fill material had to be both porous and dry, so we decided to try very fine sand, which when it fell loosely into place would be as permeable or less permeable than the fairly compacted formation. To test this we sewed a 4" diameter cloth "sock" that would fit over the probe and leave an annulus similar to that between the probe and the formation. This was put in place in the barrel full of coarse sand by driving a 4" ID pipe vertically into the coarse sand in the barrel to the desired depth. The sand inside the pipe was removed with a vacuum. The "sock" was inserted into the pipe, then the probe was placed inside the "sock", and the annulus between the probe and the "sock" was then filled with very fine 100 mesh sand. Finally the 4" diameter pipe was removed from over the top of the "sock" and probe and the test was conducted as described above.

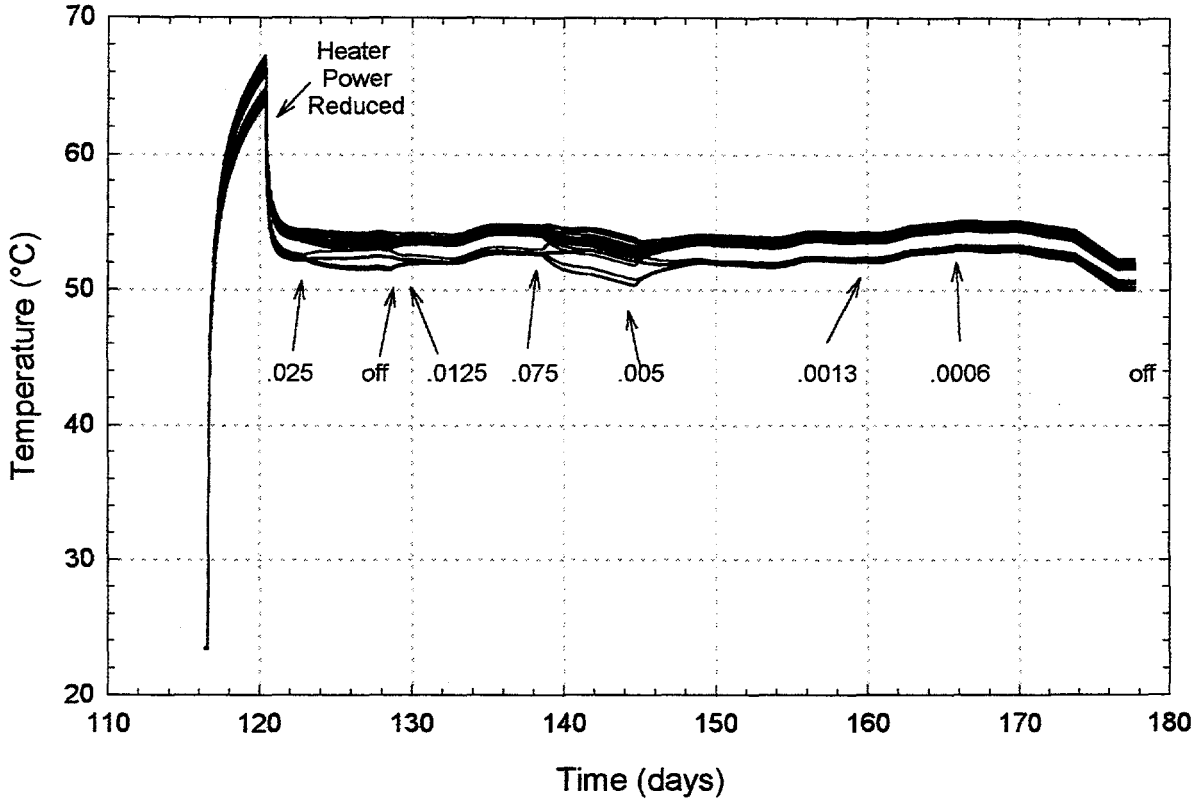

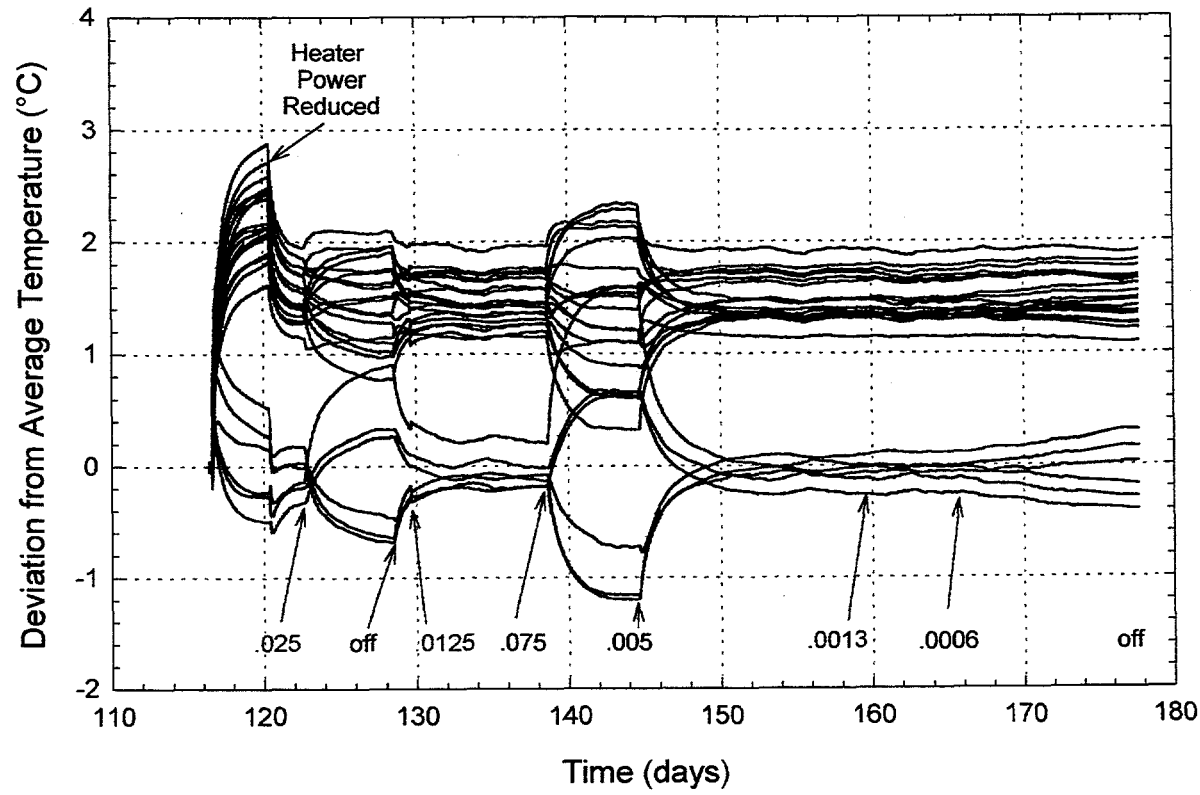

Figure 22: Laboratory test of 3-D Probe at 30° a) Raw Data b) Deviation from Reference and Average

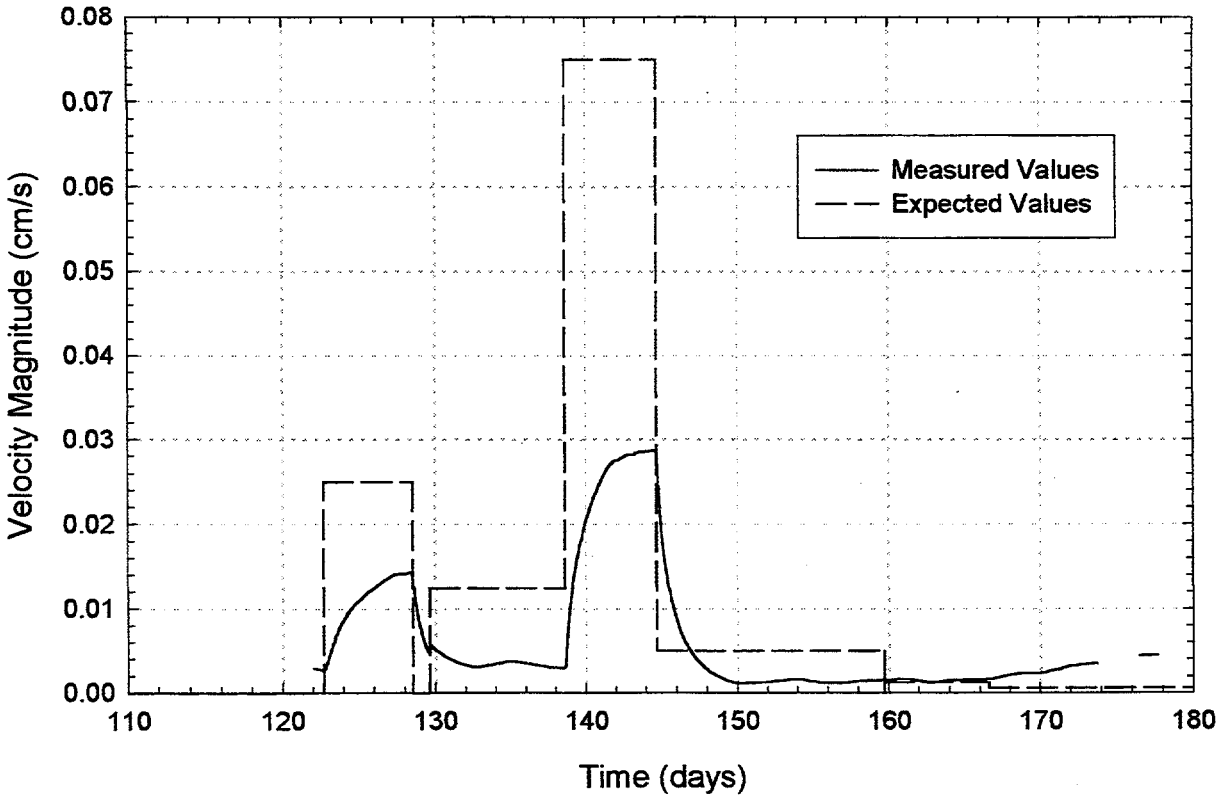

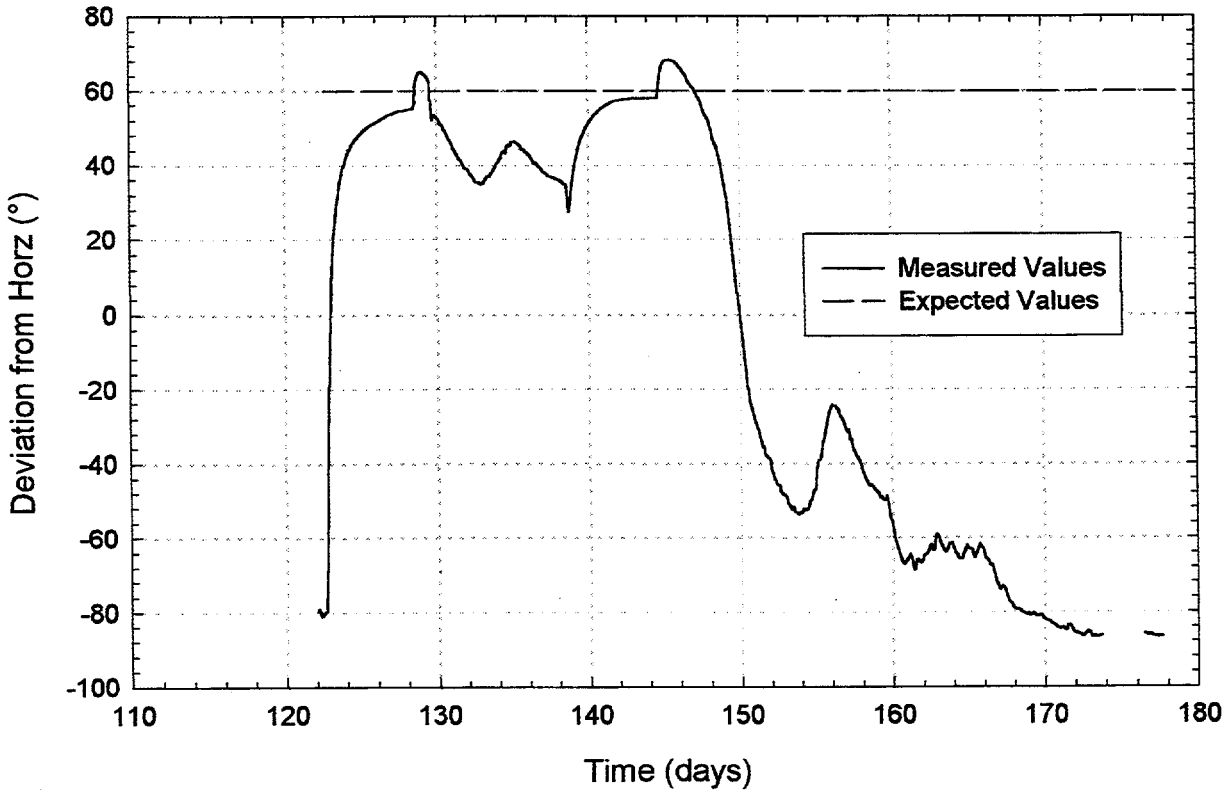

Figure 23: Laboratory test of 3-D Probe at 30° a) Velocity magnitude b) Angular deviation from horizontal on probe

Sequence of Events:

Julian Day	Date	Time	Event
190	7/8/96		3-D Probe installed vertically in sand sock
191	7/9/96		Turned heater ON for ~ 40 minutes
192	7/10/96	8:45 a.m.	Heater ON at 12 watts
198	7/16/96	1:00 p.m.	Heater accidentally set too high, reset to 12 watts
200	7/18/96	12:00 a.m.	Flow ON at 0.5 SLM
204	7/22/96	4:30 p.m.	Brief power outage, flow and heater came back ON but lost some data
205	7/23/96	6:30 a.m.	Data logger back ON
206	7/24/96	10:55 a.m.	Flow ON at 0.25 SLM
213	7/31/96	3:15 p.m.	Heater OFF, flow still ON
220	8/7/96	3:40 p.m.	Flow OFF, heater ON at 12 watts.
228	8/15/96	8:05 a.m.	Flow ON at 10 SLM
236	8/23/96	4:00 p.m.	Flow ON at 30 SLM
249	9/5/96	2:15 p.m.	Flow ON at 1 SLM
284	10/10/96	11:00 a.m.	Flow OFF, heater OFF, removed probe

Figure 24a shows the raw data from a portion of this test, and figure 24b shows the deviation from reference and average. The known flow rate at various times is shown by the arrows. As can be seen, the changes in flow rate are clearly evident in both of these plots. Figure 25 shows the measured air velocity and the known air velocity for this time period. As can be seen by comparing this with figure 23a, the results are at least as good as with all coarse sand. That is, the presence of this annulus of fine sand did not damp the response of the probe. This is probably due to the fact that the temperature distribution on the probe is affected by a large volume of the "formation" sand, and since the "formation" sand and the back-fill sand have similar thermal properties, the fact that the fine back-fill sand in the annulus restricts the flow along the probe does not affect the indicated velocity for this larger volume of "formation" sand.

Test #4: Point Source Probe

A probe was fabricated to investigate whether a point source probe would offer advantages over a finite length cylinder probe. The probe was constructed using a short ~1" long x 0.5" diameter cartridge heater, with an array of thermistors above and below the heated region. The probe was tested with both steady state power and with oscillating power in various velocity flow fields. Due to funding limitations this idea was not pursued beyond the initial laboratory tests. See Appendix C for a discussion of these tests.

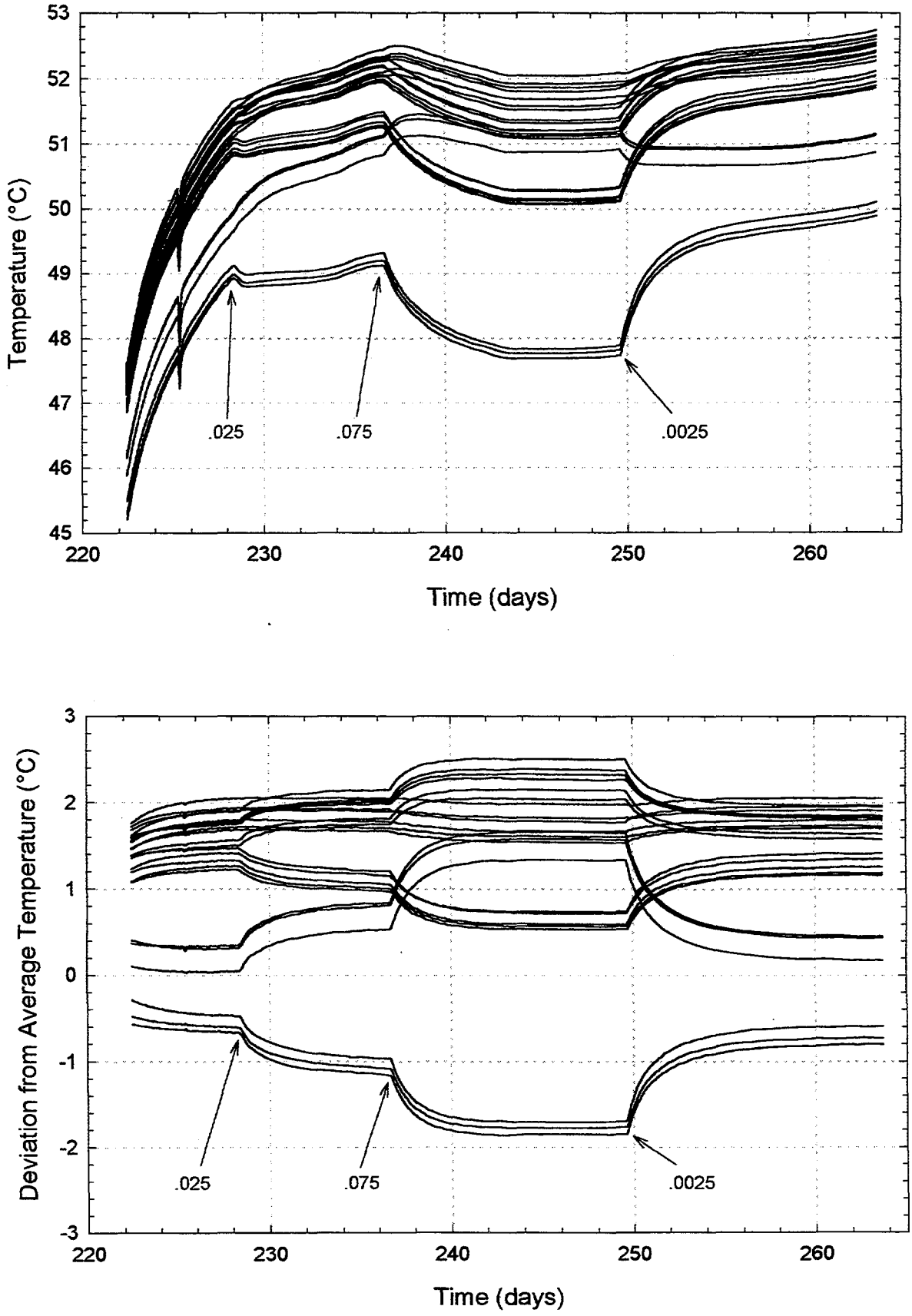

Figure 24: **Laboratory test of 3-D Probe with Permeability Contrast a) Raw Data b) Deviation from Reference and Average**

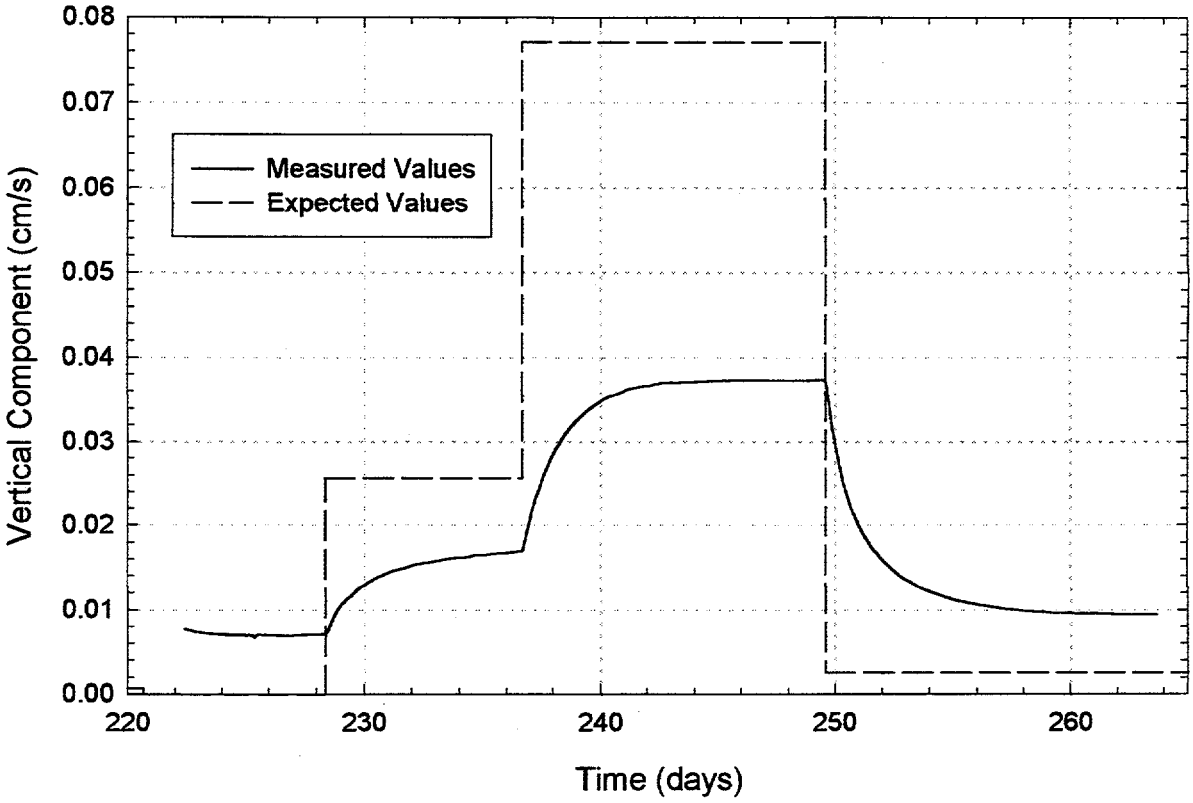

Figure 25: **Laboratory test of 3-D Probe with Permeability Contrast—Measured Vertical Component of Flow vs. Actual Velocity Data**

Field Tests

Overview:

In addition to the laboratory tests, three in situ test series were conducted on the flow probes. The first was a series of tests in a large buried tank filled with homogenous media and with known air injection rates similar to the laboratory test fixtures, but installed outdoors in the ground. These tests are referred to as the Tank Tests. Next we did a brief test at a vapor extraction site, which is referred to as the Chemical Waste Landfill Test (CWLF). The third test was a long term test at an active remediation site of an abandoned gas station, and is referred to as the Remediation Site Test.

Tank Tests

The test setup for these outdoor controlled flow tests was very similar to the laboratory test setup. The purpose of these tests was to resolve some of the variables involved in in situ testing, including daily temperature fluctuations, atmospheric pressure changes, etc., yet to maintain as much control as possible over these variables by using a homogenous medium and imposing a uniform known air flow rate. As in the laboratory tests, we controlled the inlet air flow rate with a mass flow controller. We continuously recorded inlet air temperature, ambient air temperature, probe thermistor temperatures, and sand temperatures near the wall of the tank. We also installed unheated thermistor grids at various depths outside the test tank to monitor daily and seasonal temperature changes vs. depth. Figure 27 shows the location of the flow probe, the external unheated temperature probes, the tank, air inlet manifold, and the thermistors on the inside wall of the tank.

In these tests, the probe was placed in a 10' tall by 4' diameter pressure vessel buried in the ground. The top of the tank extended 1.5 ft above the ground. The tank was filled with construction grade sand. Figure 26 shows the test tank being installed in the ground, the construction grade sand used to fill the tank, and the finished test set-up. We used a pressure vessel anticipating that it would be useful to exclude the effects of atmospheric pressure changes, to be able to pump large amounts of air through the sand which could generate significant pressure differentials, and in the future to be able to circulate water through the tank for testing the water flow probes. However, for these tests the tank was left vented to atmosphere.

An air inlet manifold was buried in the bottom of the tank to allow pressurized air from an air compressor to be ported into the bottom of the tank, flow up through the sand surrounding the flow probe, and exit through a vent at the top of the tank where it was vented to atmosphere. The air compressor had a maximum output of 8.5 CFM, and the flow was controlled by a mass flow controller.

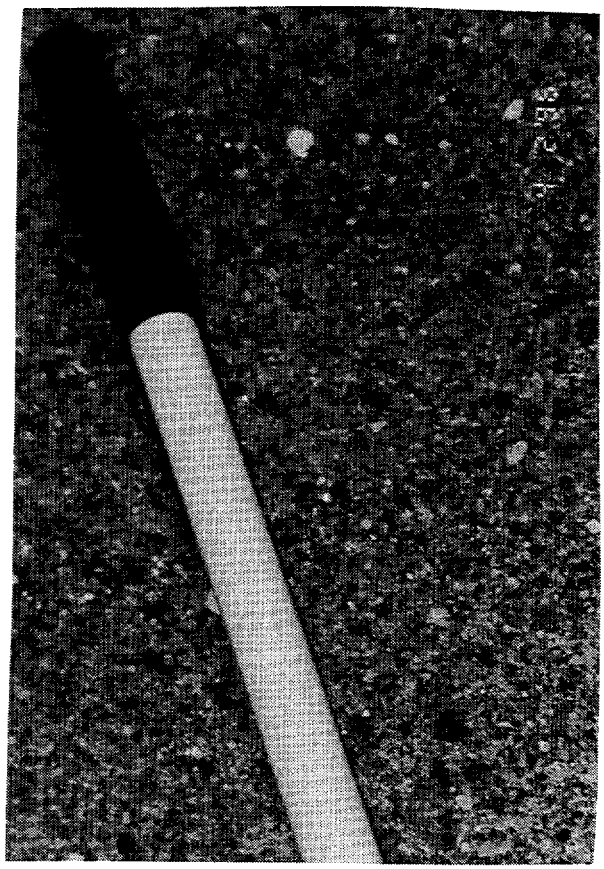

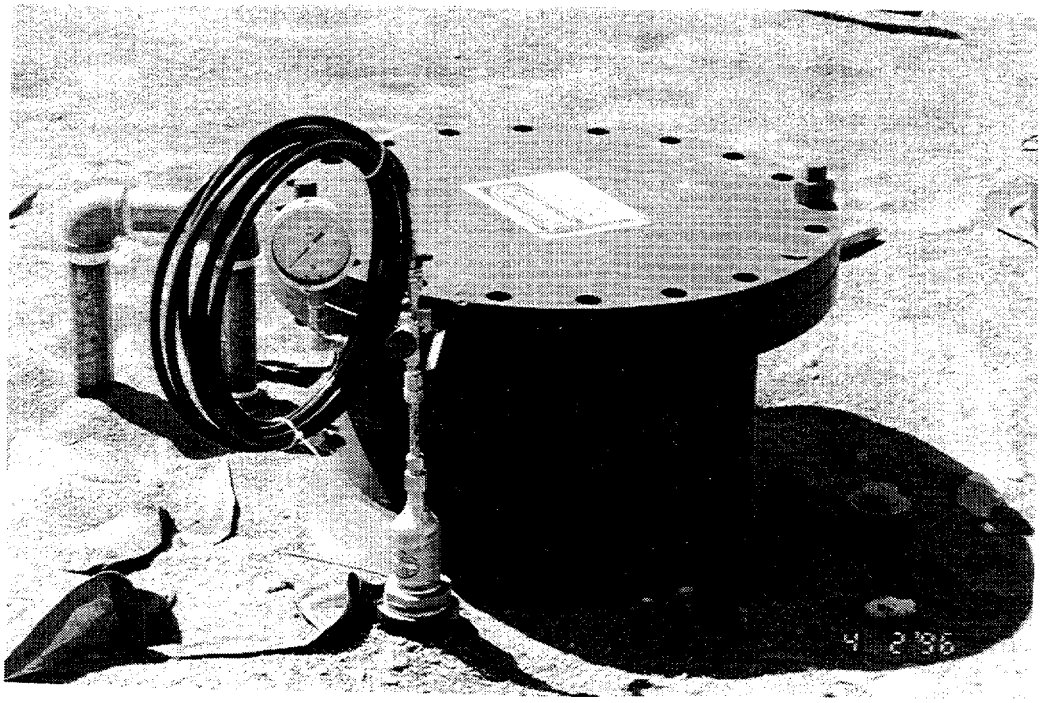

Figure 26: Tank Test a) Installation of Tank b) Construction grade sand in tank c) Tank installed in ground

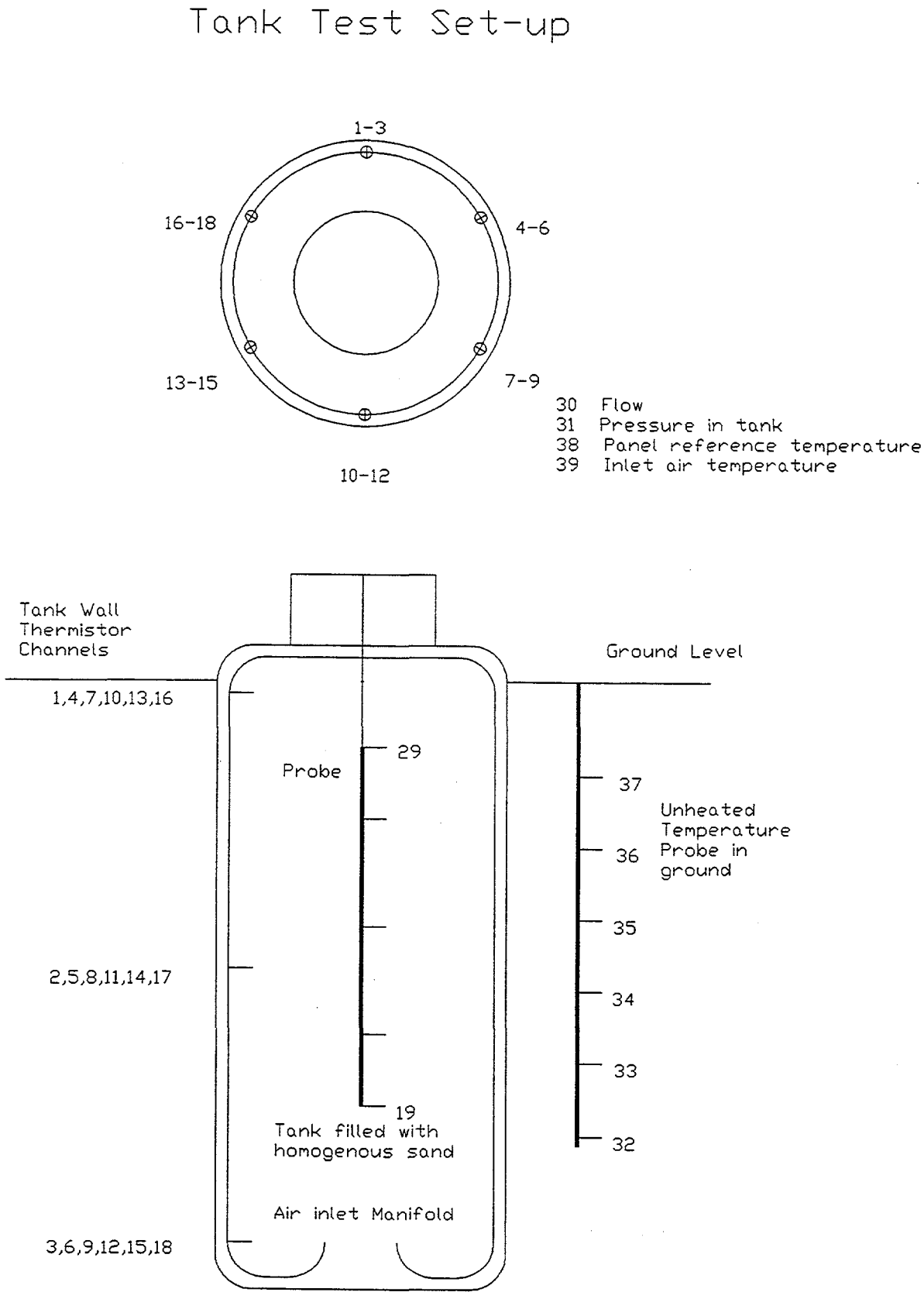

Figure 27: Tank Test—Test set-up

The probe for these tests was a 1-D probe (see Figure 5). It consisted of a metal tube approximately 0.75" diameter x 60" long. A nickel-chromium heater wire 35.5" long was placed in the tube. A linear array of 11 thermistors, spaced on 4.5" centers, was also placed inside the tube, with the middle thermistor aligned with the middle of the heater wire. The entire tube was then potted. While this produced a probe which was physically very robust, the probe had several serious thermal problems, which added to the data problems encountered in the field. The radial location of the heater wire and the thermistors within the tube was not well controlled, leaving a variable thickness of potting material between the heater wire and any given thermistor, and between that thermistor and the wall of the probe. This manifested itself as a non-optimal temperature distribution, as measured by the probe thermistors, along the length of the probe.

A number of tests were conducted over a period of several months. Figure 28a shows a small subset of the test data, with the 7 middle probe thermistors and the known flow rate. Figure 28b shows the same time period, with all 11 probe thermistors. As can be seen, during times of high air flow, the thermistor data tends to converge and diverge as expected. However, notice the large daily oscillations in the temperature data.

Unfortunately, most of the data from these tests was ultimately determined to be unusable due to various test set-up and instrumentation problems, including the following:

1. The air compressor was run continuously for long periods of time but broke down a number of times during the tests.
2. There were several power failures at this remote site.
3. The sand in the tank became very damp due to daily temperature changes, formation of dew, etc. and would not flow, so when new probes were placed in the tank, there were preferential paths for the air flow. Efforts were made to uniformly compact the sand with both hand packers and mechanical vibrators, but with limited success.
4. We monitored the differential pressure between the bottom of the tank and the top of the tank, and saw as much as 15 psi differential, indicating that the permeability of the outdoor tank was dramatically different than that of the indoor laboratory test setup.
5. Because of test set-up pressure and flow rate limitations, we were not able to generate as high an air flow past the probe as we had wanted.
6. There were also electrical instrumentation problems which were traced to changes in resistance across terminal strips in a junction box, which coincided with the daily temperature and humidity changes, which masked most of the true signal. We feel that this was by far the most important contributor to the problems with the data.

Efforts were made to isolate these various problems, including placing passive temperature probes inside and outside the tank, filtering the data, removing the sand and replacing it with dry, non-compacted sand, monitoring the humidity inside the tank, etc. While much was learned by trial and error about how to deploy and field the probes, most of the actual data from the tank tests was not usable.

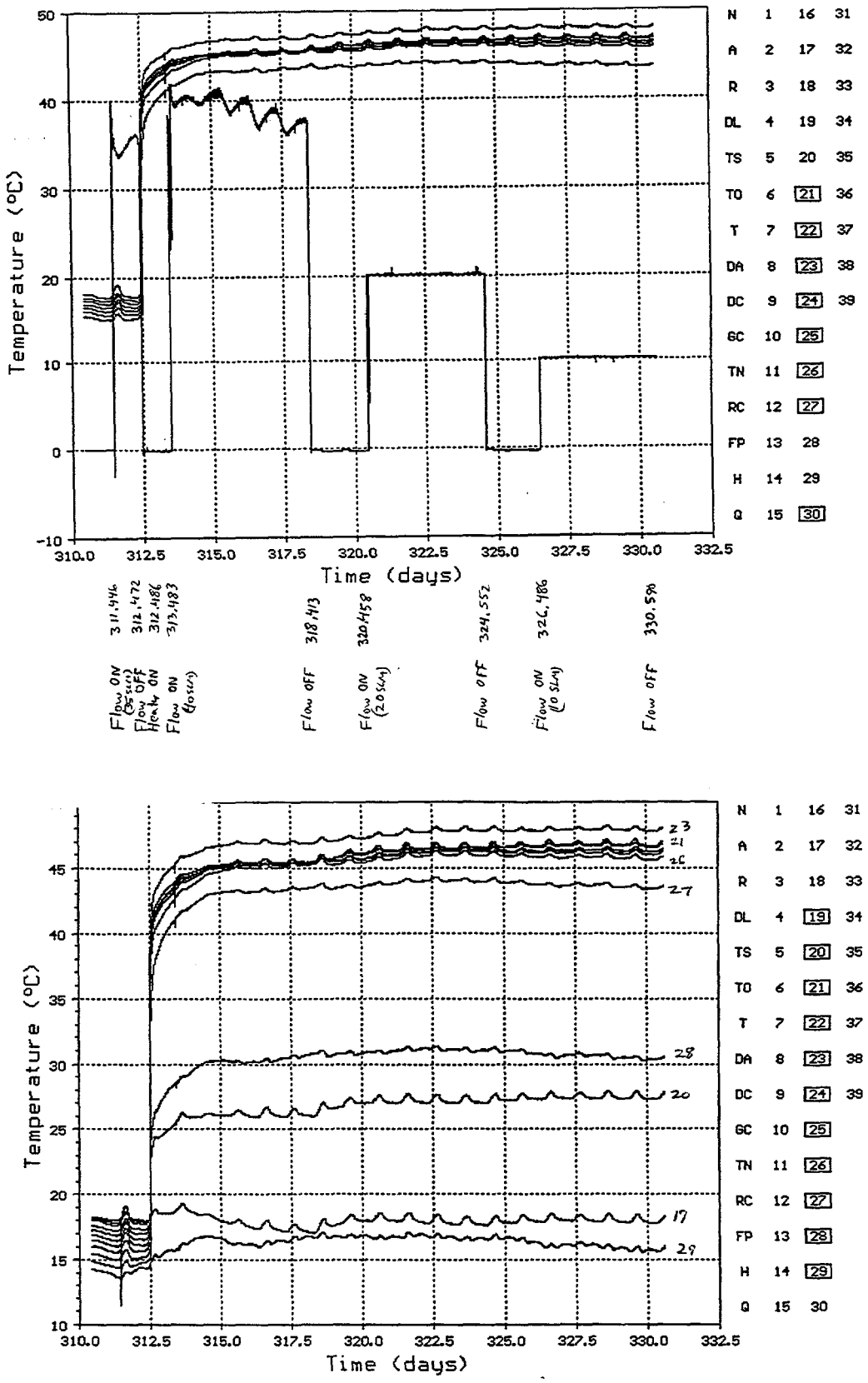

Figure 28: Tank Test a) Raw Temperature of 7 middle thermistors and Known Flow Rate b) Raw Temperature of all 11 thermistors

Figure 29a shows data from the unheated probe outside the tank (channels 32-37), and from the thermistors at the two ends of the heated probe inside the tank (channels 19 and 29). Notice that thermistors 19 and 29 (inside the tank) and 33 and 37 (outside the tank) see very different daily temperature variations, despite being at the same depths, and regardless of whether the flow is ON or OFF. In this figure, channels 32-35 are very flat, with no discernible daily oscillation. These daily oscillations in the data on the probe inside the tank were found to be related to daily changes in humidity on a terminal strip inside the tank, rather than changes in daily or seasonal temperature.

In addition to these instrumentation problems, there were long term heating and cooling trends in the data. Figure 29b shows the temperature vs. thermistor number for three flow rates in the tank tests. The shape of these curves is used by the analysis software to calculate the air velocity. The shape of the 10 SLM curve should be much more horizontal, like the 20 SLM curve, and the 20 SLM and 40 SLM curves should each tilt more vertically. Although the probe was measuring changes in flow rate, there were larger trends in the data that swamped the signal, making it impossible to obtain accurate velocity numbers. These trends look like an externally imposed temperature gradient, possibly due to seasonal changes, which is skewing the angle of the Temperature vs. Thermistor data.

Sequence of Events:

Julian Day	Date	Time	Event
297	10/24/95		Flow OFF. Buried passive temperature probe outside tank. Prior data suspect due to instrumentation problems.
304	10/31/95		Compacted sand. Heater turned ON, Flow still OFF
310	11/6/95		Compressor broke. Data since 11/2/96 bad due to ground loop problem
311	11/7/95		Flow ON at 35 SLM, heater OFF
312	11/8/95		Flow OFF, heater ON
313	11/9/95	11:36 a.m.	Flow ON at 40 SLM
314	11/10/95	9:00 a.m.	Flow ON at 41 SLM
318	11/14/95	10:00 a.m.	Flow OFF, heater still ON
320	11/16/95	11:00 a.m.	Flow ON at 20 SLM
324	11/20/95	1:17 p.m.	Flow OFF
326	11/22/95	11:45 a.m.	Flow ON at 10 SLM
331	11/26/95		Flow OFF
333	11/29/95	1:48 p.m.	Flow ON at 5 SLM
337	12/3/95		Flow OFF
341	12/7/95		Heater OFF

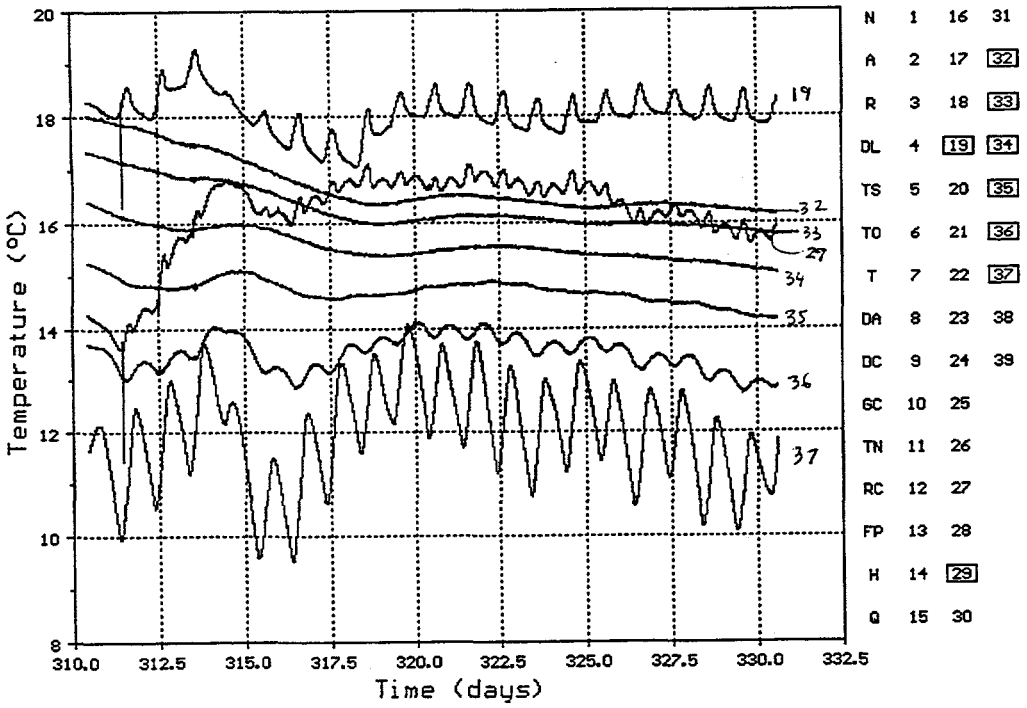

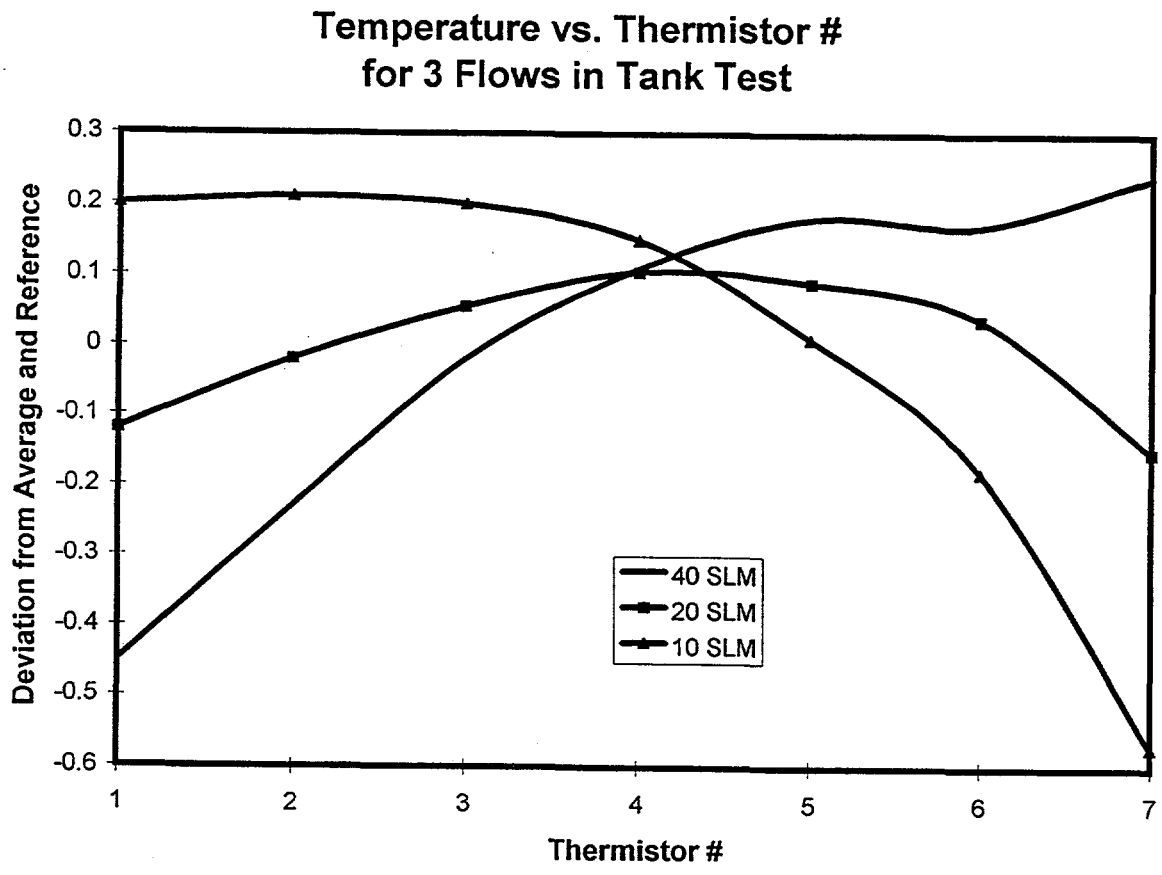

Figure 29: **Tank Test a) Raw Temperature of unheated probe outside tank and two end thermistors on flow probe in tank b) Temperature vs. Thermistor number for 3 flow in the tank**

Chemical Waste Landfill Tests:

While working on the tank tests we learned that researchers from Sandia and from Intera would be conducting a short term vapor extraction test on a nearby well at Sandia's Chemical Waste Landfill. We received permission to place three of our flow probes near this well during their experiment. Our objective in this test was to gather data from both a 3-D flow probe and a 1-D flow probe placed in the ground during a vapor extraction experiment, for comparison to the previous tests in the tank and in the laboratory, and to compare the signals with the known extraction rate at the well. The vapor extraction experiment was only scheduled to last for a few days, much too short to let the probes stabilize and determine accurate velocities, but it would give us the opportunity to monitor an active vapor extraction project under realistic field conditions and to gain experience in emplacing the probes and monitoring their performance. Our test was conducted at the same time as Intera's vapor extraction test, but on a non-interference basis.

Two 3D probes and one 1D probe were installed near the extraction well. Figure 30 shows a cross section and a plan view of the extraction well and of the probe emplacement. The first 3-D probe was placed in a hole 8' 8" East of the vapor extraction well. This probe had 3" thermistor spacing. A 6" diameter hole was augered 30' deep. The material from the hole was a mixture of fine sand and silt, with a few pieces of gravel up to 3/4" diameter and two larger rocks approximately 4" in diameter. The drillers encountered a layer that was difficult to drill through from 7' to 11' below grade, but no evidence of caliche came up with the auger and it is felt that they may have hit several large rocks. The hole slumped in to 26.5' deep. The probe was placed against the side of the hole nearest to the well, and the hole was backfilled with the soil from the auger. Two cement plugs were poured in the hole to prevent any movement of surface air directly through the augered hole to the probe.

The 1-D probe was placed in a hole 8' 10" East of the vapor extraction well and approximately 2' north of the 3-D probe. A 3" diameter hole was augered 8' deep. The probe was placed 7.5' deep and centered in the hole and the hole was backfilled with the soil from the auger. The top 12-14" of the hole was plugged with cement.

It became apparent that the method of emplacement and backfilling of the borehole are much more critical than in ground water sensing applications. Initially we had planned to install only one 3-D probe and one 1-D probe and compare their performance. However, after monitoring the first 3-D probe and the 1D probe for several days we had doubts about the data quality from these probes. These probes were placed in the ground against one side of the augered hole and the holes had been backfilled with the material that had come out of the augered holes. Both of these probes showed significant non-symmetrical temperature distributions, which persisted for a number of days. There were significant differences from one thermistor to another, even at the same depth along the probe.

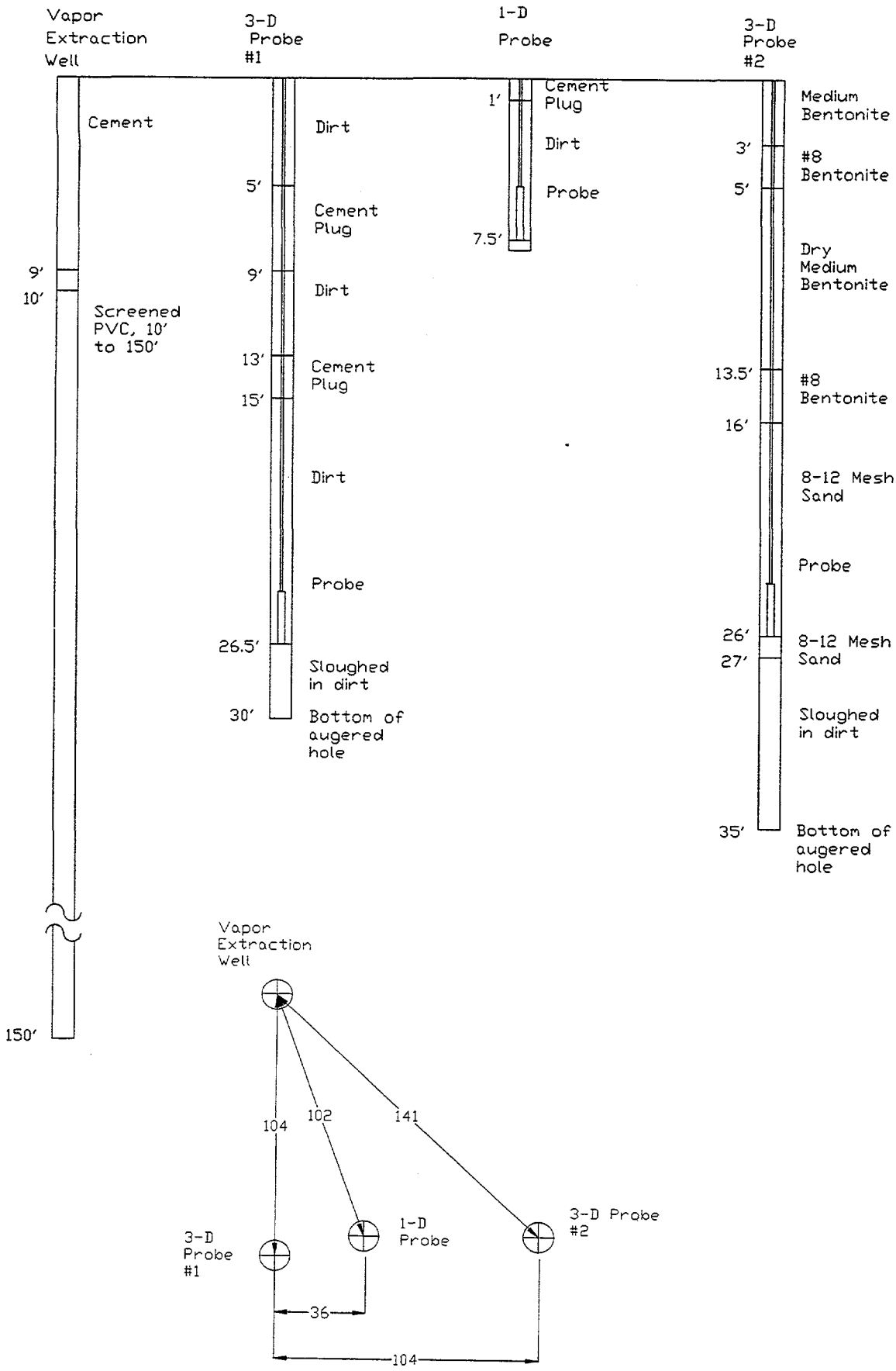

Figure 30: CWLF Test a) Probe and Well Cross-section b) Plan View

We compared these results with the proof of concept test conducted at Hanford. In that case, the probe had been centered in the hole and backfilled with sand, and it showed a very smooth, symmetric temperature distribution. We concluded that the unusual signals from the probes at the CWLF must be due to the way in which the probe was emplaced. Therefore, a second 3-D probe was installed for comparison. The second 3-D probe was placed in a hole 11' 9" North East of the extraction well. This probe had 4" thermistor spacing. A 6" diameter hole was augered 35' deep. The hole slumped in to 27' deep. A 1' layer of sand was placed in the bottom of the hole. The probe was then centered in the hole, and the hole was filled with 8-12 mesh sand to 16'. A Bentonite plug was placed from 13.5' to 16' using #8 Bentonite and 2 quarts of water. The hole was then filled with dry medium Bentonite to 5', and then another wet bentonite plug was put in place. This second 3D probe was centered as closely as possible in the hole, and was backfilled with the same homogenous coarse sand that was used in the barrel experiments in the laboratory. It showed an excellent, symmetrical temperature distribution. The data from the first two probes was so non-symmetrical that it was very difficult to calculate the velocities.

Figure 31 shows the probes being installed, the extraction well and probe locations, a picture of a 1-D and a 3-D probe, and the dirt and gravel augered from the hole which was used to backfill two of the probes.

Sequence of Events:

Julian Day	Date	Time	Event
16	1/16/96	12:00 a.m.	Installed 3-D Probe #1
17	1/17/96	4:25 p.m.	3-D Probe #1 ON at 15 watts
19	1/19/96	11:00 a.m.	Installed 1-D probe
19	1/19/96	12:00 a.m.	3-D probe #1 increased to 20 watts
20	1/20/96		1-D probe ON at 20 watts
22	1/22/96		1-D probe reduced to 13 watts
25	1/25/96		Installed 3-D probe #2
44	2/13/96	12:32 p.m.	Flow ON at 100 CFM
44	2/13/96	4:19 p.m.	Flow OFF
45	2/14/96	8:55 a.m.	Flow ON at 150 CFM
45	2/14/96	12:23 p.m.	Flow increased to 200 CFM
45	2/14/96		Flow OFF
46	2/15/96	9:00 a.m.	Flow ON at 250 CFM
46	2/15/96	12:30 p.m.	Flow decreased to 150 CFM
47	2/16/96		Flow OFF
50	2/19/96	2:15 p.m.	Wells capped off
54	2/23/96	2:20 p.m.	Heaters OFF
60	2/29/96	2:15 p.m.	Heaters ON

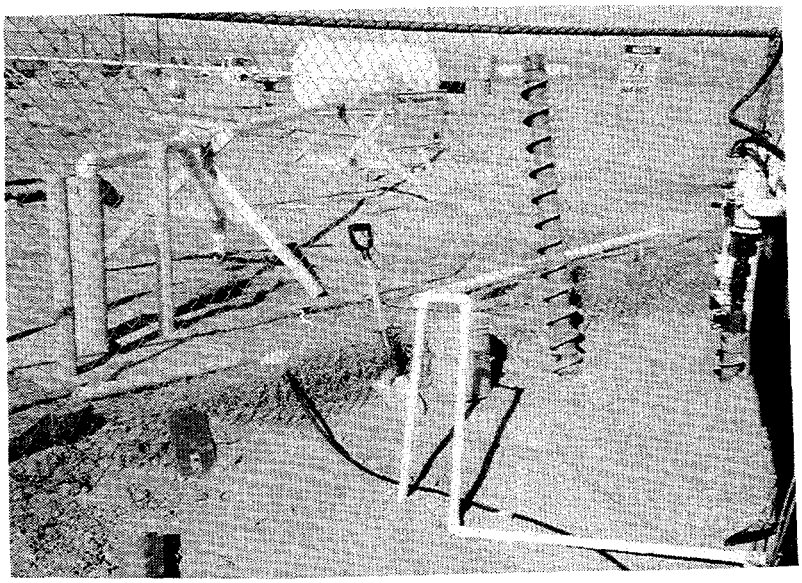

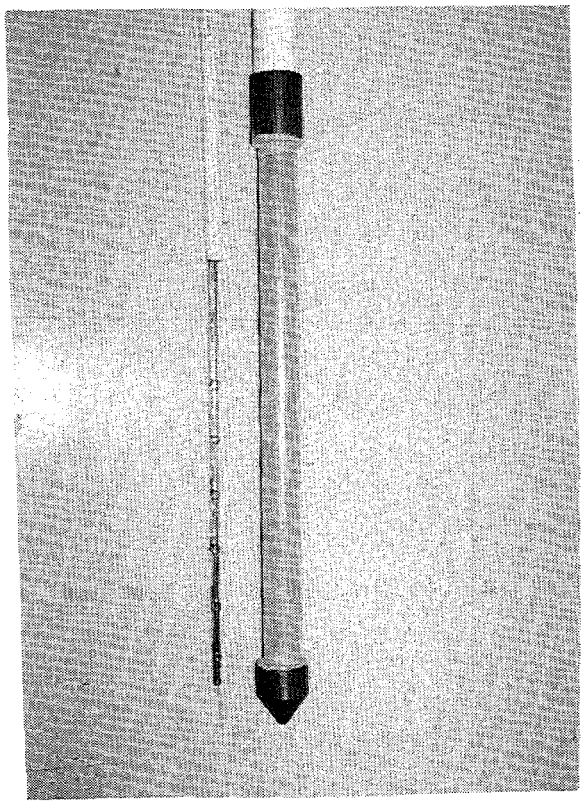

Figure 31: CWLF Test a) Installing 3-D Probe b) Probe well and piping location c) 1-D and 3-D Probes d) Dirt and gravel from augered hole used for backfill

Test Sequence:

We began recording data from the probes as soon as they were placed in the well in order to watch the temperature stabilize both before and after heater turn-on. The probes were monitored continuously from 1/17/96 through 3/5/96. The data from the probes was recorded using a data logger and computer located in a trailer next to the probes. Typically it takes 2-3 days for the temperature of the probe to stabilize following a change in heater power. It takes a shorter, but still appreciable time, to stabilize after a change in flow rate.

The vapor extraction consisted of approximately 4 hours at 100 CFM, 17 hours off, 3 hours at 150 CFM followed by 3 hours at 200 CFM, 16 hours off, 3 hours at 250 CFM followed by 26 hours at 150 CFM. The presence of all of these events is discernible on all three probes. The time constant of the probe is considerably longer than the duration of these flows, so no absolute correlation can be made between the measured flows and the known flow rates. However, the relative magnitudes of the various flow rates are as expected.

The thermal conductivity of the soil at the CWLF was measured using a conductivity probe, and was found to be 0.0015 cal/sec °C cm, which is about twice the value of the sand used in the laboratory tests.

The vertical flow probe produced much higher surface temperatures than the 3-D probe for the same total probe energy input. This is probably due to the smaller diameter and hence smaller surface area of the probe. This higher temperature resulted in higher sensitivity. The larger signals on the vertical probe may also be due in part to larger gas flows at this shallower depth.

Nearly all of the measured flow is strictly vertical. While this could be what actually happened, it is likely that there is significant vertical channeling of the flow within the augered hole. Concrete and/or bentonite caps were placed at two levels in each augered hole, but later modeling showed the possibility of significant channeling even with plugs directly above and below the probes.

There was no daily temperature oscillation on any of the probes. However, there was a very long term gradual temperature gradient which gave the appearance of a steady-state flow. In addition, there were several days before active vapor extraction began which showed a noticeable flow signal. These corresponded with days when the ambient temperature was lower than normal, and could either have been artifacts from temperature effects in the data collection instrumentation, or could correspond to weather fronts moving through the area.

Figure 32 shows raw data and deviation from reference and average for the 1-D vertical flow probe. Note that in figure 32b that all of the flow events are clearly visible, and the relative magnitudes are as expected. Figure 33 shows the calculated vertical velocity for this 1-D probe.

Figure 33 shows the raw data and deviation from reference and average for the first 3-D probe. The extraction air events are also discernible in this data. However, note the high background noise level and the long term drift in the data, which make it much harder to calculate the velocities. These are even more apparent in figure 35, which shows the calcualted vertical and

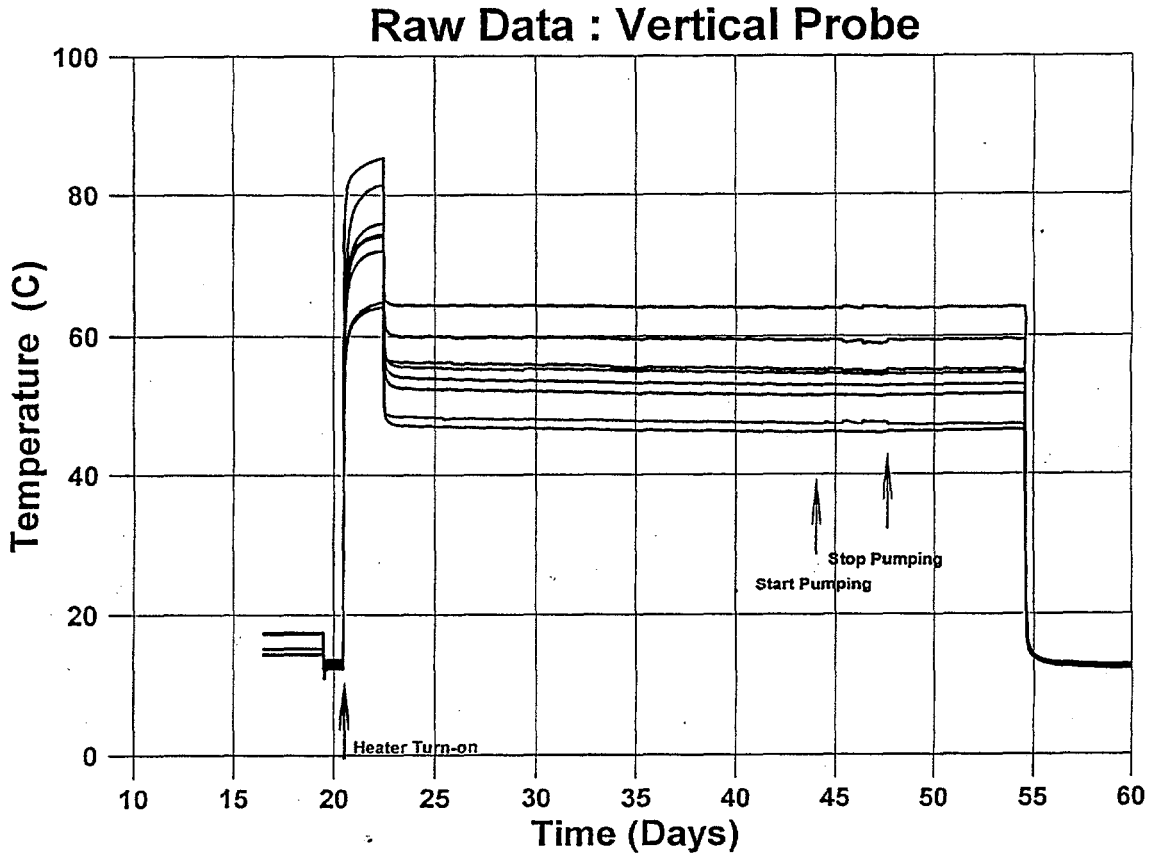

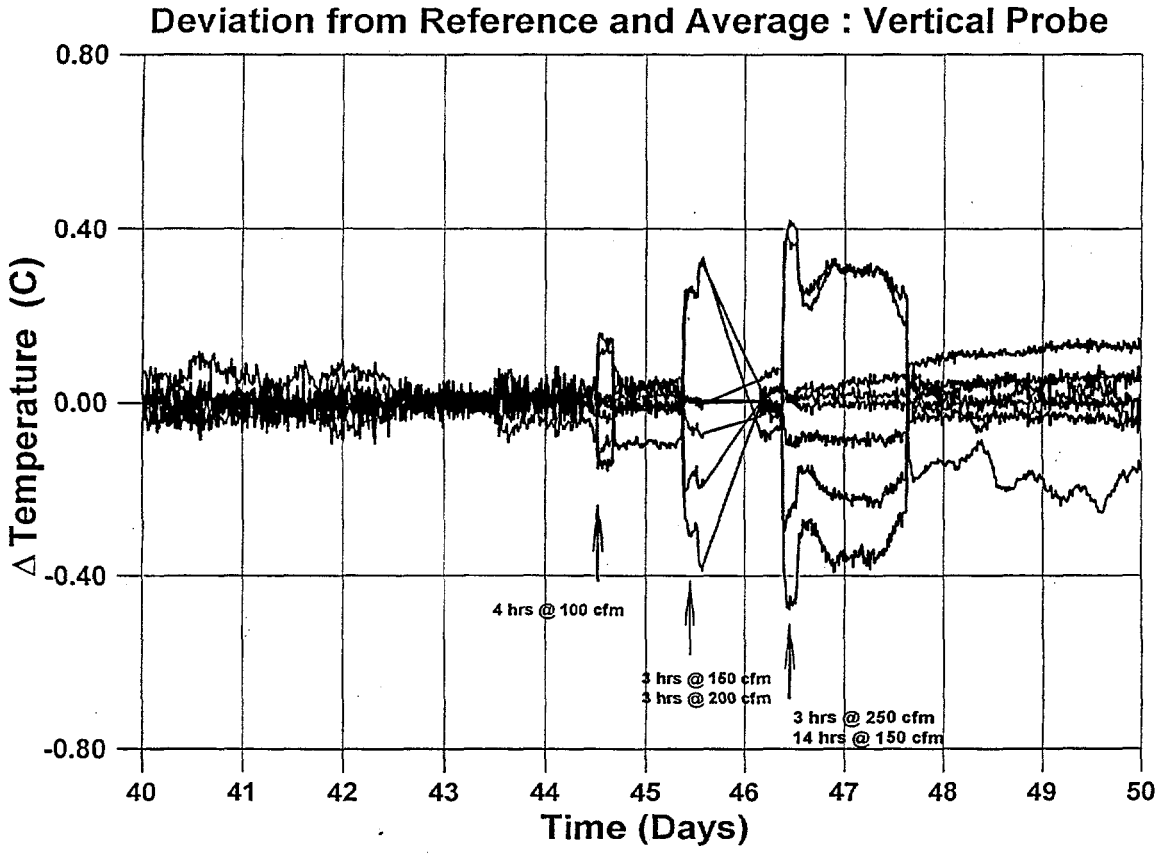

Figure 32: CWLF Test 1-D Probe a) Raw Data
b) Deviation from Reference and Average

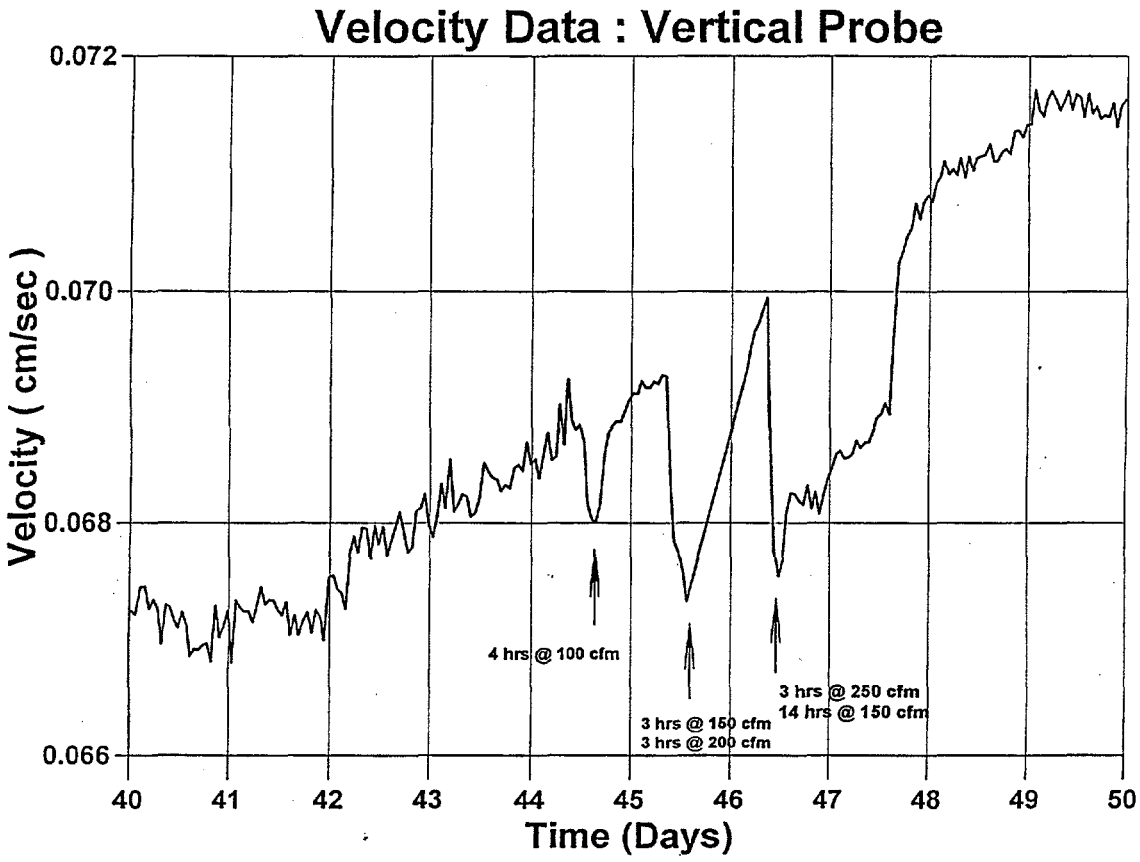

Figure 33: CWLF Test Velocity from 1-D Probe

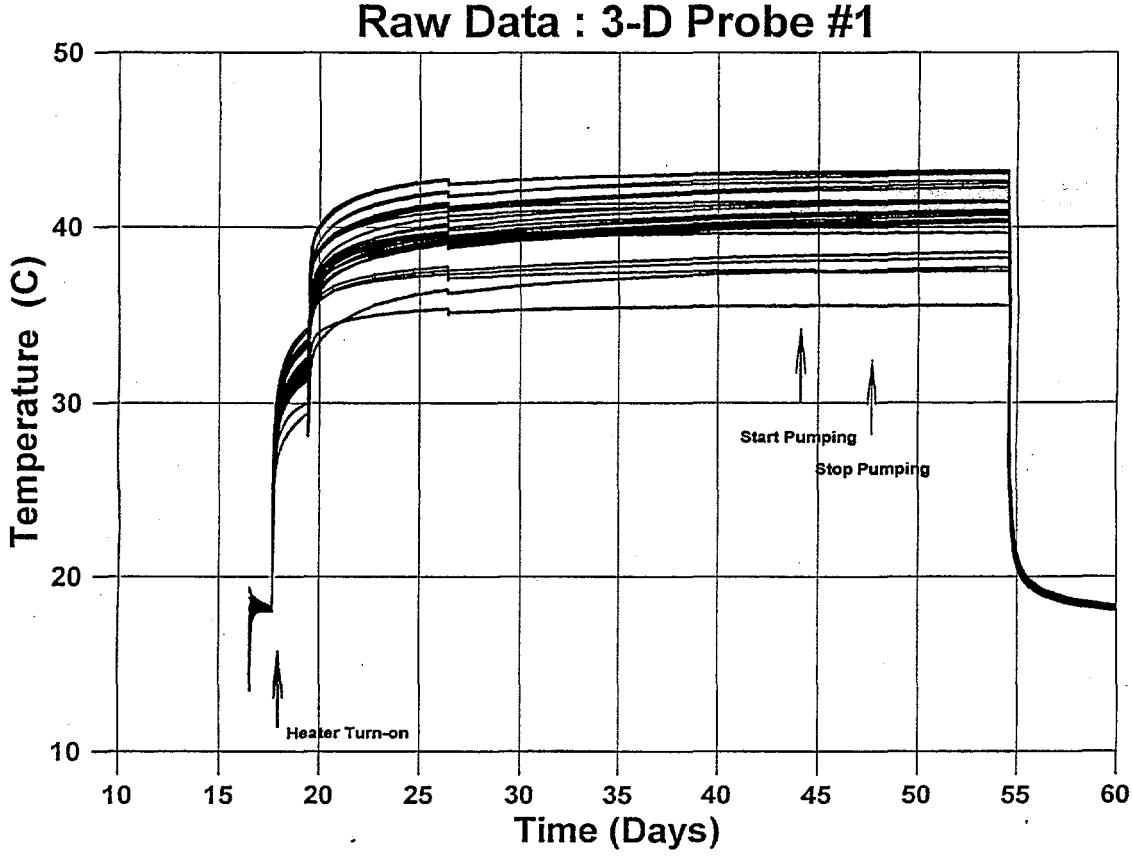

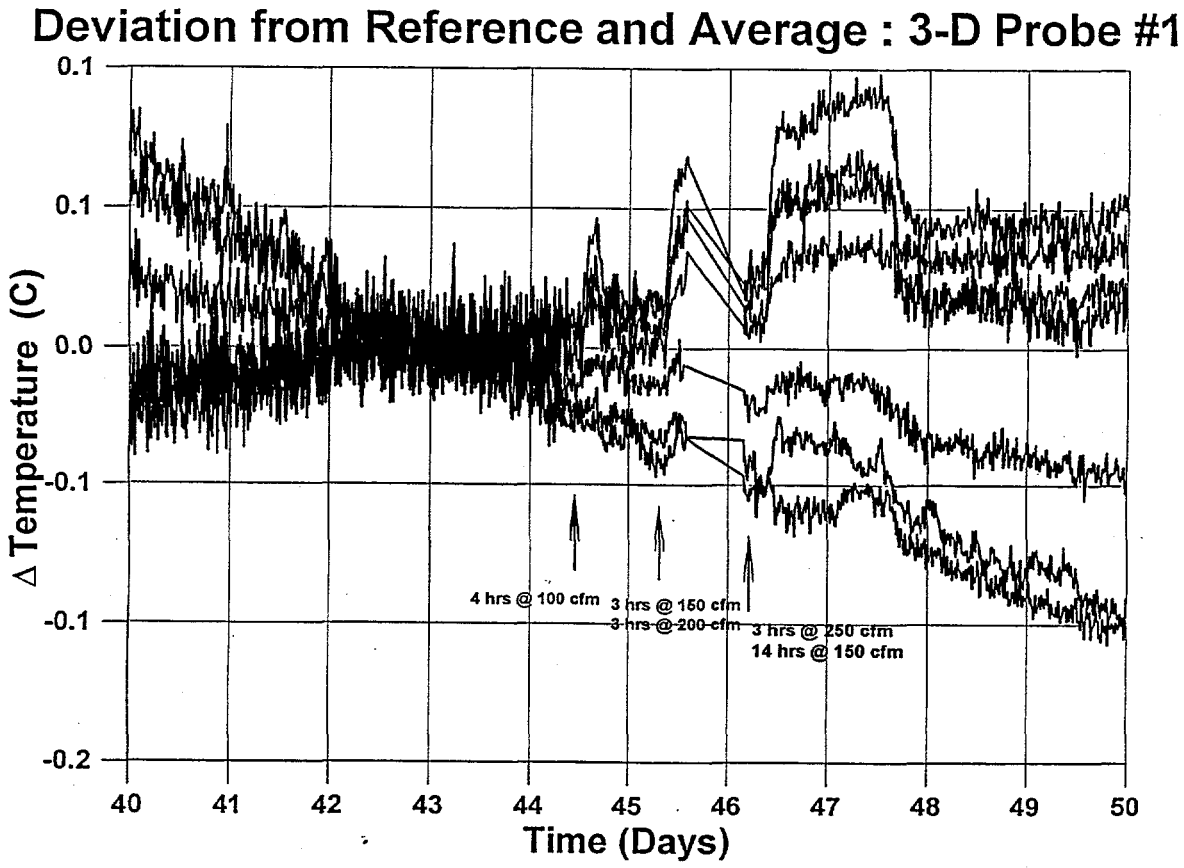

Figure 34: CWLF Test 3-D Probe #1 a) Raw Data
b) Deviation from Reference and Average

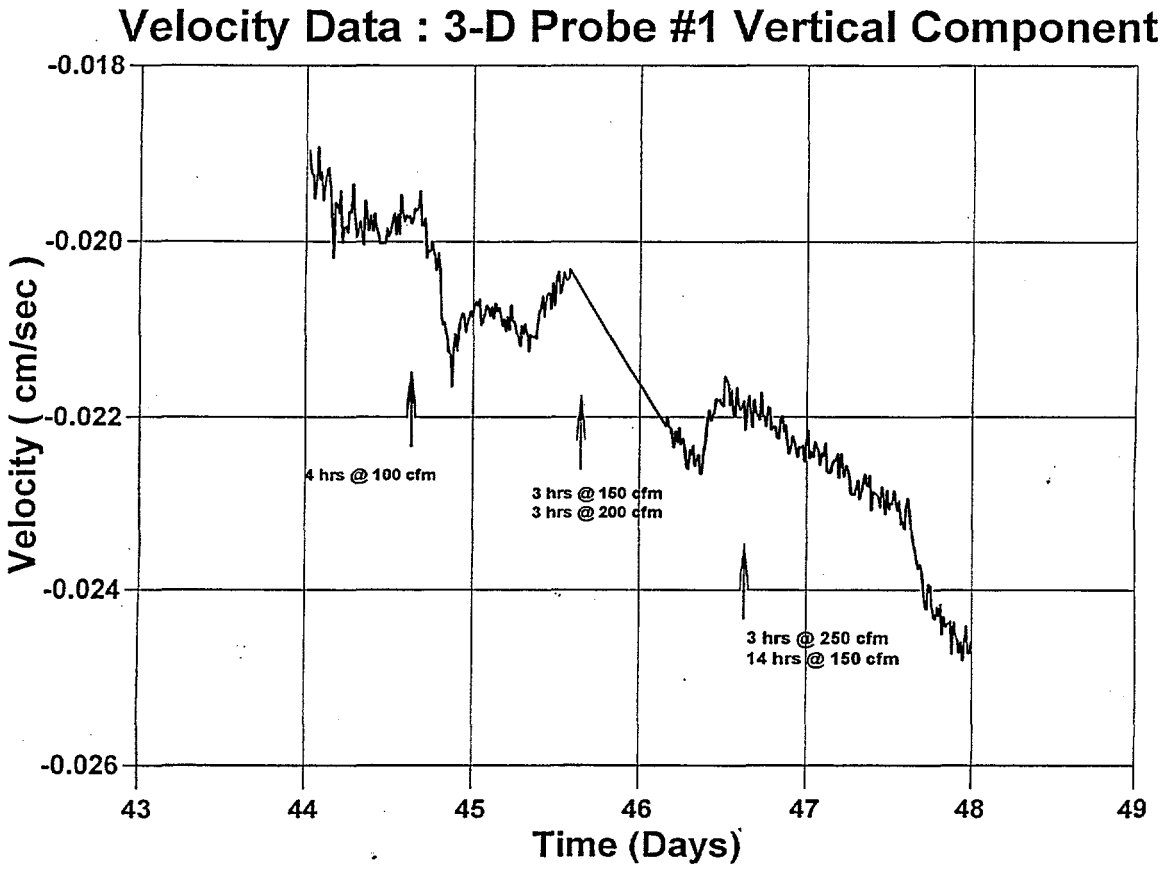

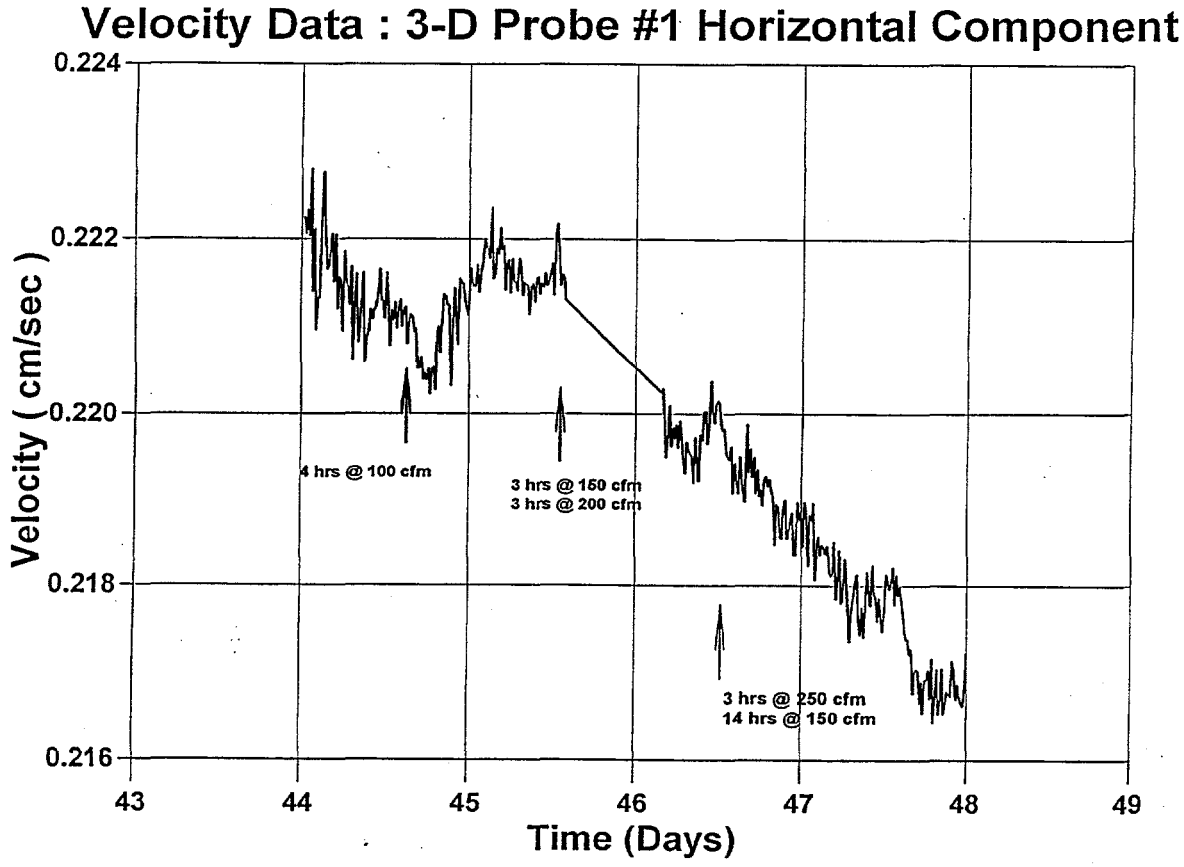

Figure 35: CWLF Test Velocity from 3-D Probe #1 a) Vertical Component b) Horizontal Component

horizontal components of velocity for this probe. Note that the pumping events are hidden in the background noise and long term trends.

Figure 36 shows the raw data and the deviation from reference and average for the second 3-D probe. Notice how much lower the background divergence is. In figure 37, which shows the calculated velocities, the vertical velocity component clearly shows all of the vapor extraction events, and the relative magnitudes are as expected. However, almost all of the flow is vertical, rather than horizontal. From the test geometry and at this depth we would have expected nearly all of the flow to be horizontal. We believe the discrepency is due to flow channeling in the coarse sand used to backfill the probe hole, which greatly increased the apparent vertical flow past the probe.

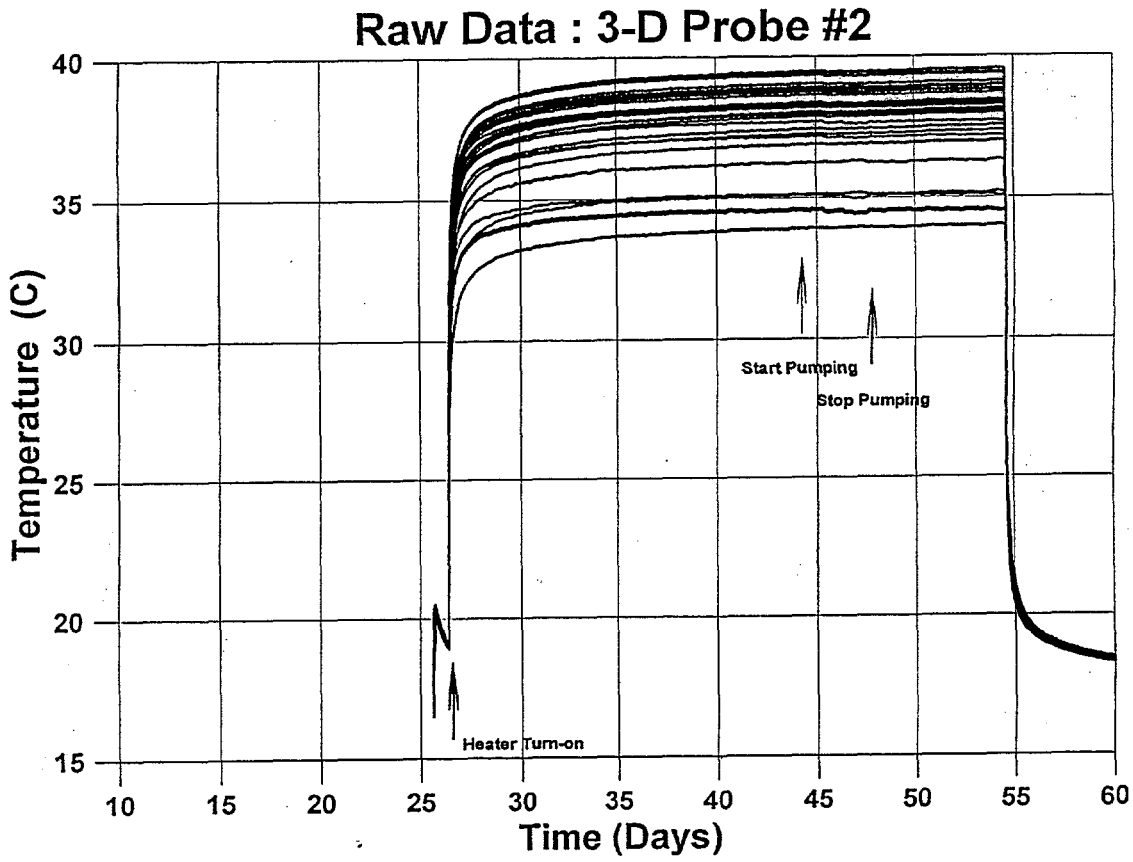

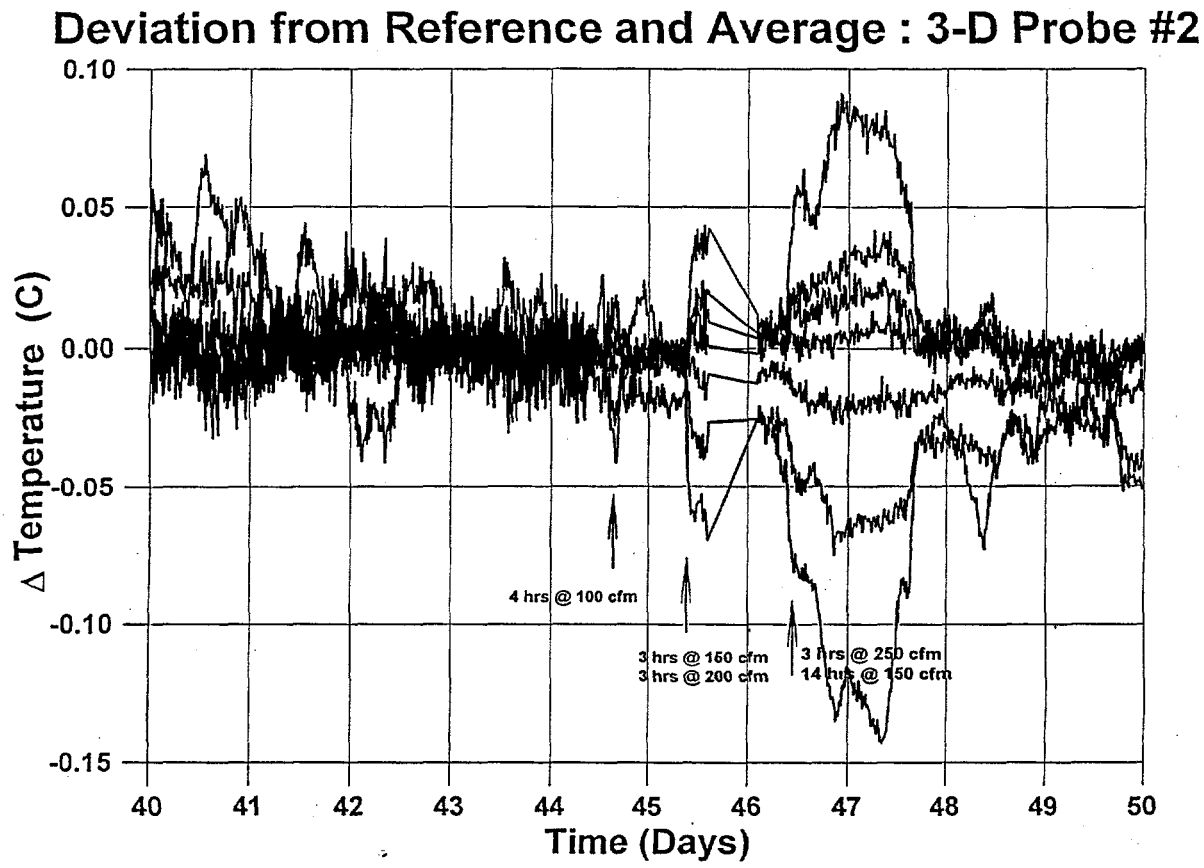

Figure 36: CWLF Test 3-D Probe #2 a) Raw Data
b) Deviation from Reference and Average

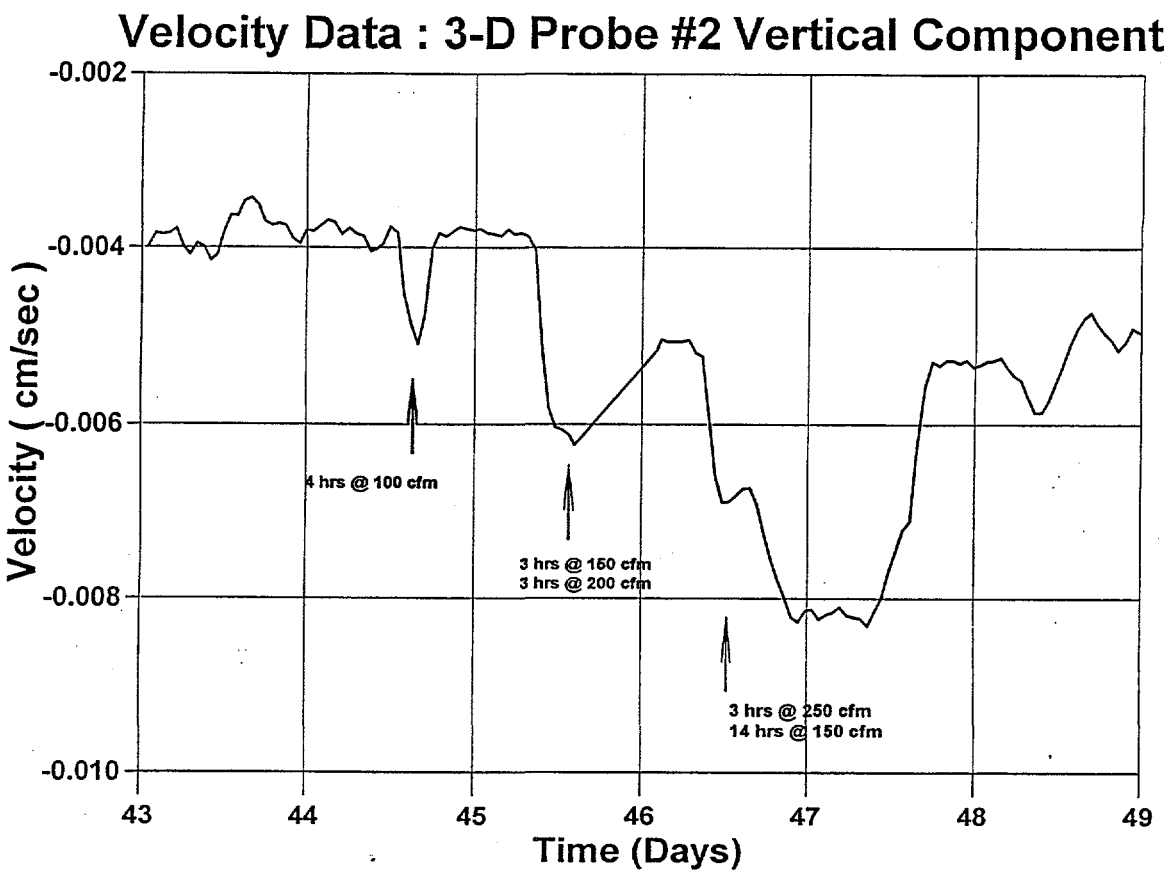

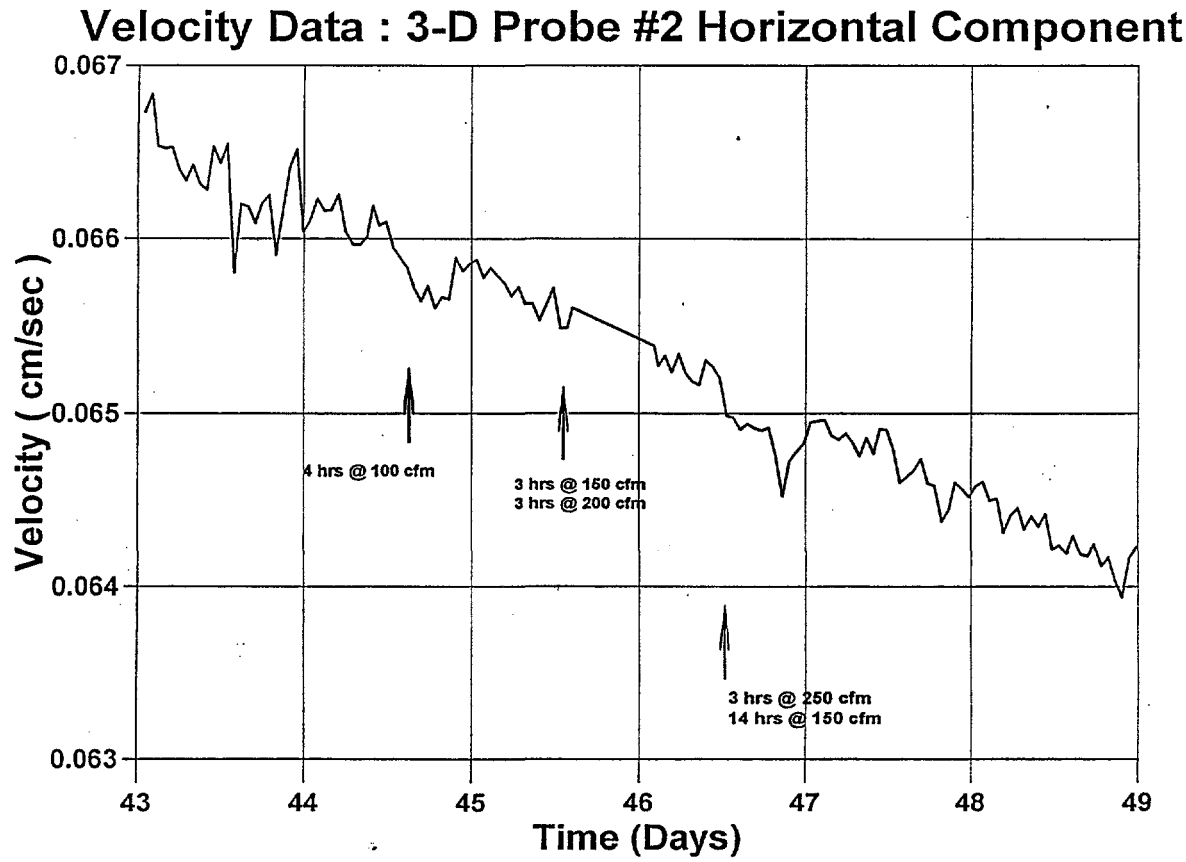

Figure 37: CWLF Test Velocity from 3-D Probe #2 a) Vertical Component b) Horizontal Component

Remediation Site Test

Following the brief field test at the Chemical Waste Landfill, we conducted a two month field test of the flow probes at an active remediation site being operated by Intera. The purpose of deploying these probes at this remediation site was to better characterize the probes and to gain additional field experience with deploying them. It was also hoped that the data from this test would help to validate and refine Intera's predictive model of underground air flow directions and velocities and of the interaction of several nearby wells on the flow from an individual well, in order to help in planning future remediation efforts at other sites.

Figure 38 shows a site map of this location, and Figure 39 shows a cross-section. It contains a combined air sparging and vapor extraction system consisting of 34 wells divided up into 6 branches. For our test purposes we only used the vapor extraction portion of the system. Three 3-D probes and one 1-D probe were installed in the ground, at depths of 5-10 feet, between a group of three vapor extraction wells. These probes are designated at Probe #1, #2, #3 (all 3-D probes) and #4 (1-D probe), and Wells A, B, and C.

The holes for the 3D probes were dug using a conventional auger rig. No water was used during drilling. The dirt removed from the holes was all fine sand, with no rocks or gravel to the full depth. The sand appeared very damp, and it had rained very hard the night before. This site is within a few blocks of the river and the water table is at a depth of 10' to 12' below grade. A micrometer was used to measure a number of representative grains of sand so that we could try to match the permeability when we backfilled the holes. The dirt that had slumped into the holes was removed with an industrial vacuum with a long PVC pipe attached. The probes were centered in the holes using a stainless steel centralizer attached to the PVC pipe above the top of the probe. The holes were then backfilled with very fine sand. The borehole above the probe was backfilled with precision non-shrink grout to prevent vertical air flow. The heater wires and data wires were run underground in PVC pipe to a small shed housing the instrumentation. The heater wires were connected to a power supply and the multiplexer leads to the data logger.

The hole for the 1D probe was drilled using a 1" ships auger and a power hand drill to a depth of ~ 6'. The probe was inserted and we poured fine sand in, but the annulus was so small that it did not fill well, and we also could not pull the probe out. We grouted the top 1' or so of the hole with precision non-shrink grout, and also the surface approximately 18" diameter over the probe.

Figure 40 shows the holes being augered, the sloughed in dirt being removed using a vacuum, a 3-D probe being installed, and the hole for the 1-D probe being drilled. Figure 41 shows one of the 3-D probes with centralizers, and the underground wiring connecting the four probes to the instrumentation shed.

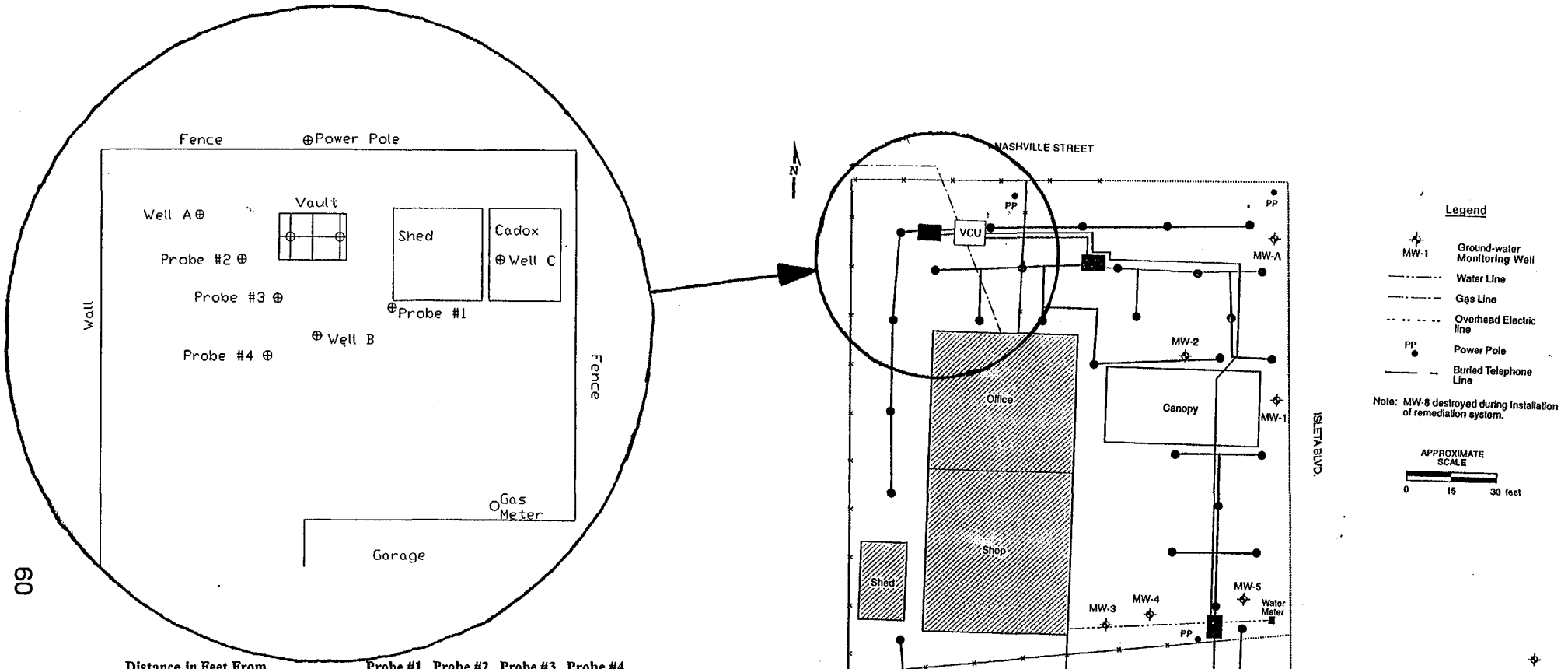

Distance in Feet From	Probe #1	Probe #2	Probe #3	Probe #4
Well A	23.8	6.8	12.6	17.1
Well B	8.9	11.8	6.0	6.0
Well C	13.2	28.9	25.3	28.0
Angles in Degrees				
Original zero on Probe relative to North	145	130	84	NA
Reference angle from Well B to Probe	-105	-5	-49	NA
Relative angle to Well A	45	~180	~180	NA
Relative angle to Well C	183	46	~46	NA

Figure 38: Map of Remediation Test Site

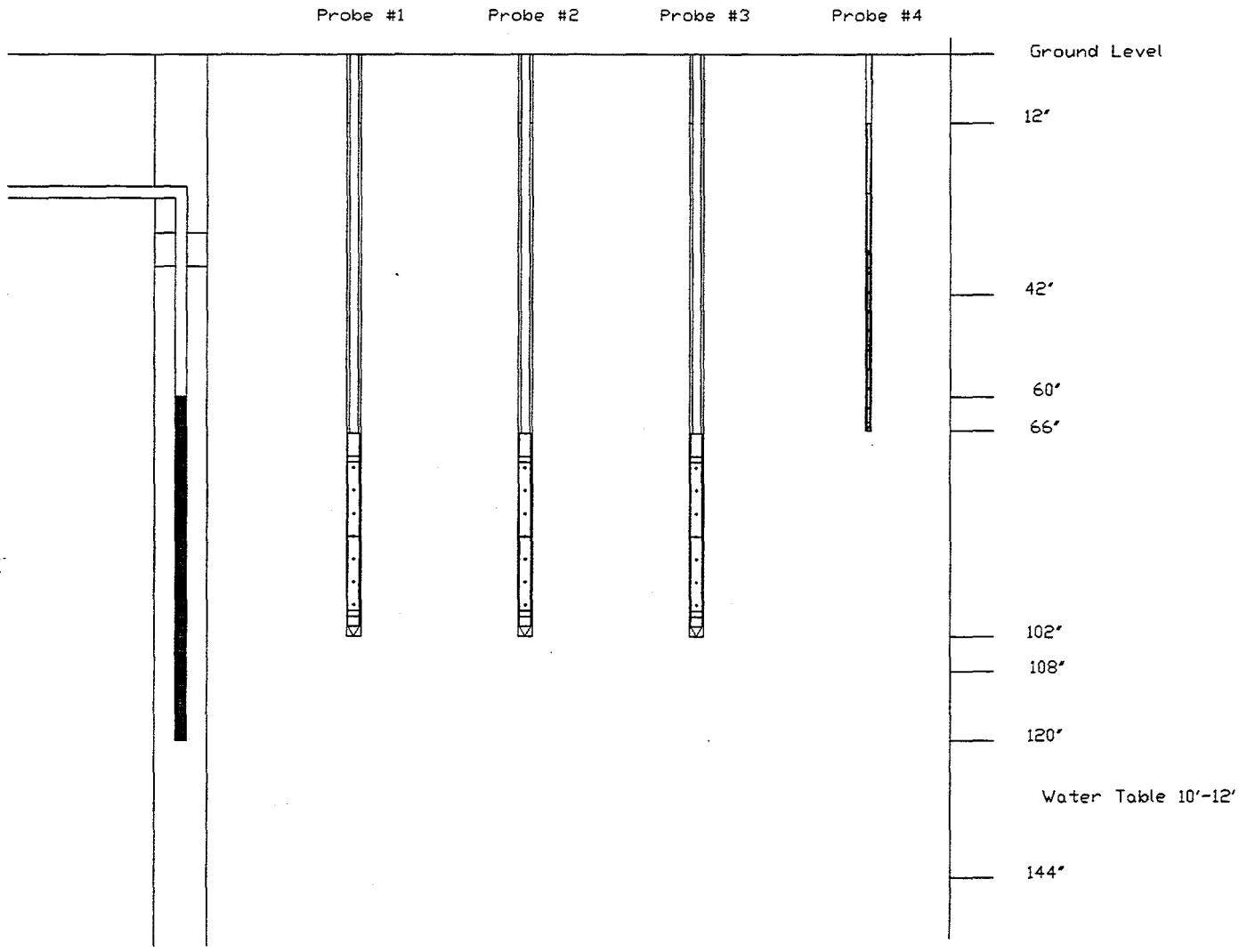

Figure 39: Remediation Site Test—Cross-section of Probes and Wells

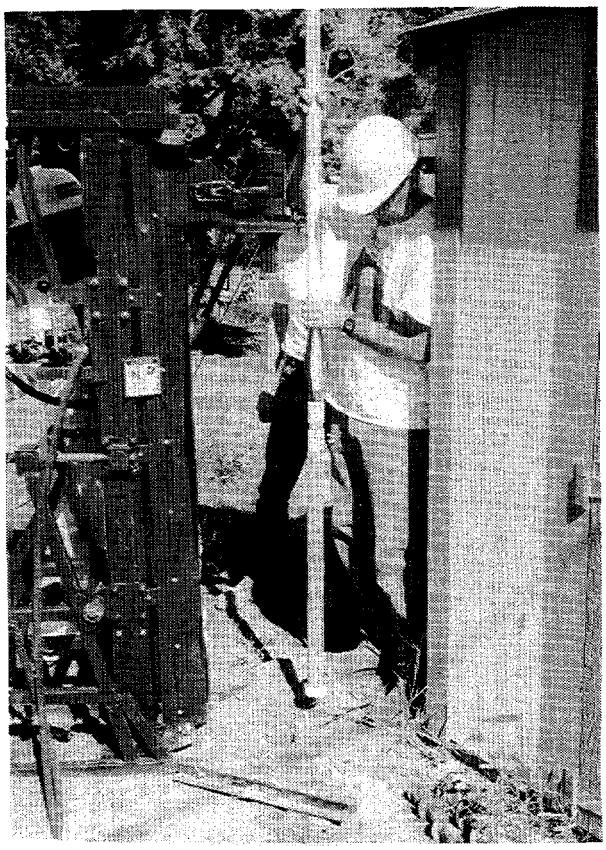

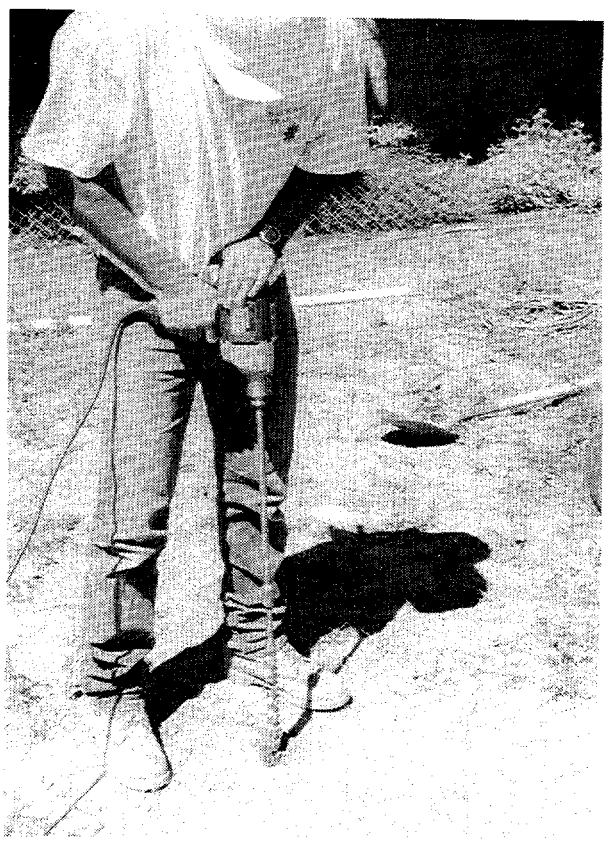

Figure 40: Remediation Site Test a) Augering Hole for 3-D Probe b) Vacuuming Dirt from Hole c) Installing 3-D Probe d) Augering Hole for 1-D Probe

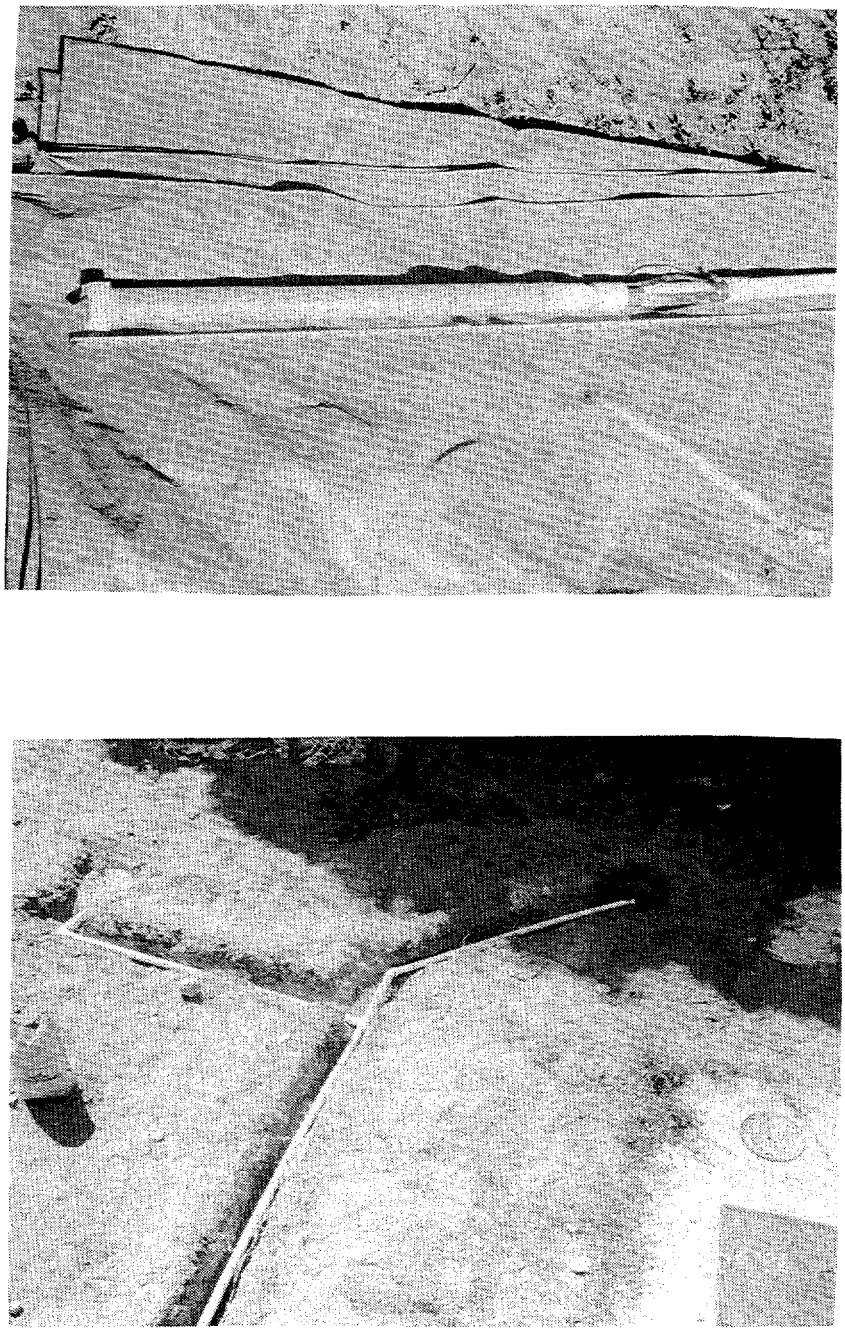

Figure 41: Remediation Site Test a) 3-D Probe with centralizers b) Wiring in PVC pipe to four probes

After the probes were placed in the holes and backfilled, they were allowed to equilibrate for 4 days. The probe heater power was turned ON on 8/28/96, but was turned off again on 8/29/96 because of data logger problems. The probes were allowed to cool down until 8/31/96 and then were turned back on. The 3-D probes were turned on at 12 watts each, and the 1-D probe at 10 watts.

All of the probes exhibited very unusual behavior, very different from our prior laboratory experiments. The temperatures measured by the various thermistors kept slowly wandering and crossing, rather than the probe heating up evenly and reaching a symmetric temperature distribution. This unusual data continued for the first 1-2 days after the heater power was turned on. We speculated that this might be due to the moisture from the rains passing down through the sand, or to the sand near the probe drying out slightly due to the heater and hence changing its thermal conductivity.

On 9/3/96 the vapor extraction equipment was turned ON. We could control the air flow from groups of wells on the same branch, but not from individual wells. Also, we could not turn off all but one of the branches due to air intake requirements on the vapor extraction pumps. However, we had located the probes between three wells on three different branches and the other wells were far enough away that they should not have had any effect. With 4 of the six branches ON, the inlet vacuum was 22" of water and the total air flow coming from 26 of the 34 wells was 250 CFM, for an average air flow of 10 CFM per well.

On 9/5/96 3-D probe #3 was turned OFF and allowed to cool down to ambient. It was turned back ON on 9/10/96 to see if the unusual startup behavior we had initially seen on all of the probes would occur again, or if it could have been due to the heavy rains or some other factor. When probe #3 was turned back ON, it exhibited the same unusual behavior as the first time, with the temperatures slowly wandering on several of the channels. On 9/17/96 the vapor extraction system shut itself down, possibly due to lightning problems. On 9/27/96 the vapor extraction system was turned back ON, with well B ON and well A OFF. This time there were 20 of 34 wells ON, with an average flow per well of 13 CFM.

On 10/11/96 the heater on the 1-D probe was turned OFF so that its thermistors could be used to monitor the long term temperature trends which we were seeing on all of the probes. Well B was turned OFF and well A was turned ON. On 10/21/96 the vapor extraction system shut itself down. It was allowed to remain off, but we continued to record data. On 11/7/96 all of the probes were turned OFF, as was the data recorder, and the experiment was ended.

We had planned on extracting vapor from all three wells, one well at a time, for approximately 1 week each, over a period of two months. After the system had run for approximately two weeks at a fixed level, the results were still somewhat puzzling. We could definitely see a change in signal when the flow was turned on, the signal was present on all four probes, and it was strongest on the probes near the extraction well. However, the temperatures measured by the probes "wandered" in a rather random fashion at heater turn-on continued to diverge over that two week period. As a result, even though we saw the start of vapor extraction, we were not able to

calculate a believable velocity (for example, on one probe, the bottom of the probe showed flow in one direction, the top of the same probe showed flow in the opposite direction).

We speculated that part of this was due to changes in soil moisture content with the numerous heavy rains we have had from the day before probe installation until the present. Another possibility was that the heat from the probe was modifying the local moisture content of the ground immediately surrounding the probe, and hence modifying the local thermal properties of the ground surrounding the probe. This effect would vary over the length of the probe since the temperature varies over the length of the probe. All of our laboratory testing was conducted in barrels of dry sand. Another possibility was that the seasonal temperature changes in the ground due to a cold snap that began about the same time as the probe emplacement was being superimposed on the flow temperature distribution.

Due to the non-stable readings we were seeing, we decided to continue monitoring that same flow rate and well for an additional week, and then to switch to one of the other two nearby wells and run for approximately three weeks. Following the end of the vapor extraction period, we continued to record for several weeks to get a second "background, no-flow" reading to compare with our initial readings. We ended up not using well C because of the long time spent monitoring wells A and B, and because well C was the farthest from the probes and hence would produce the smallest signals.

Sequence of Events:

Julian Day	Date	Time	Event
237	8/24/96	3:00 p.m.	Three 3-D and one 1-D probes installed
240	8/27/96	8:30 a.m.	Flow turned ON. Well C ON, A and B OFF
240	8/27/96	1:50 p.m.	Flow turned OFF
241	8/28/96		Heaters turned ON
242	8/29/96		Heaters turned OFF
244	8/31/96		3-D heaters ON at 12 watts, 1-D ON at 10 watts
247	9/3/96	2:30 p.m.	Flow ON at well A, OFF at well B (26 of 34 wells ON)
249	9/5/96		3-D probe #3 turned OFF
254	9/10/96		3-D probe #3 turned back ON
261	9/17/96	6:00 p.m.	Flow OFF (automatic shut down)
271	9/27/96	5:30 p.m.	Flow OFF at well A, ON at well B
285	10/11/96	3:15 p.m.	Probe #4 (1-D) OFF, well A ON, well B OFF
295	10/21/96		Flow OFF (automatic shut down)
312	11/7/96		All probes OFF, end of experiment

Figure 42 shows the raw data from probe #2. This probe showed by far the best data. All of the vapor extraction events are clearly visible in the raw data. Figure 43 shows the velocities measured by probe #2 and probe #3. The velocity has been seperated into components in line with the probe and well A, and perpendicular to that line. As can be seen, all of the events are clearly visibile in the velocity data on the component in-line with well A, while the velocity

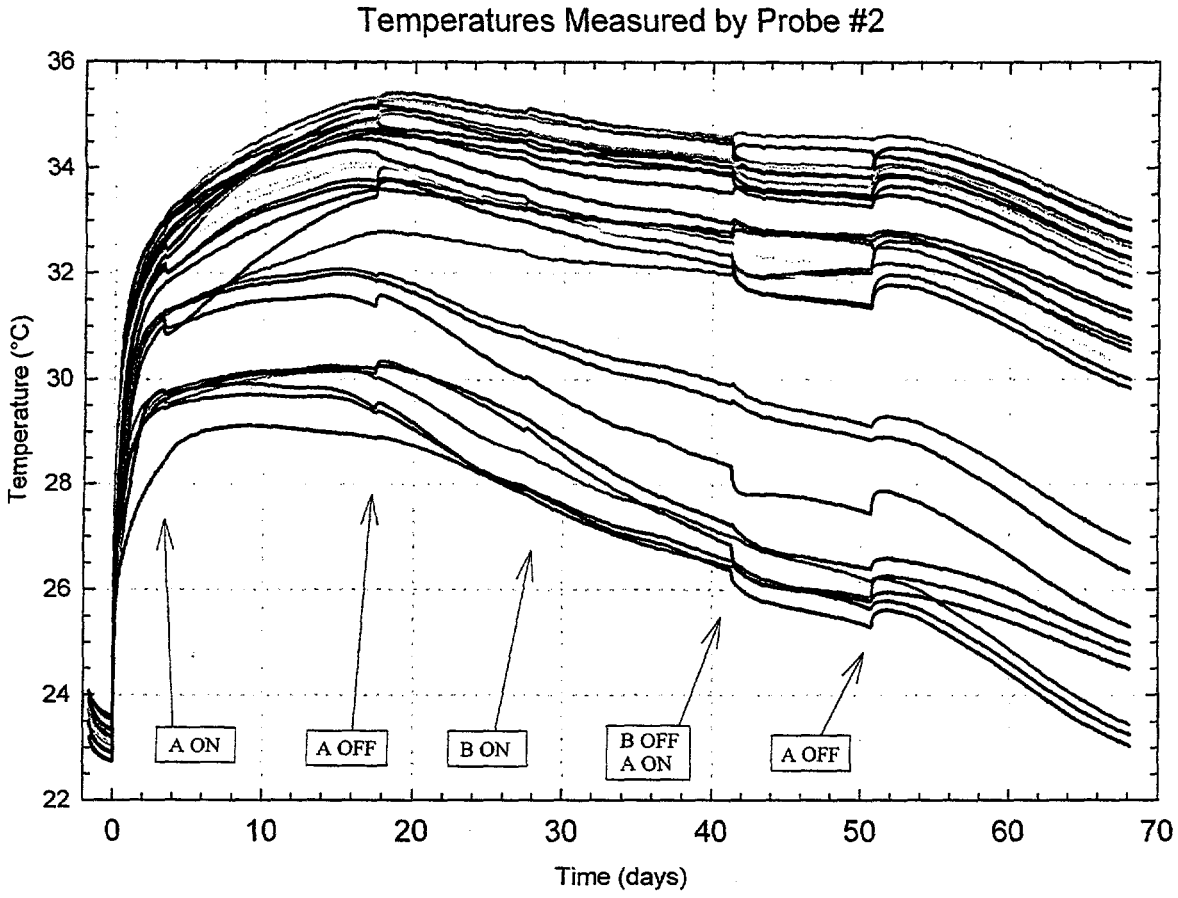

Figure 42: Remediation Site Test—Raw Temperatures Measured by Probe #2

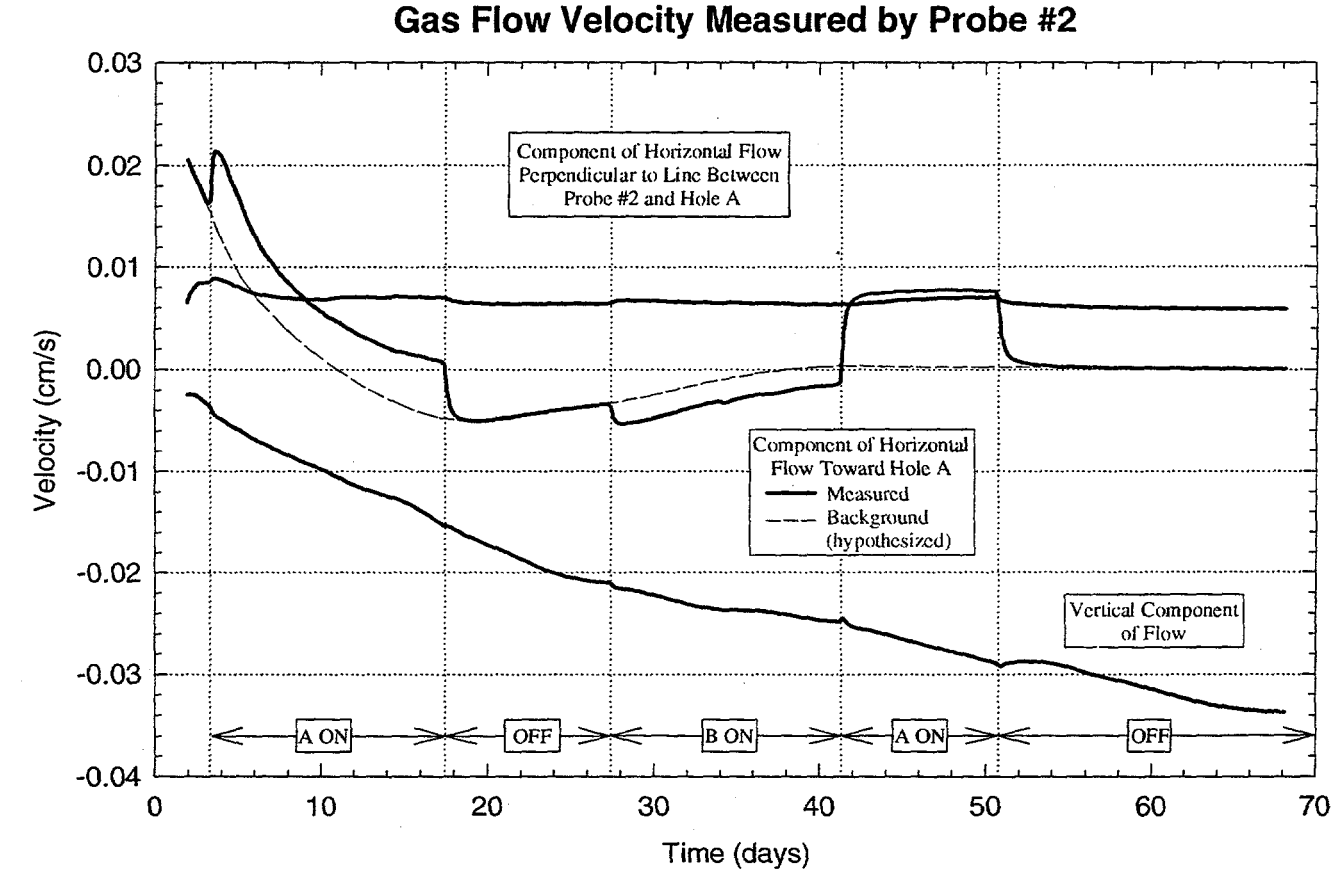

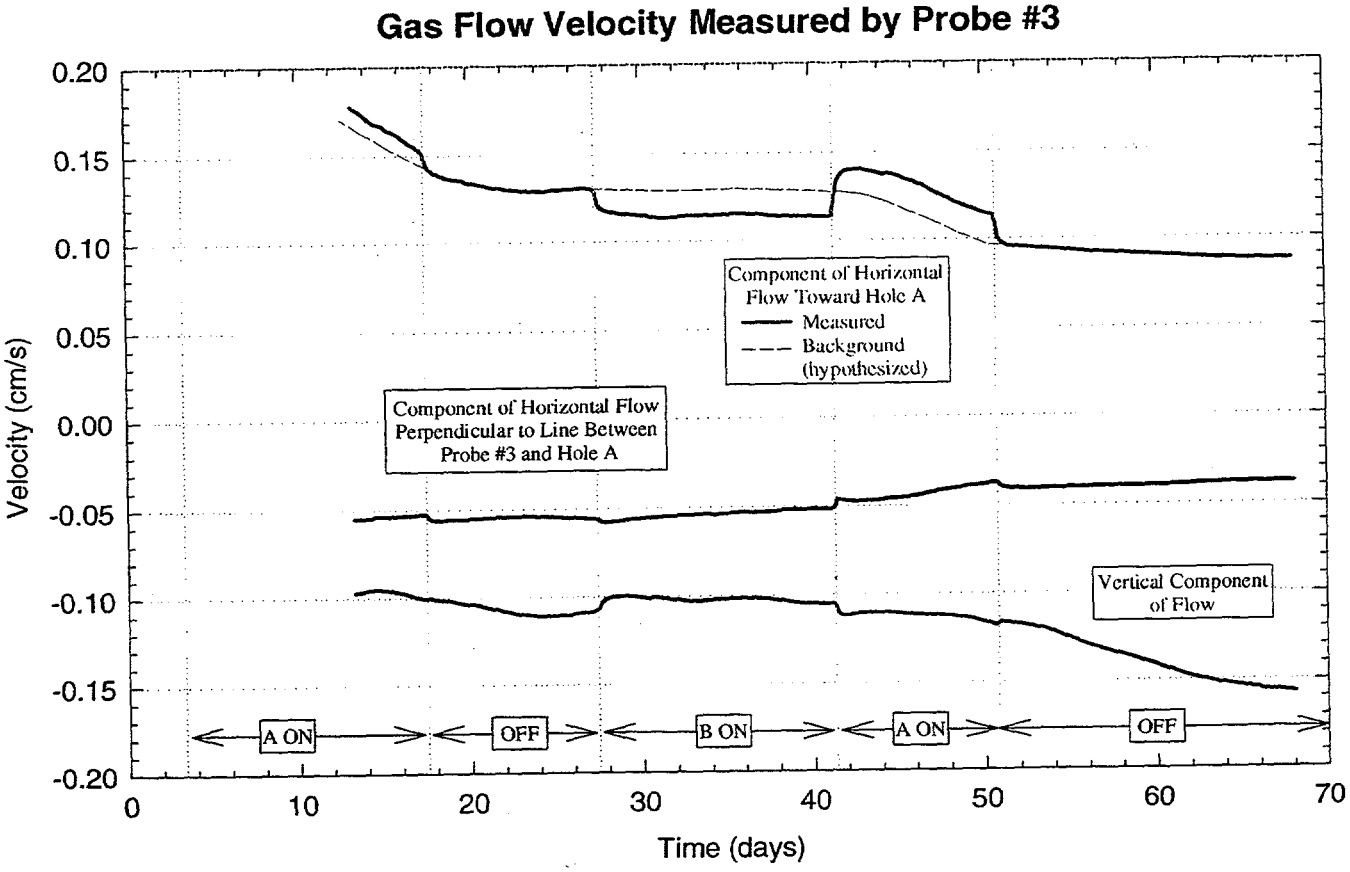

Figure 43: Remediation Site Test a) Gas Flow Velocity Measured by Probe #2 b) Gas Flow Velocity Measured by Probe #3

component perpendicular to the well and the verical velocity component remain essentially unchanged. This is as would be expected, and was very encouraging. However, there are also long term trends in the data, even when the flow is OFF or is unchanging with time. These are shown by the hypothesized dashed line in the figures. We do not know what is causing these long term changes. We were not able to correlate them with hourly weather data, including precipitation, air temperature, and air pressure.

Results

1. Modeling: Indicates there is preferential flow channeling near the probe due to perturbations caused by probe emplacement hole.
2. Laboratory tests: There was excellent agreement between air velocities calculated from the probe data and known air velocities under controlled laboratory experiments. The minimum perceptible change in flow is approximately 0.001 cm/sec. The probe is accurate in laboratory flow conditions to within ~30% over a range of 0.01 to 1 cm/sec.
3. Chemical Waste Land Fill Test: All of the vapor extraction events are clearly visible on this short term field test. However, the test was too short for the temperatures to stabilize. The test did show that probe emplacement technique is critical.
4. Remediation Site Test: All of the vapor extraction events are clearly visible. The velocity signals are superimposed on very large, long-term background trends in the signal, possibly due to changes in soil moisture content or seasonal ground temperature variations, making interpretation difficult. However, the plots of gas velocity along the line between the probe and the well, vs. perpendicular to that line, show that a reasonable estimate of gas flow velocity can be obtained.

Conclusions

1. The probe is very sensitive and quite accurate in controlled, laboratory experiments in dry homogenous media at flow rates of 0.00 to 1 cm/sec.
2. The probe response is very slow (on the order of 2-3 days to stabilize).
3. The probe is not sensitive enough to monitor air flows induced by atmospheric pressure changes.
4. The probe is sensitive to long term environmental effects unrelated to the air flow, including seasonal temperature changes and possibly changes in formation water content near the probe.
5. The probe is sensitive enough to pick up changes in vapor extraction rates in remediation setups like that described in the report at distances up to approximately 20'.

References

1. Ballard et al, "The In Situ Permeable Flow Sensor: A Device for Measuring Groundwater Flow Velocity", Sandia Report SAND93-2765.
2. Ballard, S., "The in situ permeable flow sensor: a groundwater flow velocity meter", Ground Water, Vol. 34, No. 2, March - April 1996.
3. Romero, L. A., "Forced Convection past a slender body in a saturated porous medium", SIAM Journal of Applied Mathematics, Vol. 55, No. 4, pp. 975-985, August 1995.
4. Pruess, K. (1991) "TOUGH2—A General Purpose Numerical Simulator for Multiphase Fluid and Heat Flow", LBL-29400 (UC-251) Lawrence Berkeley Laboratory, 102 pp.

Appendix

Appendix A: The Temperature Distribution Outside The Heated Section
Appendix B: An Analysis of a Groundwater Probe with a Core of Highly Conductive Material
Appendix C: Point Source Probe Summary

THE TEMPERATURE DISTRIBUTION OUTSIDE THE HEATED SECTION

L.A. ROMERO *

1. The Slender Body Approximation . We will use the following notation

- R is the radius at the center of the probe
- $2L$ is the length of the probe
- $\epsilon = R/L$ is the aspect ratio of the probe
- $\hat{z} = z/L$ is the dimensionless distance along the axis of the probe
- $Rh(\hat{z})$ is the radius of the probe as a function of $\hat{z}$
- $Qg(\hat{z})$ is the flux of heat per unit area as a function of $\hat{z}$.
- $\hat{T} = T\frac{k}{QR}$ is the dimensionless temperature

Our slender body analysis shows that for a purely vertical flow the dimensionless temperature on the surface of the probe is given by

$$\hat{T}(h(\hat{z}),\hat{z}) = -h(\hat{z})g(\hat{z})ln\left(h(\hat{z})\epsilon\right) + e^{\frac{1}{2}Pe\,\hat{z}}G(\hat{z}), \tag{1a}$$

where,

$$G(\hat{z}) = H(\hat{z})ln\left(4(1-\hat{z}^2)\right) + \int_{-1}^{1} \frac{H(\xi)e^{-\frac{1}{2}Pe|\hat{z}-\xi|} - H(\hat{z})}{|\,\hat{z}-\xi\,|}d\xi. \tag{1b}$$

and

$$H(\hat{z}) = \frac{1}{2}e^{-\frac{1}{2}\,Pe\hat{z}}h(\hat{z})g(\hat{z}) \tag{1c}$$

The equation (1a) is valid provided $\epsilon << 1$ and $\epsilon Pe << 1$.

* Applied and Numerical Mathematics Division, Sandia National Laboratories ,Albuquerque N.M. 87185

2. The Temperature Distribution Outside the Heated Section. We will assume that the radius $h(\hat{z})$ is uniform on the whole probe, and that the heat flux $g(\hat{z})$ is uniform for $\mid \hat{z} \mid < \delta$. In this case the temperature on the surface of the probe outside of the heated section is given by

$$\hat{T}(\hat{z}) = \frac{1}{2}\int_{-\delta}^{\delta} \frac{e^{Pe/2(\hat{z}-\xi)}e^{-Pe/2|\hat{z}-\xi|}}{\mid \hat{z}-\xi \mid} d\xi \tag{2}$$

If $\hat{z} > \delta$ we have

$$\hat{T}(\hat{z}) = \frac{1}{2} ln\left(\frac{\delta+\hat{z}}{\hat{z}-\delta}\right) \quad for \;\; \hat{z} > \delta \tag{3a}$$

When $\hat{z} < -\delta$ we have

$$\hat{T}(\hat{z}) = \frac{1}{2}\int_{-Pe(\delta+\hat{z})}^{Pe(\delta-\hat{z})} \frac{e^{-t}}{t} \quad for \;\; \hat{z} < -\delta \tag{3b}$$

You already have a routine that evaluates the integral

$$A(z) = \int_0^z \frac{1-e^{-t}}{t} dt$$

In terms of this integral we can write

$$\hat{T}(\hat{z}) = \frac{1}{2}\left(ln\left(\frac{z-\delta}{z+\delta}\right) + A(-Pe(z+\delta)) - A(Pe(\delta-z))\right)$$

3. The Point Source Solution. When $\delta << 1$, the solution given in the last section is very close to the point source solution in an infinite medium. It is easily verified that

$$T = \frac{Q_T}{4\pi kr} e^{-\frac{U_T}{2\kappa}(1-cos(\theta))}$$

satisfies

$$\kappa \nabla^2 T = (0, 0, U) \cdot \nabla T$$

and satisfies

$$\lim_{R \to 0} -k \int_{r=R} \frac{\partial T}{\partial n} ds = Q_T$$

If $\delta << 1$ in the last section, we might expect the solution to approach the point source solution. In this case the total amount of heat generated by the probe is $4\pi\delta RLQ$. It follows that we should put $Q_T = 4\pi QRL\delta$ in the point source soution.

In terms of our dimensionless variables from the last section, we have

$$\hat{T} = \frac{\delta}{\hat{z}} \ for \ \hat{z} > 0$$

and

$$\hat{T} = -\frac{\delta}{\hat{z}} e^{-Pe\hat{z}} \ for \ \hat{z} < 0$$

An examination of the solution in eqn. (2) of the last section shows that this agrres with the point source solution when $\delta << 1$.

4. The Point Source for a Cross Fl;ow. The point source solution remains valid no matter what direction the flow is in. However, In this section we discuss the nature of the solution when we do not take our measurements on an axis that is aligned with the flow. Suppose that rather than taking measurements along the axes $\theta = 0$ and $\theta = \pi$, we take our measurements along $\theta = \theta_0$ and $\theta = \theta_0 + \pi$. In this case we get

$$T(r,\theta_0) = \frac{Q_T}{r} e^{-Pe/2r(1-cos(\theta_0))}$$

and

$$T(r,\theta_0) = \frac{Q_T}{r} e^{-Pe/2r(1+cos(\theta_0))}$$

Although we cannot determine the absolute direction of the flow from these measurements, we can in theory determine the inclination of the flow to the axis that we take our measurements on.

5. Oscillatory Behavior. Suppose the source of heat is oscillating periodically with time. In this case we must consider the time dependent equations

$$\frac{\partial T}{\partial t} + U\frac{\partial T}{\partial z} = \kappa \nabla^2 T$$

Tet $T = T^* e^{\frac{Uz}{2\kappa}}$. A direct substitution shows that

$$\frac{1}{\kappa}\frac{\partial T^*}{\partial t} + \frac{U^2}{4\kappa^2} T^* = \nabla^2 T^*$$

If the flow is periodic, we can write

$T^* = e^{i\omega t} F$

and hence,

$$F\left(\frac{i\omega}{\kappa} + \frac{U^2}{4\kappa^2}\right) = \nabla^2 F$$

This has the solution

$$F = \frac{Q_T}{4\pi r} e^{r(i\omega/\kappa + U^2/(4\kappa^2))^{1/2}}$$

The temperature T associated with this solution is

$$T = \frac{Q_T e^{i\omega t}}{4\pi r} e^{-r\alpha(\theta,\omega,U,\kappa)}$$

where

$$\alpha(\theta,\omega,U,\kappa) = (\frac{i\omega}{\kappa} + \frac{U^2}{4\kappa^2})^{1/2} - \frac{U cos(\theta)}{2\kappa}$$

This solution clearly corresponds to a point source of heat that is oscillating periodically. We get a physically realizable solution by taking the real part of this solution. There is alot of information in this temperature distribution. Not only do we get information from the spatial variation in temperature, we also get information from the temporal variation in temperature. In particular, the tempoaral variation at any point in space can be written as

$$T = G(r,\omega,U,\kappa,\theta) cos(\omega t - r\beta(U,\omega,\kappa))$$

where

$$\beta(U,\omega,\kappa) = \frac{U}{2\kappa} Im\left(1 + 4i\omega\kappa/U^2\right)^{1/2}$$

Note that the phase shift increases linearly with r, and is independent of θ.

The parameter

$$\Gamma = \frac{4\omega\kappa}{U^2}$$

is crucial in determining the behavior of the system. If $\Gamma << 1$ we have

$$\beta \approx \omega/U$$

In this case the phase shift is independent of the diffusivity.

On the other hand, if $\Gamma >> 1$, we have

$$\beta \approx \sqrt{\frac{\omega}{2\kappa}}$$

In this case the phase shift is independent of the velocity and can be used to determine the diffusivity.

An Analysis of a Groundwater Probe with a Core of Highly Conducting Material

L.A. Romero *

February 28, 1996

1 Introduction

Consider the following set of dimensionless equations.

$$\nabla^2 T = Pe\frac{\partial T}{\partial z} \quad for \quad r > \epsilon \tag{1a}$$

$$\nabla^2 T = 0 \quad for \quad \epsilon_0 < r < \epsilon \tag{1b}$$

$$\frac{\partial T(\epsilon_0, z)}{\partial r} = \epsilon_k/\epsilon_0 \quad for \quad |\, z \,| < \delta \tag{1c}$$

$$\frac{\partial T(\epsilon_0, z)}{\partial r} = 0 \quad for \quad |\, z \,| > \delta \tag{1d}$$

*Applied and Numerical Mathematics Division, Sandia National Laboratories ,Albuquerque N.M. 87185

$$T(\epsilon - 0, z) = T(\epsilon + 0, z) \tag{1e}$$

$$\frac{\partial T(\epsilon - 0, z)}{\partial r} = \epsilon_k \frac{\partial T(\epsilon + 0, z)}{\partial r} \tag{1f}$$

$$T(r, z) \to 0 \ \ as \ \ r^2 + z^2 \to \infty \tag{1g}$$

These are the dimensionless equations for vertical flow past an infinite cylinder in a porous media that has an aspect ratio of $\epsilon = L/R$, and that has an inner region of highly conducting material. The ratio of the conductivity of the porous medium to the inner core is given by

$$\epsilon_k = \frac{k_m}{k_c}$$

where k_m is the conductivity of the porous medium, and k_c is the conductivity of the inner core. The ratio of the inner diameter of the core to its outside diameter is given by

$$\epsilon_R = \frac{\epsilon_0}{\epsilon}$$

The parameter δ is really unnecessary in this formulation, but it is a remnant of the previous analysis,

If ϵ_k is too small, the temperature distribution inisde the core will be nearly uniform both axiallly and radially. We now argue that if ϵ is also small, it is possible to have the temperature distribution be nearly uniform radially, but still be nearly the same as if the core did not exist.

2 Observations Using Perturbation Theory

In order to get a basic feel for how small the parameter ϵ_k must be in order to start influencing the temperaure profile, we will consider the simpler problem where the Peclet number is zero. We will analyze this problem assuming that ϵ is very small. In my previous slender body analysis I did a formal perturbation expansion by making the radial variable dimensionless using the radius R, and the axial variable dimensionless using the length L. For the sake of brevity I will not carry out such a formal perturbation analysis here, however such an analysis is the motivation behind all of my remarks.

Assuming that ϵ is very small, we might expect that we can ignore the axial temperature gradients relative to the radial gradients. This is the basis of the slender body analysis . If we ignore all axial gradients in our problem we end up with a two dimensional radially symmetric problem where z is merely a parameter. Under this assumption we find that for $\mid z \mid < \delta$ we have

$$T(r,z) = \begin{cases} \epsilon_k ln(r) + F(z) + (1-\epsilon_k) ln(\epsilon) & for \;\; \epsilon_0 < r < \epsilon \\ ln(r) + F(z) & for \;\; r > \epsilon \end{cases}$$

and for $\mid z \mid > \delta$we have

$$T(r,z) = F(z) \;\; for \;\; r > \epsilon_0$$

Note that in this approximation, the temperature exterior to the body has the

same form as if there were no inner core. As in the previous slender body solution, the function $F(z)$ is determined by matching to the solution valid for large values of r (compared to ϵ). In this approximation, the function $F(z)$ and hence the temperature on the surface of the probe will be the same as if no inner core existed. We now check to see if the assumptions we made in getting this solution were in fact valid.

In deriving this solution we assumed that the terms in $\frac{1}{r}\frac{\partial}{\partial r}\left(r\frac{\partial T}{\partial r}\right)$ was large compared to $\frac{\partial^2 T}{\partial z^2}$. We see that this will be the case for our solution provided

$$\epsilon_k/\epsilon^2 >> \frac{\partial^2 F}{\partial z^2}$$

If we assume that $\frac{\partial^2 F}{\partial z^2}$ is order one, this means that our solution will be valid provided that

$$\epsilon_k >> \epsilon^2$$

This would imply that the inner core would not effect the temperature profile until the ratio of the conductivities was very high. Unfortunately, figure 1) shows that as $\epsilon \rightarrow 0$, the derivatives of T (and hence F become very large at the end of the heated section. This reasoning implies that we expect to get into trouble where the heated section ends.

I have not done a thorough asymptotic analysis of this problem, but numerical results seem to indicate that the proper condition is more like

$$\epsilon_k > \epsilon$$

in order to be able to ignore the inner core.

3 Numerical Computations

We will numerically compute the solution to eqns. (2) by analytically determining the Fourier transform

$$\hat{T}(r,\alpha) = \int_{-\infty}^{\infty} T(r,z)e^{-i\alpha z}dz$$

and then numerically computing the inverse transform. The Fourier transformed equations satisfy

$$\frac{1}{r}\frac{\partial}{\partial r}\left(r\frac{\partial \hat{T}}{\partial r}\right) = \alpha^2\hat{T} + i\alpha Pe\hat{T} \quad for \quad r > \epsilon \tag{2a}$$

$$\frac{1}{r}\frac{\partial}{\partial r}\left(r\frac{\partial \hat{T}}{\partial r}\right) = \alpha^2\hat{T} \quad for \quad \epsilon_0 < r < \epsilon \tag{2b}$$

$$\frac{\partial \hat{T}(\epsilon_0,\alpha)}{\partial r} = \epsilon_k/\epsilon_0\,(2sin(\alpha\delta)/\alpha) \tag{2c}$$

$$\hat{T}(\epsilon - 0,\alpha) = \hat{T}(\epsilon + 0,\alpha) \tag{2d}$$

$$\frac{\partial \hat{T}(\epsilon - 0,\alpha)}{\partial r} = \epsilon_k \frac{\partial \hat{T}(\epsilon + 0,\alpha)}{\partial r} \tag{2e}$$

$$\hat{T}(r,\alpha) \rightarrow 0 \ \ as \ \ r \rightarrow \infty \tag{2f}$$

These equations have the solution

$$\hat{T}(r,\alpha) = \begin{cases} A(\alpha)K_0(\alpha r) + B(\alpha)I_0(\alpha r) & for \ \ \epsilon_0 < r < \epsilon \\ C(\alpha)K_0(\sqrt{\alpha^2 + i\alpha Pe}r) & for \ \ r > \epsilon \end{cases} \tag{3}$$

Here K_0 and I_0 are modified Bessel functions of the first and second kind. These functions were evaluated using standard mathematical libraries. In order to satisfy the boundary conditions $A(\alpha)$,$B(\alpha)$, and $C(\alpha)$ must satisfy the following system of linear equations.

$$-\alpha A(\alpha)K_1(\alpha\epsilon_0) + \alpha B(\alpha)I_1(\alpha\epsilon_0) = \epsilon_k/\epsilon_0 \, (2sin(\alpha\delta)/\alpha) \tag{4a}$$

$$A(\alpha)K_0(\alpha\epsilon) + B(\alpha)I_0(\alpha\epsilon) = C(\alpha)K_0(\sqrt{\alpha^2 + i\alpha Pe}\epsilon) \tag{4b}$$

$$-\alpha A(\alpha)K_1(\alpha\epsilon) + \alpha B(\alpha)I_1(\alpha\epsilon) = -\sqrt{\alpha^2 + i\alpha Pe}\epsilon_k K_1(\sqrt{\alpha^2 + i\alpha Pe}\epsilon) \tag{4c}$$

Here we have sued the fact that the derivative of K_0 is $-K_1$, and that the derivative of I_0 is I_1. We solve this sytem of equations in order to determine $A(\alpha)$, $B(\alpha)$, and $C(\alpha)$. Once we do this we know the Fourier transform analytically, and we can compute the inverse Fourier transform by numerically evaluating the integral

$$T(r,z) = \frac{1}{2\pi}\int_{-\infty}^{\infty} e^{i\alpha z}\hat{T}(r,\alpha)d\alpha$$

Figures 2 and 3 show the results of these numerical calculations when $Pe = 0$.. We see that for a given value of ϵ_k, the core has less of an effect when the aspect ratio ϵ is smaller. We further see that the region of trouble occurs near the boundary between the heated and unheated regions ($\delta = .8$).

Figures 4 and 5 show the same calculations with $Pe = .5$. In these figures we plot the temperature differences between symmetrically placed points on the probe. It should be noted that when $\epsilon_k = .01$ the temperature profile differs considerably from the profile with $\epsilon_k = 1$, however, the temperature is still far from being uniform axially. It is very likely that the probe would still operate well in this situation, but that you would have to use a different solution than my previous slender body analysis. As you can see, I have a numerical code that predicts the temperature in this case. The code currently gives one data point in under a second of computing time on a SUN workstation. I am confident that I could either greatly speed this code up, or come up with an analytical solution that replaces my previous solution.

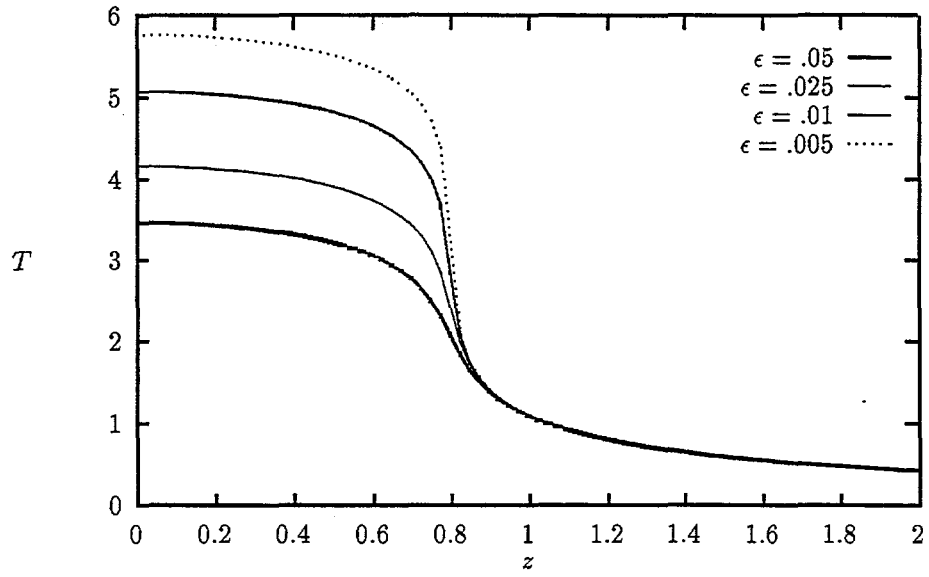

Figure 1: This shows the temperature profile on the probe as a function of z for different values of the aspect ration ϵ. All of the caculations are done assuming that the ratios of conductivities R is equal to one , and that the heated section ends at $z = \delta = .8$. As ϵ decreases there is an overall raising of the temperature of the probe in the heated region as well as a steepening of the gradients near the region where the heated section ends.

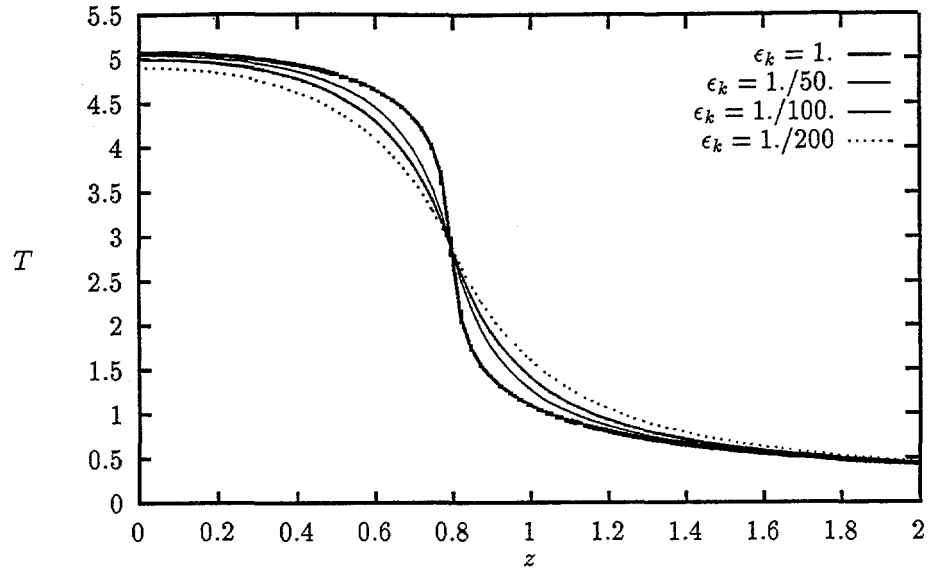

Figure 2: This shows the temperature as a function of z for $\epsilon = .01$ and various values of the ratio of conductivities $i\epsilon_k$.

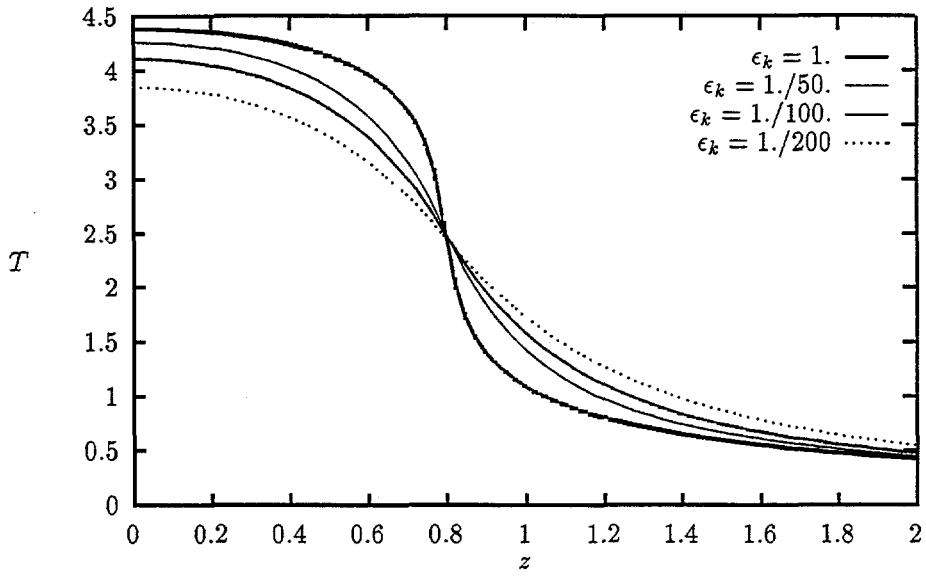

Figure 3: This shows the temperature as a function of z for $\epsilon = .02$ and various values of the ratio of conductivities ϵ_k.

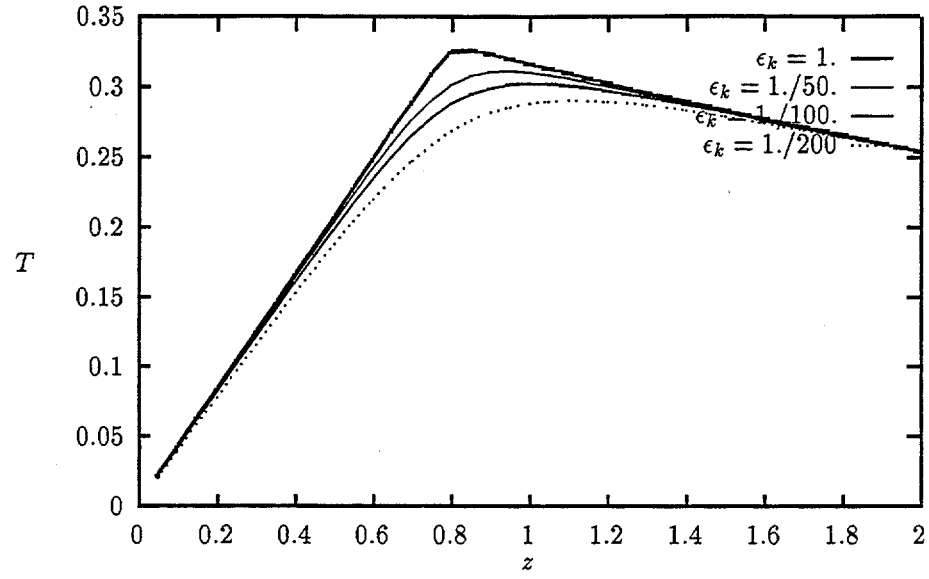

Figure 4: This shows the temperature differences between symmetrical pointsas a function of z for $\epsilon = .01$ and various values of the ratio of conductivities $i\epsilon_k$. All plots have $Pe = .5$.

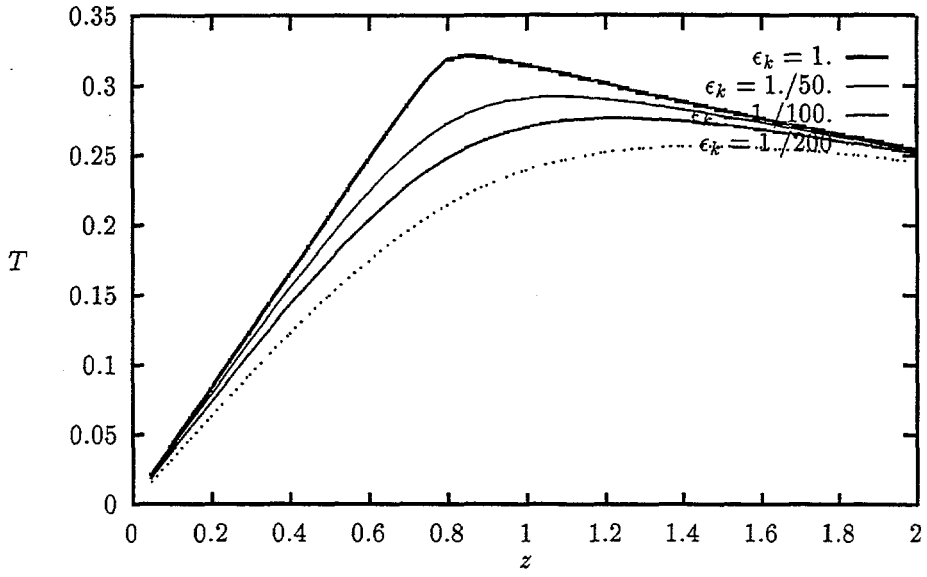

Figure 5: This shows the temperature differences between symmetrical pointsas a function of z for $\epsilon = .02$ and various values of the ratio of conductivities $i\epsilon_k$. All plots have $Pe = .5$.

Point Source Probe Summary

Abstract:
A variation on the vertical gas flow probe was constructed and calibrated in mid July 1996. Following calibration, the probe was excised in a series of lab tests conducted in bldg. 823 room 1296. The lab tests were conducted in an insulated sand-filled barrel ~110 gal size (2 plastic 55 gal drums connected vertically). The sand filling the barrel was a 4-9 mesh obtain from Rodgers and Co. In total, data was collected from 2 flow rates plus background data while the heater was powered with a steady-state DC source; and 1 flow rate with 3 frequencies of cycled heater power. The lab tests were conducted from July through September 1996.

Probe Components and Construction Technique:
Ten Fenwal thermistors P/N 135-105-QAG-J01 were attached to an ~40 ft length of Alpha cable type 3490/25C at the spacing shown on the figure below. Each end of each thermistor had connected to it a single conductor (i.e. no common returns). Also attached to this cable were both leads of an Omega cartridge heater type CIR-1035/120V. The assembly was stretched out tightly on a bench top and the distance between the midpoints of each thermistor was recorded and marked on the outside of an ~45" length of CPVC which was used to house the assembly.

The length of the CPVC was sufficiently long to allow a significant length beyond the uppermost thermistor. This allowed room for additional potting compound to water-proof the probe. The assembly was installed in the CPVC pipe using tie wire and held in place (and stretched taught) by hose clamping the tie wire to the outside of the bottom of the CPVC pipe. A make-shift injection system was made for the potting compound from a length of 1-1/2" diameter PVC pipe and connected to the bottom of the vertically oriented probe with plastic tubing and a hose clamp (tubing and hose clamp clamped the tie wire in position). The entire length of CPVC was then injected full of 3M brand Scotchcast #4 insulation compound and allowed to cure.

Data Acquisition System
The end of the cable was terminated with a KPSE06F20-39P connector using a 1" slip-slip PVC coupling for a potting backshell. The connector and AM416 were wired such that thermistor #1 (refer to sketch) was connected to input channel number 1 thermistor 2 to channel 2 and so on. The data was also stored in final memory and in data files in this same order. The Table 1 contains the pin assignments.

A means for measuring heater power to the probe was accomplished using a series 0.1Ω current viewing resistor in the heater circuit. Physically this resistor was mounted in a Bud box ~4" x 2-1/2" x 2-1/2" along with a Crydom relay and a free wheeling diode. The relay provides a way of turning on and off the heater power under program control, while the free wheeling diode prevents relay damage from large voltage spikes that occur at relay turn-off times. The current viewing resistor was a 2 watt 0.1Ω which developed 100mV across it for every 1A of current flow through it. The high and low sides of the CVR were connected to the 4H and 4L differential input channels on the CR10. Due to small leakage currents through the relay and the 5% resistance tolerance of the resistor a 2-point linear correction scheme was employed based on the CR10 measured values for 0 watts and 10 watts (the power range which was anticipated to be operated at). The correction scheme produced a slope of m=1.0255 and b=6.769. The heater power data was stored on channel #11 in all the data files.

A Tylan mass flow controller model FC-202 max. flow connected to a 4 channel power supply and readout type 20A and provided the 0-5V analog voltage proportional to 0-100% of max. flow (30SLPM). Due to the ±2500 mV limitations of the datalogger, that voltage was voltage divided using two 500kΩ resistors. As with the case of the heater power measurement a 2 point linear correction scheme was employed to compensate for errors due to mismatched resistors and dc offsets from cable length. The

Point Source Flow Probe

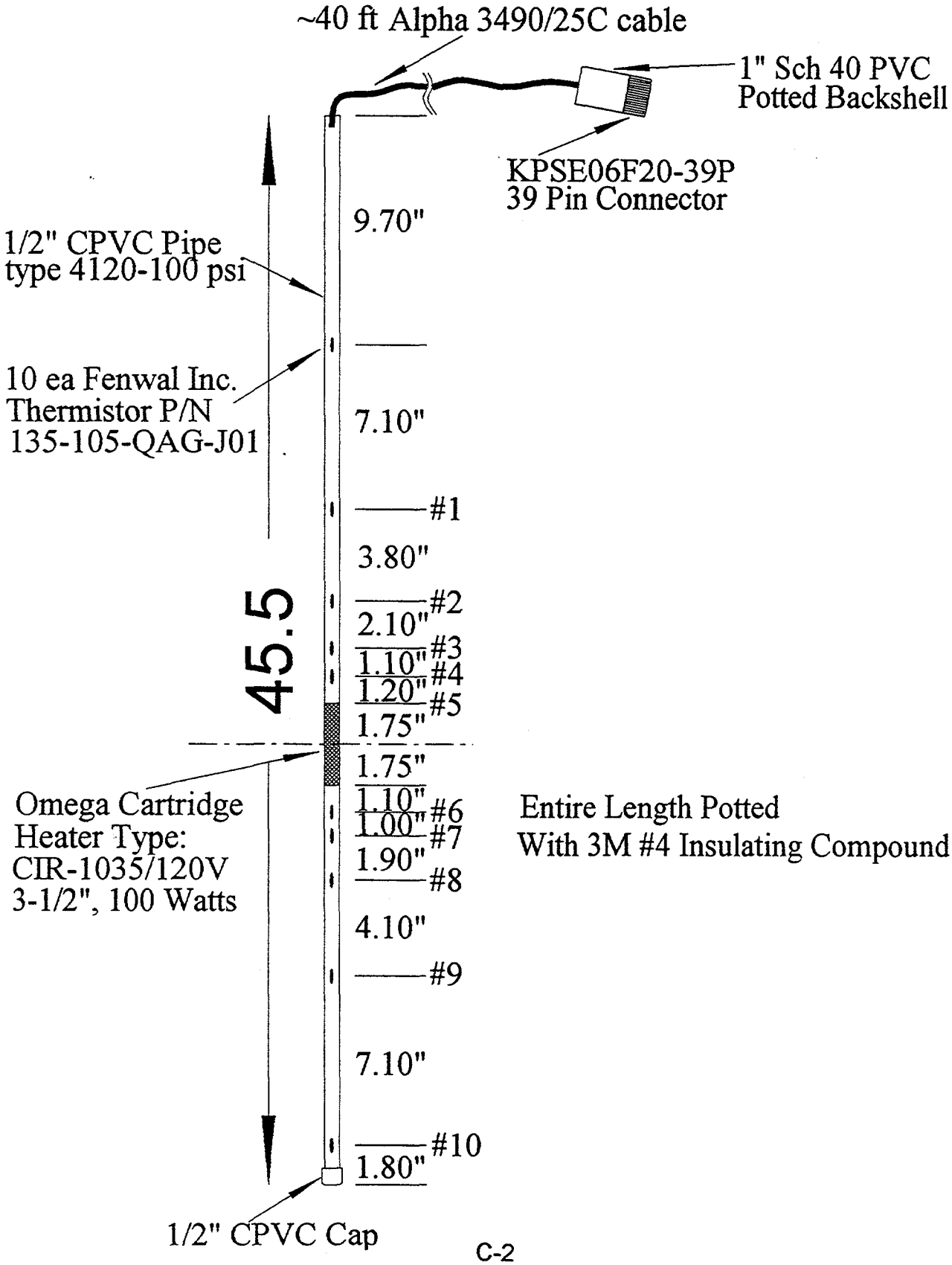

corrections were calculated from data collected at 0 SLPM and 30 SLPM and came out to be: m=1.0639 and b=-24.58. This flow rate information was collected and stored in channel #12.

THERMISTOR	39 PIN CONNECTOR	AM416 MULTIPLEXER
#1 High	B	1 H1
#1 Low	C	1 L1
#2 High	D	2 H1
#2 Low	E	2 L1
#3 High	F	3 H1
#3 Low	G	3 L1
#4 High	H	4 H1
#4 Low	J	4 L1
#5 High	K	5 H1
#5 Low	L	5L1
#6 High	N	6 H1
#6 Low	P	6 L1
#7 High	R	7 H1
#7 Low	S	7 L1
#8 High	T	8 H1
#8 Low	U	8 L1
#9 High	V	9 H1
#9 Low	W	9 L1
#10 High	X	10 H1
#10 Low	Y	10 L1
Heater High	Z	DC Power Supply (+)
Heater Low	a	DC Power Supply Return
Shield	p	CR10 "G"

Table 1 Connector/Thermistor Pin Assignment.

Continuous Power Flow Tests

The probe was installed into the 4-9 mesh sand by first driving an ~5' length of 1" schedule 40 PVC pipe using a rubber mallet to a depth such that the center of the heater section was at the center of the barrel. Next an ordinary shop vacuum was used to remove the sand from within the 1" PVC pipe. The point source probe was then lowered into place and the 1" PVC pipe was retracted from the sand using a chain wrench and pry bar. The probe was allowed to equilibrate in temperature overnight.

A DC power supply was connected through the relay/CVR box to the cartridge heater inside the tool. The voltage was adjusted to provide 10 Watts of power into the 151.7Ω load. After ~ 24 hours the temperature immediately adjacent to the cartridge heater got hot enough to melt the wires which passed by the heater and connected the lower thermistors. This was discovered by the fact that the 2 bottom thermistors #9 and #10 were getting too warm when compared to channels #1 and #2 which were approximately equidistant from the heat source. What actually occurred was that those two channels partially shorted out between each other. The probe heater power was turned off and allowed to cool.

After cooling off over the weekend, all thermistor channels were checked for shorts and all were found to be isolated better than ~10MΩ (the impedance of the meter). The heater power was again turned on at 15:30 PM on July 29, this time at 5 Watts. Due to inaccuracies of the CVR circuit the datalogger measurement was recorded at ~ 6 Watts, but actually was 5 Watts. The probe was allowed to equilibrate at this heater power for ~ 2 days with no gas flow. Gas flow was begun at 15:20 PM on July 31 at 30

standard liters per minute (SLPM). The gas supply was obtained from facilities provided via a wall mounted flexible hose reel/regulator unit. The 30 SLPM flow rate was continued for ~ 2 days until 13:30 on August 2 when it was reduced to 6 SLPM. Figure 2 shows the raw temperature data.

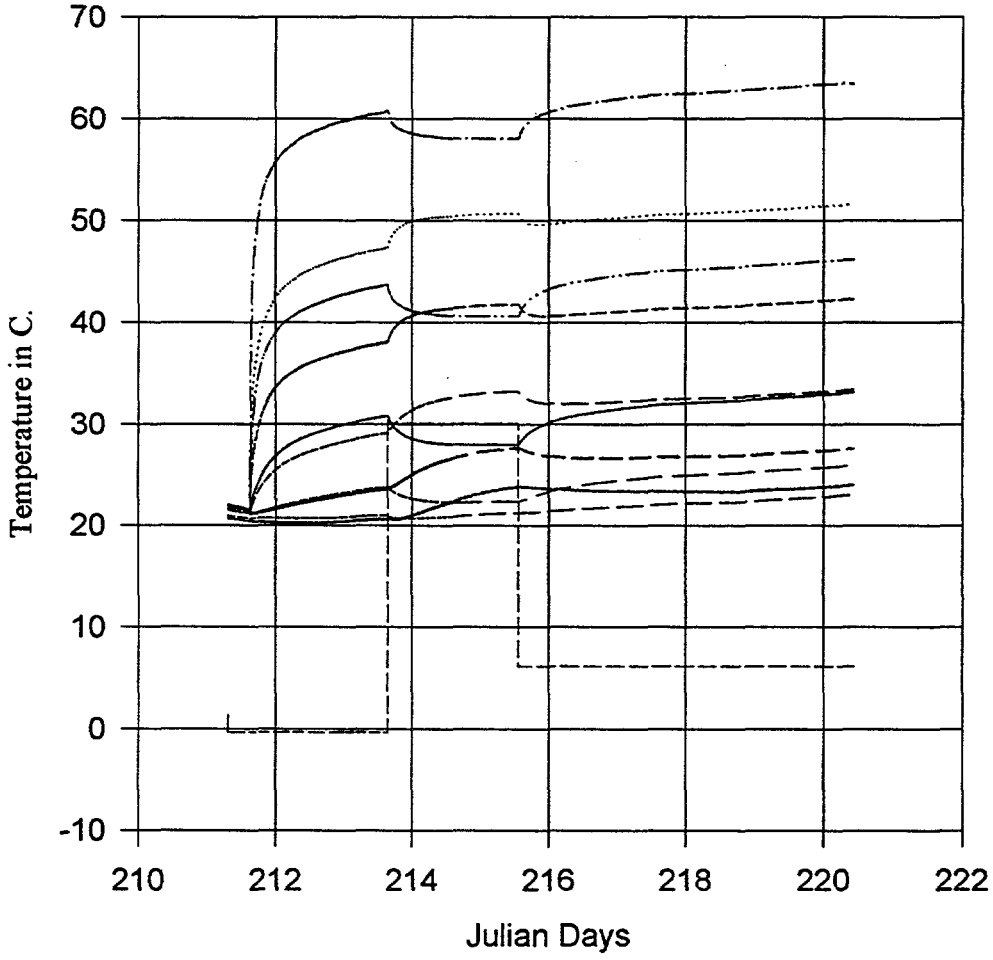

Figure 2. Temperature vs. Time for 6 Watts DC Power Over Warm-up Period, 30 SLPM Flow, and 6 SLPM Flow (Step function trace is gas flow in Standard Liters per Minute - SLPM)

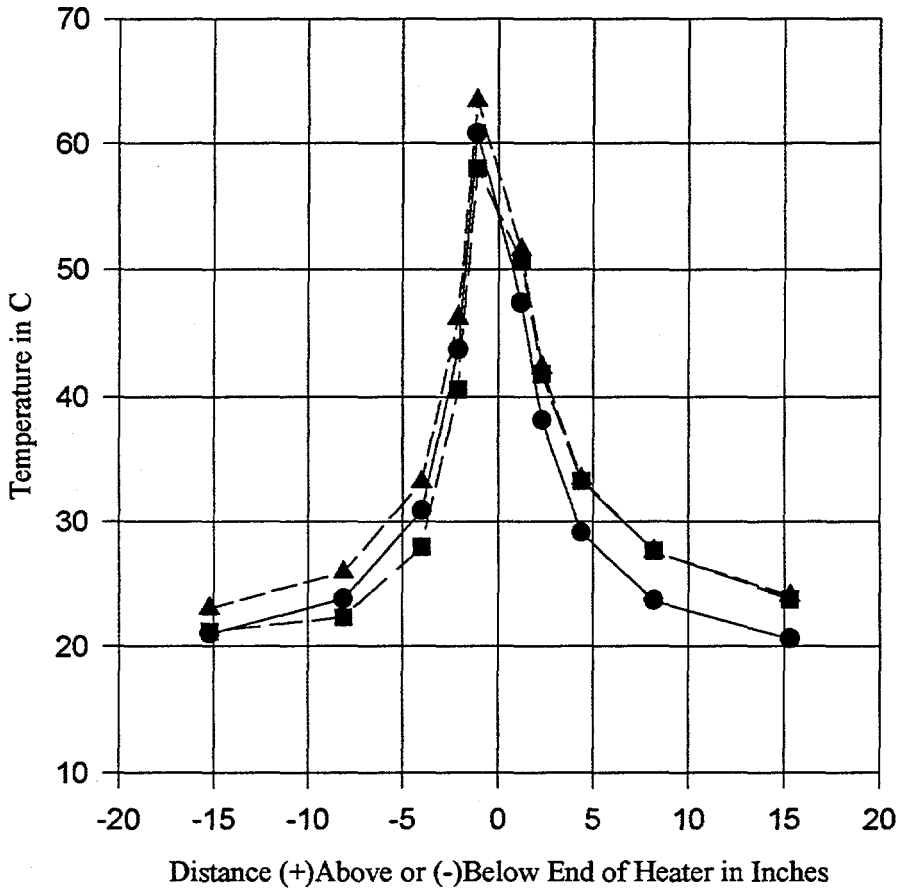

Figure 3. Temperature vs. Vertical Distance from Heater. (Circles - No Flow, Triangles - 6 SLPM, Squares - 30 SLPM).

Figure 3 illustrates the change in the vertical temperature profile during the test conditions: no flow, 6 SLPM, and 30 SLPM. Each symbol represents a thermistor location during each of the test conditions and the x axis is scaled to represent the heater section as a single point (actual length is ~3.5") and actual thermistor distances relative to either end of the heater.

Sinusoidal Heater Power Tests

Throughout the sinusoidal heater power tests the gas flow remained at 6 SLPM. Low frequency sinusoidal cycling of the DC power source was accomplished through CR10 datalogger control of an SDM-A04 4-channel continuous analog output module. The analog output voltage was connected through a break-out box to the remote programmable voltage input pin of a Sorensen DCS 80-13 DC power supply.

The program used to control the analog output module is attached and labeled "Sinusoidal Heater Power". In this program the program statements in Table 2, steps 3-5 determined the period of the sine wave output. Step #3 returns the fractional portion of the current hour in minutes, multiplied by 60 in step #4 gives seconds. Step #5's "F" value is the product of $2\pi\omega$ (in degrees). The attached program produces a sine wave with a frequency of 1cycle/20 minutes, obtained from the current time into an hour in seconds (steps3 &4) multiplied by $2\pi\omega$ (.29996 "F" term step 5). Where $\omega = 1/f$; f=20 min=1200 sec. Altogether then the "F" term is 2*3.141*(1/1200)*57.3(conversion from radians to degrees for CR10)=.29996.

10 Watts of peak heater power was tried at first with the same result as with 10 Watts of continuous power, namely the insulation on the wires for channels #9 and #10 began to melt and short out to each other. As before, luckily, when the power was reduced the insulation on the shorting wires cooled such that there was again, greater than 10MΩ isolation between those channels so that the tests could continue.

5 Watts, 60 min Period, 6 SLPM Flow

Again 5 Watts was the chosen power to operate the heater for the rest of the tests, the power reduction occurred at ~11:30 am on August 8. So then the first usable sinusoidal powered test began on Aug. 8, ~11:30 am at 6 SLPM flow rate with 5 Watts of peak heater power cycling in a sinusoidal manner with a period of 60 minutes. The test continued with these parameters until Aug. 27, ~8:30 am, however, because the data collection computer was shared with other activities in the lab, data was lost from Aug. 16, ~7:00 am through Aug. 18, ~1:30 am. Also worth noting, the storage rate of data was reduced to once per 10 min. from 1 per 2 min. on Aug. 21 ~6:45 am. This storage was adequate still for cycles of power at a period of 60 min., but when that changed to a 20 minute period on Aug. 27, ~8:30 am this was no longer true.

5 Watts, 20 min. Period, 6 SLPM Flow

At the start of the frequency change Aug. 27, ~8:30 am the storage rate was too slow to accurately depict the waveforms being measured. This was not discovered until Aug. 29, ~9:00 am. when the storage rate was changed to every 60 sec. Therefore, the data collected between Aug. 27 and Aug. 29 is not useable. Valid data with the above parameters exists from Aug. 29, ~9:00 am through Sept. 5, ~14:45 PM.

5 Watts, 180 min. Period, 6 SLPM Flow

The period of the heater power input was changed from 1 cycle per 20 min. to 1 cycle per 180 min. on Sept. 5, ~14:45 PM and continued at that frequency until flow was shut off. Gas flow was turned off during a period in which data was lost - between Sept. 17, ~13:00 PM and Sept. 18, ~7;30 am and the exact time is not known. Data for 0 SLPM gas flow was recorded for ~2 weeks prior to heater power turn-off.

Summary and Conclusions

The point source probe idea is one which merits more testing and refinement. Certainly, more thought as to how to eliminate the need to pass thermistor wires next to the cartridge heater and/or use of higher temperature insulation (e.g. Teflon) must be considered. For the same reason, a substitute for the CPVC pipe must be found - possibly stainless steel. The number of thermistors and their spacing relative to the heater, heater length, and operating power also needs more experimentation.

The continuous powered heater tests show a very clear signal occurring at flow start at 30 SLPM and also again at the flow rate change to 6 SLPM. There is promise in the use of the tool in this manner. Yet much work needs to be done to develop a method to calculate the flow rate based on the temperature distribution along the probe length.

The sinusoidally powered heater results are much less clear, however very little effort was made in processing this data. There did appear to be some phase shifts between the heater power control frequency and the sine wave frequency on the thermistor data, but it was not as evident as thought nor did it appear to change significantly with changes in control frequency.

```
Program:
   Flag Usage: Continuous Heater Power
   Input Channel Usage:
   Excitation Channel Usage:
   Control Port Usage:
   Pulse Input Channel Usage:
   Output Array Definitions:


   *  1     Table 1 Programs
    01: 60    Sec. Execution Interval

   01: P86    Do
    01: 47    Set high Port 7

   02: P87    Beginning of Loop
    01: 0     Delay
    02: 10    Loop Count

   03: P90    Step Loop Index
    01: 1     Step

   04: P86    Do
    01: 78    Pulse Port 8

   05: P4     Excite,Delay,Volt(SE)
    01: 1     Rep
    02: 25    2500 mV 60 Hz rejection Range
    03: 1     IN Chan
    04: 1     Excite all reps w/EXchan 1
    05: 80    Delay (units .01sec)
    06: 2500  mV Excitation
    07: 1--   Loc :
    08: .0004 Mult
    09: 0.0000 Offset

   06: P59    BR Transform Rf[X/(1-X)]
    01: 1     Rep
    02: 1--   Loc :
    03: .5    Multiplier (Rf)

   07: P95    End

   08: P86    Do
    01: 78    Pulse Port 8

   09: P4     Excite,Delay,Volt(SE)
    01: 1     Rep
    02: 25    2500 mV 60 Hz rejection Range
    03: 1     IN Chan
    04: 1     Excite all reps w/EXchan 1
    05: 80    Delay (units .01sec)
    06: 2500  mV Excitation
    07: 5     Loc :
    08: .0004 Mult
    09: 0.0000 Offset

   10: P59    BR Transform Rf[X/(1-X)]
    01: 1     Rep
    02: 5     Loc :
    03: .5    Multiplier (Rf)

   11: P1     Volt (SE)
    01: 1     Rep
    02: 25    2500 mV 60 Hz rejection Range
    03: 7     IN Chan
    04: 11    Loc :
    05: 10    Mult
    06: 0.0000 Offset

   12: P37    Z=X*F
    01: 11    X Loc
    02: 1.0255 F
    03: 11    Z Loc :

   13: P34    Z=X+F
    01: 11    X Loc
    02: 6.769  F
    03: 11    Z Loc :

   14: P37    Z=X*F
    01: 11    X Loc
    02: .001  F
    03: 11    Z Loc :

   15: P55    Polynomial
    01: 1     Rep
    02: 11    X Loc
    03: 11    F(X) Loc :
    04: 0.0000 C0
    05: 0.0000 C1
    06: 151.7  C2
    07: 0.0000 C3
    08: 0.0000 C4
    09: 0.0000 C5

   16: P1     Volt (SE)
    01: 1     Rep
    02: 25    2500 mV 60 Hz rejection Range
    03: 5     IN Chan
    04: 12    Loc :
    05: 1     Mult
    06: 0.0000 Offset
```

```
17: P37     Z=X*F
 01: 12     X Loc
 02: 1.0639 F
 03: 12     Z Loc :
18: P34     Z=X+F
 01: 12     X Loc
 02: -24.58 F
 03: 12     Z Loc :

19: P37     Z=X*F
 01: 12     X Loc
 02: .012   F
 03: 12     Z Loc :

20: P86     Do
 01: 57     Set low Port 7

21: P86     Do
 01: 10     Set high Flag 0 (output)

22: P80     Set Active Storage Area
 01: 1      Final Storage Area 1
 02: 94     Array ID or location

23: P77     Real Time
 01: 111    Day,Hour-Minute,Seconds

24: P78     Resolution
 01: 1      High Resolution

25: P70     Sample
 01: 12     Reps
 02: 1      Loc

26: P96     Serial Output
 01: 71     SM192/SM716/CSM1

27: P       End Table 1


*  2        Table 2 Programs
 01: 1      Sec. Execution Interval

01: P20     Set Port(s)
 01: 0000   C8,C7,C6,C5 options
 02: 1      C4..C1=low/low/low/high   02:
            P       End Table 2
```

Program: ***Sinusoidal Heater Power***
Flag Usage:
Input Channel Usage:
Excitation Channel Usage:
Control Port Usage:
Pulse Input Channel Usage:
Output Array Definitions:

* 1 Table 1 Programs
01: 60 Sec. Execution Interval

01: P86 Do
01: 47 Set high Port 7

02: P87 Beginning of Loop
01: 0 Delay
02: 10 Loop Count

03: P90 Step Loop Index
01: 1 Step

04: P86 Do
01: 78 Pulse Port 8

05: P4 Excite,Delay,Volt(SE)
01: 1 Rep
02: 25 2500 mV 60 Hz rejection Range
03: 1 IN Chan
04: 1 Excite all reps w/EXchan 1
05: 80 Delay (units .01sec)
06: 2500 mV Excitation
07: 1-- Loc :
08: .0004 Mult
09: 0.0000 Offset

06: P59 BR Transform Rf[X/(1-X)]
01: 1 Rep
02: 1-- Loc :
03: .5 Multiplier (Rf)

07: P95 End

08: P86 Do
01: 78 Pulse Port 8

09: P4 Excite,Delay,Volt(SE)
01: 1 Rep
02: 25 2500 mV 60 Hz rejection Range
03: 1 IN Chan
04: 1 Excite all reps w/EXchan 1
05: 80 Delay (units .01sec)
06: 2500 mV Excitation
07: 5 Loc :
08: .0004 Mult
09: 0.0000 Offset

10: P59 BR Transform Rf[X/(1-X)]
01: 1 Rep
02: 5 Loc :
03: .5 Multiplier (Rf)

11: P1 Volt (SE)
01: 1 Rep
02: 25 2500 mV 60 Hz rejection Range
03: 7 IN Chan
04: 11 Loc [:CVR pwr]
05: 10 Mult
06: 0.0000 Offset

12: P37 Z=X*F
01: 11 X Loc CVR pwr
02: 1.0255 F
03: 11 Z Loc [:CVR pwr]

13: P34 Z=X+F
01: 11 X Loc CVR pwr
02: 6.769 F
03: 11 Z Loc [:CVR pwr]

14: P37 Z=X*F
01: 11 X Loc CVR pwr
02: .001 F
03: 11 Z Loc [:CVR pwr]

15: P55 Polynomial
01: 1 Rep
02: 11 X Loc CVR pwr
03: 11 F(X) Loc [:CVR pwr]
04: 0.0000 C0
05: 0.0000 C1
06: 151.7 C2
07: 0.0000 C3
08: 0.0000 C4
09: 0.0000 C5

16: P1 Volt (SE)
01: 1 Rep
02: 25 2500 mV 60 Hz rejection Range
03: 5 IN Chan
04: 12 Loc [:Flow slm]
05: 1 Mult
06: 0.0000 Offset

17: P37 Z=X*F
01: 12 X Loc Flow slm
02: 1.0639 F
03: 12 Z Loc [:Flow slm]

```
18: P34     Z=X+F
 01: 12     X Loc Flow slm
 02: -24.58 F
 03: 12     Z Loc [:Flow slm ]

19: P37     Z=X*F
 01: 12     X Loc Flow slm
 02: .012   F
 03: 12     Z Loc [:Flow slm ]

20: P86     Do
 01: 57     Set low Port 7

21: P86     Do
 01: 10     Set high Flag 0 (output)

22: P80     Set Active Storage Area
 01: 1      Final Storage Area 1
 02: 96     Array ID or location

23: P77     Real Time
 01: 111    Day,Hour-Minute,Seconds

24: P78     Resolution
 01: 1      High Resolution

25: P70     Sample
 01: 15     Reps
 02: 1      Loc

26: P96     Serial Output
 01: 71     SM192/SM716/CSM1

27: P       End Table 1


*  2        Table 2 Programs
 01: 30     Sec. Execution Interval

01: P20     Set Port(s)
 01: 0000   C8,C7,C6,C5 options
 02: 1      C4..C1=low/low/low/high

02: P30     Z=F
 01: 5      F
 02: 00     Exponent of 10
 03: 28     Z Loc [:max pwr  ]

03: P18     Time
 01: 1      Minutes into current day
              (maximum 1440)
 02: 60     Mod/by
 03: 27     Loc [:sin factr]

04: P37     Z=X*F
 01: 27     X Loc sin factr
 02: 60     F
 03: 27     Z Loc [:sin factr]

05: P37     Z=X*F
 01: 27     X Loc sin factr
 02: .29996 F
 03: 27     Z Loc [:sin factr]

06: P48     Z=SIN(X)
 01: 27     X Loc sin factr
 02: 27     Z Loc [:sin factr]

07: P37     Z=X*F
 01: 28     X Loc max pwr
 02: .5     F
 03: 26     Z Loc [:1/2 pwr  ]

08: P36     Z=X*Y
 01: 27     X Loc sin factr
 02: 26     Y Loc 1/2 pwr
 03: 25     Z Loc [:sin term ]

09: P33     Z=X+Y
 01: 26     X Loc 1/2 pwr
 02: 25     Y Loc sin term
 03: 13     Z Loc [:desrd pwr]

10: P30     Z=F
 01: 151.7  F
 02: 00     Exponent of 10
 03: 24     Z Loc [:htr resis]

11: P36     Z=X*Y
 01: 24     X Loc htr resis
 02: 13     Y Loc desrd pwr
 03: 23     Z Loc [:V desired]

12: P39     Z=SQRT(X)
 01: 23     X Loc V desired
 02: 23     Z Loc [:V desired]

13: P37     Z=X*F
 01: 23     X Loc V desired
 02: .0125  F
 03: 14     Z Loc [:cntrl V  ]

14: P37     Z=X*F
 01: 14     X Loc cntrl V
 02: 5000   F
 03: 14     Z Loc [:cntrl V  ]
```

```
15: P103    SDM-A04
 01: 1      Reps
 02: 00     Address
 03: 14     Loc cntrl V
```

```
16: P1      Volt (SE)
 01: 1      Rep
 02: 25     2500 mV 60 Hz rejection Range
 03: 3      IN Chan
 04: 15     Loc [:ctl V msd]
 05: 2      Mult
 06: 0.0000 Offset

17: P       End Table 2
```

Raw Data file Legend

Pt_Src-1.dat	7/24/96 7:00am	thru	7/26/96 15:00pm	10Watts Cont. No Flow
Pt_Src-2.dat	7/29/96 7:00am	thru	8/01/96 9:00am	5Watts Cont. 30 SLPM
Pt_Src-3.dat	8/01/96 9:00am	thru	8/07/96 11:00am	5 Watts 30==>6SLPM
Pt_Src-4.dat	8/07/96 14:00pm	thru	8/19/96 6:30am	10 W Sine, 5W Sine - 1hr Period
Pt_Src-5.dat	8/19/96 6:30am	thru	9/05/96 10:00am	5W Sine 1 hr ==> 20 min Period
Pt_Src-6.dat	9/05/96 10:00am	thru	10/01/96 7:00am	5W Sine 20min==> 180min Period

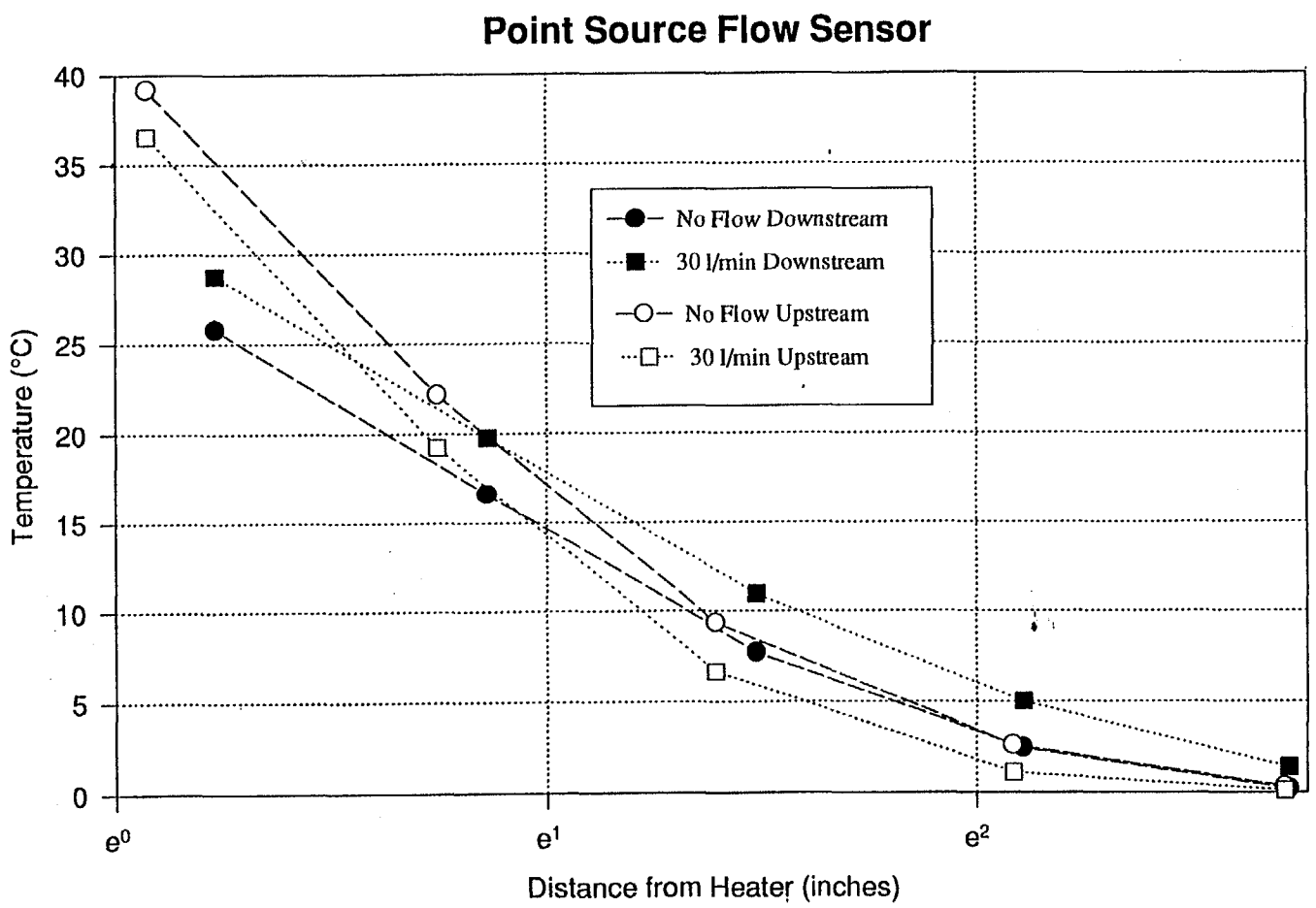
Point Source Flow Sensor
40
35
30
25
20
15
10
5
0
Temperature (°C)
No Flow Downstream
30 l/min Downstream
No Flow Upstream
30 l/min Upstream
e0
e1
e2
Distance from Heater (inches)

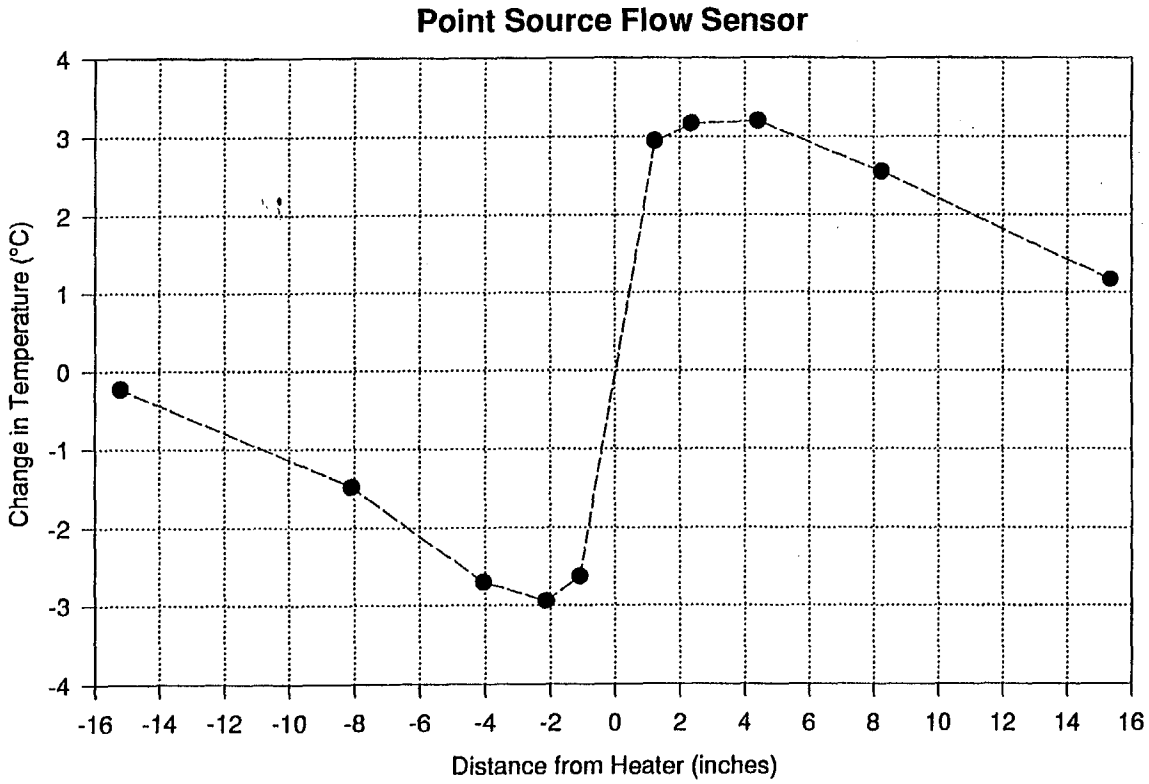
Point Source Flow Sensor
Change in Temperature (°C)
4
3
2
1
0
-1
-2
-3
-4
-16
-14
-12
-10
-8
-6
-4
-2
0
2
4
6
8
10
12
14
16
Distance from Heater (inches)

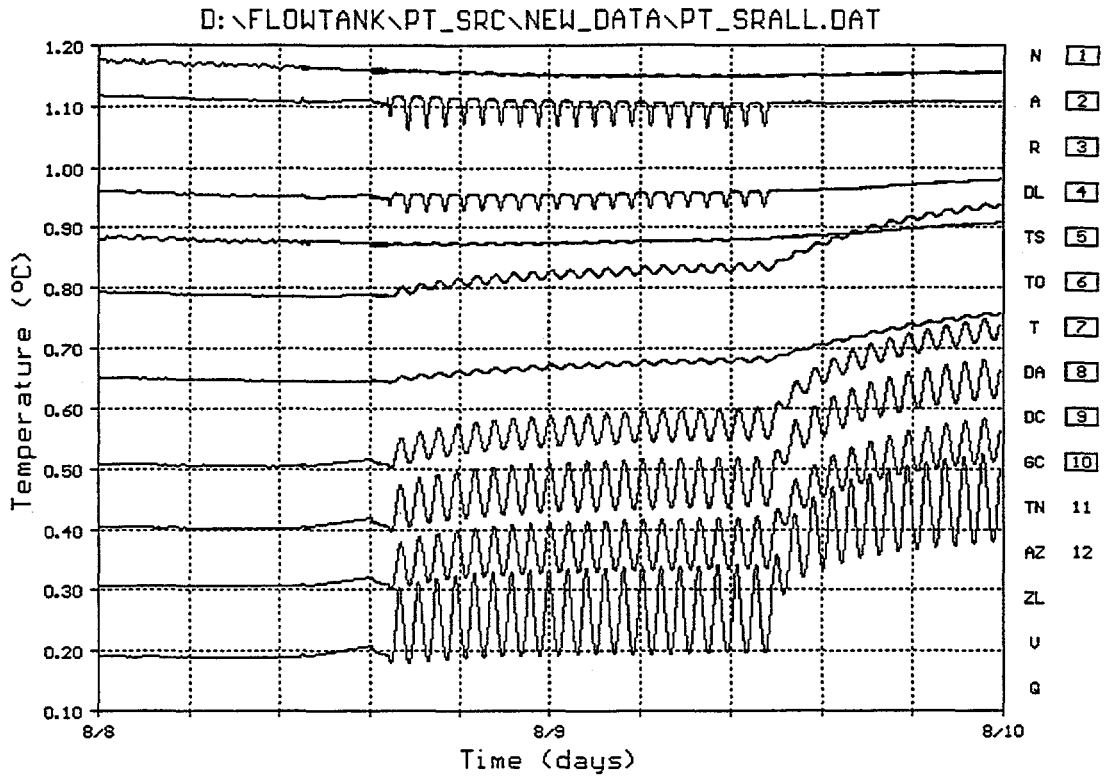
D:\FLOWTANK\PT_SRC\NEW_DATA\PT_SRALL.DAT
Temperature (°C)
1.20
1.10
1.00
0.90
0.80
0.70
0.60
0.50
0.40
0.30
0.20
0.10
8/8
8/9
8/10
Time (days)
N 1
A 2
R 3
DL 4
TS 5
TD 6
T 7
DA 8
DC 9
GC 10
TN 11
AZ 12
ZL
V
Q

DISTRIBUTION

SERDP Program Office
Attn: Dr. Femi Ayorinde
901 North Stuart Street
Suite 303
Arlington, VA 22203

Intera
Attn: James E. Studer
1650 University Blvd. NE
Suite 300
Albuquerque, NM 87102-1732

Intera
Attn: Souren Ala
1650 University Blvd. NE
Albuqueque, NM 7102-1732

Sandia Internal:

MS-0701	**Richard W. Lynch, 6100**
MS-0705	**Robert P. Cutler, 6116**
MS-0750	**Sanford Ballard, 6116**
MS-0705	**Glenn T. Barker, 6116**
MS-0750	**Michael P. Chavez, 6116**
MS-0705	**Marianne C. Walck, 6116**
MS-0751	**Ray E. Finley, 6117**
MS-0750	**Harlan W. Stockman, 6118**
MS-1110	**Louis Romero, 9222**
MS-9018	**Central Technical Files, 8940-2**
MS-0899	**Technical Library, 4414**
MS-0619	**Review & Approval Desk, 12690 For DOE/OSTI**
MS-0161	**Patent & Licensing Office, 11500**